IMPACT OF COSOLVENTS ON THE INTERPHASE MASS TRANSFER OF NAPLs IN POROUS MEDIA

by

Korcan Yakşi

B.Sc. in Chemistry, Middle East Technical University, 2014

Submitted to the Institute of Environmental Sciences in partial fulfillment of the requirements for the degree of

Master of Science

in

Environmental Sciences

Boğaziçi University

2019

Dedicated to all those who endeavor to keep the light of science alive.

ACKNOWLEDGEMENTS

First and foremost, I would like to express my gratitude to Prof. Dr. Nadim Copty for his constant support and guidance on the coming this thesis to existence. He has provided motivation and encouragement since the day I started to participate in his research lab. It has been a privilege to be his student, and to acquire his academic perspective throughout my time in this graduate program. Besides my advisor, I also would like to thank the members of my thesis committee; Assoc. Prof. Dr. Nihat Hakan Akyol and Assoc. Prof. Dr. Başak Güven for their valuable contributions.

A very special thanks to Prof. Dr. İnci Gökmen from the chemistry department of METU, whom raised my awareness and inspired me as well as many other chemists to actively take part in various fields of environmental studies.

I am very lucky to have met Defne Şahin, the most remarkable companion I have in our institute, and a friend for life. I am grateful to her for all the support when I needed the most, and for making my days at Boğaziçi University among the best in my life.

I am thankful to Derya Aydın Sarıkurt and Zeynep Demiray for their valuable help in the experimental work of this thesis. I also would like to thank Gülşah Günel, İlknur Temizel, Ece Özön, Öykü Sefiloğlu and Berivan Ülger for making the institute a warm and welcoming place for my time there.

I also gratefully appreciate the countless support of Deniz Göçhan to this thesis, as well as helping me building up the academic perspective I have now.

Last but not least, I owe my deepest gratitude to my family; Aycan Yakşi, Ayfer Sevinç and İsmet Yakşi. Words fail to describe the meaning of their endless support and love; I cannot be thankful enough for their help throughout my academic studies. What I have achieved could not be possible without them.

ABSTRACT

IMPACT OF COSOLVENTS ON THE INTERPHASE MASS TRANSFER OF NAPLs IN POROUS MEDIA

Contamination of the subsurface with organic contaminants in the form of non-aqueous phase liquids (NAPLs) is a widespread and critical environmental threat. Due to their low aqueous solubilities, high adsorption rates and potentially high toxicities, these compounds act as long-term contamination sources and are among the most challenging to remediate. Conventional pump-and-treat techniques for the remediation of NAPLs have proven to be inefficient and cost-intensive. Among many remediation techniques introduced in the recent years, cosolvent flushing for enhanced dissolution of NAPLs is demonstrated as a cost-efficient and convenient method for in-situ remediation of NAPLs. Interphase mass transfer of the NAPL mass into the flushing solution is a key process that controls the effectiveness of the enhanced dissolution remediation technology; yet very few direct studies have rigorously investigated the effect of cosolvents on it. This study investigates the effect of cosolvents on the mass transfer of NAPLs into flushing solutions. The cosolvent and NAPL selected for this purpose are ethanol and 1,2-dicholorobenzene (DCB), respectively. A series of experiments are conducted to test the effect of ethanol content and flushing velocity on mass transfer. The experimental results are interpreted using a one-dimensional analytical solution and a two-dimensional pore network model. The mass transfer coefficients estimated from the two models are used to develop Sherwood correlations. It is observed that cosolvent presence has a significant impact on mass transfer coefficient. The developed Sherwood correlations can potentially be used in further modeling studies and field applications involving the remediation of entrapped NAPLs.

ÖZET

GÖZENEKLİ ORTAMDAKİ NAPL'LERİN FAZLAR ARASI KÜTLE AKTARIMINA YARDIMCI ÇÖZÜCÜLERİN ETKİSİ

Yüzeyaltı ortamlarının, susuz faz sıvıları (NAPL'ler) formundaki organik kirleticilerle kirlenmesi, yaygın ve ciddi bir çevresel tehdittir. Sudaki düşük çözünürlükleri, yüksek adsorpsiyon oranları ve potansiyel olarak yüksek toksisiteleri nedeniyle, bu bileşikler uzun vadeli kirletici kaynakları olarak davranış gösterirler ve iyileştirmesi en zorlu olanlarındandır. NAPL'lerin iyileştirilmesi için geleneksel "pompaj ve arıtma" tekniklerinin verimsiz olduğu ve yüksek maliyet gerektirdiği kanıtlanmıştır. Son yıllarda ortaya konan birçok iyileştirme tekniği arasında, NAPL'lerin daha iyi çözünmesi için yardımcı çözücülerle yıkama yöntemi, NAPL'lerin yerinde iyileştirilmesi için düşük maliyetli ve uygun bir yöntem olarak gösterilmektedir. NAPL kütlesinin yıkama çözeltisine fazlar arası kütle aktarımı, artırılmış çözünmeyle iyileştirme teknolojisinin tesirini kontrol eden kilit bir süreçtir; fakat henüz çok az sayıda doğrudan çalışma, yardımcı çözücülerin bu süreçlerin üzerindeki etkisini titizlikle araştırmıştır. Bu çalışma, yardımcı çözücülerin NAPL'lerin yıkama çözeltisine kütle transferi üzerindeki etkilerini araştırmaktadır. Bu amaç için seçilen yardımcı çözücü ve NAPL, sırasıyla etanol ve 1,2-diklorobenzendir (DCB). Etanol içeriğinin ve yıkama hızının kütle transferi üzerindeki etkisini sınamak için bir dizi deney yapılmıştır. Deneysel sonuçlar, tek boyutlu bir analitik çözüm ve iki boyutlu bir gözenek ağı modeli kullanılarak yorumlanmıştır. Bu iki model üzerinden hesaplanan kütle transfer katsayıları, Sherwood korelasyonları geliştirmek için kullanılmıştır. Yardımcı çözücü varlığının kütle transfer katsayısı üzerinde önemli bir etkiye sahip olduğu gözlemlenmiştir. Geliştirilen Sherwood korelasyonları, ilerideki modelleme çalışmalarında ve hapsolmuş NAPL'lerin iyileştirilmesini içeren saha uygulamalarında kullanılabilir.

TABLE OF CONTENTS

LIST OF FIGURES

LIST OF TABLES

LIST OF SYMBOLS/ABBREVIATIONS

Symbol	Explanation	Unit
A	Cross Sectional Area of the Tank	L^2
a	Contact Area per Unit Volume of Porous Medium	L^2/L^3
C	Aqueous Phase Concentration	M/L^3
C_{eff}	Steady-State Effluent Concentration	M/L^3
C_i	Aqueous-Phase Concentration in Chamber i	M/L^3
C_m	Concentration Associated with Q_m	M/L^3
C_s	Aqueous Solubility of Contaminant	M/L^3
ΔC_{im}	Difference in Concentration Between Chamber i and Adjacent Chambers m	M/L^3
D	Dispersion Coefficient	L^2/T
D_m	Molecular Diffusion Coefficient	L^2/T
d_m	Mean Grain Diameter of the Porous Medium	L
i	Chamber Index	-
J	Contaminant Mass Flux	L/T
k_f	Explicit Interphase Mass Transfer Coefficient	L/T
K_L	Lumped Interphase Mass Transfer Coefficient	1/T
L	Length of the Flow Cell (=0.1 m)	L
M	Number of Adjacent Chambers	-
n	Porosity of Porous Medium	-
Q	Flow Rate	L^3/T
Q_m	Flow Rate into/out of Chamber i to Adjacent Chambers	L^3/T
Re	Reynolds Number	-
S_c	Schmidt Number	-
S_h	Explicit Sherwood Number	-
S_h'	Lumped Sherwood Number	-

S_n	Initial NAPL Saturation	-
t	Time	T
v	Velocity	L/T
V_s	Volume of Chamber *i*	L^3
x	Length in the Direction of Flow	L
x_d	Travel Distance into the Region of Residual Organic Phase	L
α	Contact Angle	-
θ_n	Saturation of the Organic Phase	-
μ	Aqueous Phase Kinematic Viscosity	L^2/T
μ_w	Aqueous Phase Dynamic Viscosity	M/LT
ρ_w	Aqueous Phase Density	M/L^3

Abbreviation	**Explanation**
BTEX	Benzene-Toluene-Ethylbenzene-Xylene
CTC	Carbon Tetrachloride
DCB	1,2-Dichlorobenzene
DNAPL	Dense Non-Aqueous Phase Liquid
EtOH	Ethanol
GC-MS	Gas Chromatography-Mass Spectroscopy
IFT	Interfacial Tension
LNAPL	Light Non-Aqueous Phase Liquid
NAPL	Non-Aqueous Phase Liquid
PCB	Polychlorinated Biphenyl
PCE	Perchloroethylene
PRB	Permeable Reactive Barrier
TCE	Trichloroethylene
TCA	1,1,1-Trichloroethane

1. INTRODUCTION

Organic compounds such as hydrocarbons, halogenated organics and BTEX are widely used for energy or in various industry applications such as the synthesis of monomers, solvents, paints, coatings, degreasing and cleaning agents, heat-transfer fluids, pesticides, nutrients, pharmaceuticals, oil extractors, automobiles, foods, beverages, etc. (Pankow et al., 1996; Testa and Winegardner, 2000; Arpe, 2010; Grodowska and Parczewski, 2010; Nagasawa et al., 2013; Wypych, 2014). Considerable number of these compounds have toxic/carcinogenic effects on human health as well as other biota and long-lasting harmful effects to the environment upon direct or indirect contamination (Carter, 2011). Once these compounds leak into subsurface, the remediation of these contaminations becomes very difficult and costly (Stroo and Ward, 2010) because of the properties of these compounds such as low solubility, low degradability etc. These properties tend to keep these compounds trapped within the subsurface for many years. The persistencies of such anthropogenic organics are putting groundwater resources at high risk.

Because of their non-polar molecular structures, many organic contaminants have low aqueous solubilities (hydrophobic nature) and high interfacial tension. As a result, these contaminants tend to form a separate phase referred to as NAPLs – non-aqueous phase liquids as a particular class of the chemicals. When the contaminants are present in the form of NAPLs it is very challenging to remediate the soil and groundwater with high efficiency and to prevent further contamination of water resources. Two general classifications for NAPLs exist: LNAPLs for light non-aqueous phase liquids and DNAPLs for dense non-aqueous phase liquids. LNAPLs have lower densities than water and upon spillage, they tend to infiltrate downwards through the vadose zone and accumulate at or around the water table. On the other hand, DNAPLs have higher densities than water, which causes them to penetrate to deeper layers of soil following their release.

The leakage of NAPLs in the subsurface causes multi-dimensional complications as they either migrate through soil in bulk, forming entrapments (residual NAPLs) within pores or accumulate as pools upon encountering barriers. These barriers can be bedrock, the water table (for LNAPLs), low permeability layers with high clay content or other geographical structures depending on the nature of the NAPL present. Once entrapped in the subsurface, these compounds are gradually dissolved in the flowing groundwater. The resultant dissolved plume is then transported downgradient due to the interaction of different fate and transport mechanisms like dispersion, advection, sorption, etc.

The recognition of NAPLs, especially chlorinated solvents, as serious pollutants did not take place until the mid-1980s, when North American and European regulatory bodies classified them as hazardous; although their industrial usage continued unabated throughout the 20th and 21st centuries (Kueper et al., 2014b). Initial attempts for the remediation of groundwater have mostly considered the pump-and-treat technology, whereby extraction wells are placed downgradient of the NAPL zone and the extracted contaminated groundwater is treated ex-situ (at the ground surface). Numerous applications however, have shown that this technique is quite inefficient and more aggressive treatment technologies are needed, as NAPLs exhibit low dissolution and degradation rates (Grubb and Sitar, 1994; Childs et al., 2006). Over the past two to three decades, various technologies for the remediation of NAPLs from groundwater systems were developed such as bioremediation, sparging, venting, and vacuum-enhanced recovery, in situ thermal remediation, phytotechnologies, reactive walls and in-situ chemical agent flushing (Suthersan et al., 2017).

Among these methods, in-situ flushing with cosolvents has been shown to be a promising remediation option. It is a mass recovery operation, which introduces a single or multi-component agent (such as alcohols, humic substances, cyclodextrins) into the subsurface with definitive velocities, compositions and durations and creating a consistent material cycle via vertical wells. Cosolvent flushing accelerates NAPL remediation through two mechanisms. Firstly, cosolvents tend to increase the aqueous solubility of hydrocarbons for further acceleration of mass transfer into aqueous phase. Also, cosolvents at higher compositions drastically lower the interfacial tension leading to the mobilization of NAPLs to recover entrapped liquid mass. However, once NAPL is mobilized it can potentially be collected through extraction wells, but it can also lead to uncontrolled downward migration and further contamination of groundwater resources. Therefore, it is of crucial importance to choose the most suitable cosolvent agent(s) with the most effective methodology and to conduct laboratory testing and/or modeling studies prior to their application in the field to ensure that their use would not exasperate the contamination problem.

When NAPLs are present in the subsurface, interphase mass transfer, which is the rate of mass dissolution from the entrapped NAPL phase into the flowing aqueous phase is one of the most important processes controlling the rate and the persistence of the contamination. Interphase mass transfer plays a significant role in remedial applications that include surfactants and cosolvent flushing. Although a number of studies have examined the factors influencing interphase mass transfer from the NAPL phase to the aqueous phase, very few studies have investigated the problem when a surfactant or cosolvent is present in the aqueous solution. The focus of this study is therefore to examine the impact of cosolvents on interphase mass transfer and to develop mass transfer

expressions that can be used in future modeling studies and in remedial investigations when cosolvents are used as flushing agents.

2. BACKGROUND AND LITERATURE REVIEW

In this chapter, NAPLs and their properties are first reviewed. Subsequently, state-of-the-art in-situ remediation methods for NAPLs will be summarized. Related mass transfer expressions and correlations, which are the main focus of this study, will also be presented and discussed.

2.1. Non-aqueous Phase Liquids as Hazardous Chemicals

Dating back to the beginning of the last century, groundwater resources have become critically vulnerable to contamination by anthropogenic organic compounds (Perry et al., 1989; Llamas and Custodio, 2002). Various substances such as petroleum hydrocarbons, BTEX and chlorinated organic compounds in the form of non-aqueous phase liquids (NAPLs) pose a significant threat not only to freshwater sources but also to the environment. NAPLs have several release mechanisms including, but not limited to, accidental leakage from storage tanks, transport pipelines, unsanitary industrial landfills, refineries, bulk-product terminals, gas stations, airports, military bases, and domestic & industrial facilities of various scales (Pankow et al., 1996; USGS, 1998; U.S. Environmental Protection Agency, 2009; Molins et al., 2010; Tomlinson et al., 2014; European Environment Agency, 2015).

Having desirable chemical properties, stable nature and low production costs, chlorinated solvents started to been implemented in production cycles of various industries on a frequent and regular basis (Huling and Weaver, 1991; Geller and Hunt, 1993; Shevah and Waldman, 1995; Wang et al., 1996; U.S. Environmental Protection Agency, 2004; Birak and Miller, 2008; European Environment Agency, 2018). As noted previously, NAPLs are classified as two general groups namely LNAPLs (light non-aqueous phase liquids) and DNAPLs (dense non-aqueous phase liquids). Their fate as contaminants in the subsurface are heavily influenced by their relative densities to water. Figure 2.1 represents general migration pathways for both contaminant sub-classes upon entering the subsurface.

LNAPLs, once released to the unsaturated subsurface, tend to move downwards under the influence of gravity. Once they reach the saturated zone (water table), they spread horizontally, almost floating-like, along the water table. This liquid body forms dissolved phase (aqueous) plumes in groundwater body via dissolution (Illangasekare et al., 1995; Hu et al., 2010), as well as vapor plumes

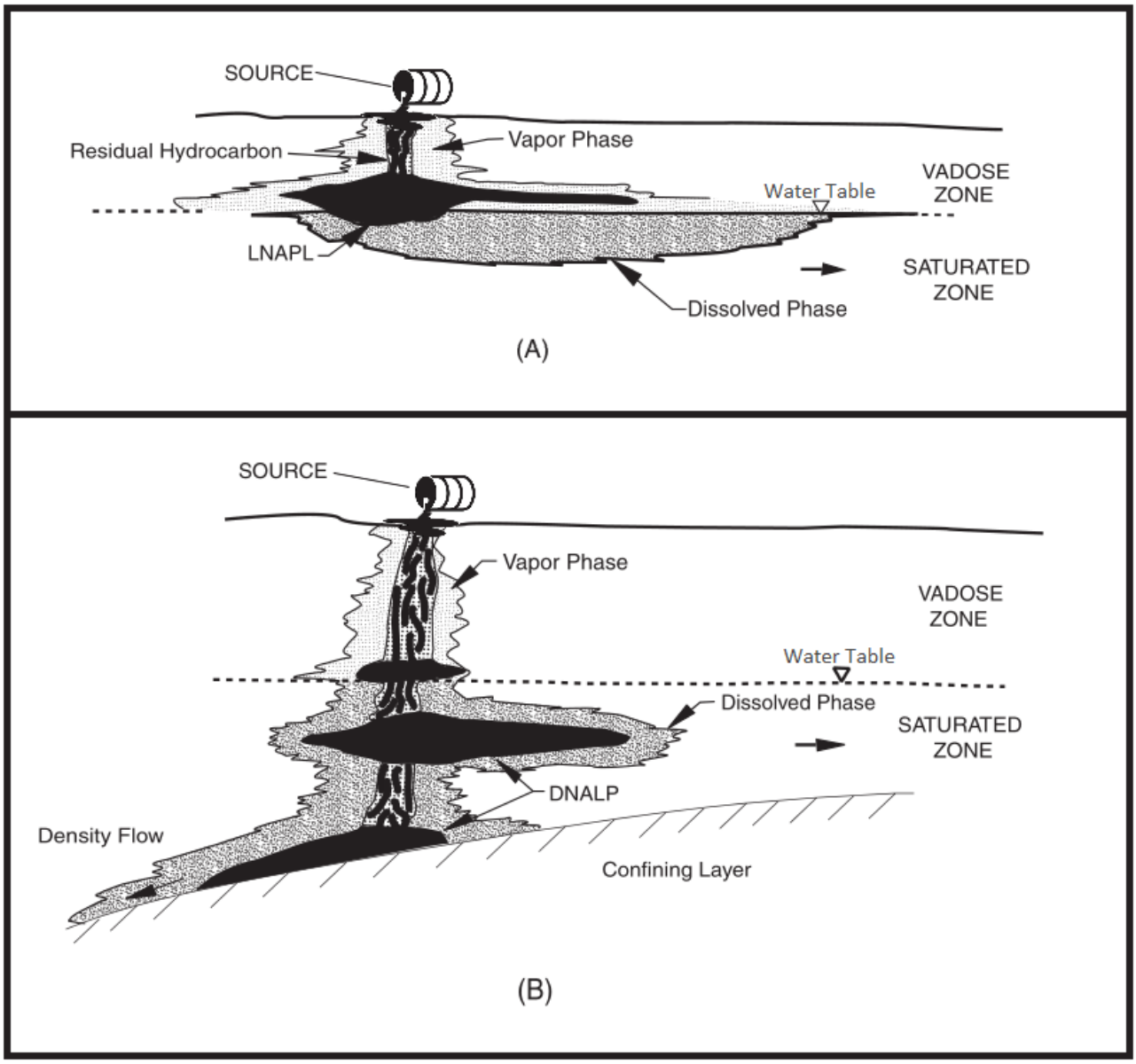

Figure 2.1. Illustration showing general distribution trends of LNAPLs (A) and DNAPLs (B) in the subsurface. Adapted from Figure 5.1 of (Testa and Winegardner, 2000).

in the vadose zone (USGS, 1998). Overall, LNAPLs do not migrate downwards over significant distances below the water table (Gerhard et al., 2014).

DNAPLs, on the contrary, tend to penetrate into deeper layers of the subsurface environment upon spillage (Figure 2.1). As stated in (U.S. Environmental Protection Agency, 2004) “DNAPLs generally migrate under the influence of gravity and stratigraphy rather than through groundwater flow”. Mostly chlorinated substances, as a result of gravitational forces, tend to migrate well below the water table up to the point where they reach an impermeable barrier like a clay layer or bedrock. DNAPLs migrate both vertically and horizontally in the subsurface, and tend to preserve equilibrium between organic phase, air, water and soil in accordance with the saturation level of the vadose zone

(Huling and Weaver, 1991; Testa and Winegardner, 2000). Residual DNAPL, in the form of randomly spread blobs and ganglia of organic liquid, is formed at the trailing end of a migrating DNAPL body. Residual DNAPL masses also occur in response to pore-scale hydrodynamic instabilities (Kueper et al., 2003). These residual/pooled DNAPL masses create further challenge to remediation processes as they are often poorly accessible by the flushing fluids (Akyol, 2018). Chlorinated solvents are a major group of DNAPLs and are recognized to pose a significant threat to the subsurface environment. They are considered as the most prevailing organic contaminants in groundwater considering their widespread usage in numerous industries such as manufacturing, degreasing and commercial dry cleaning (Mercer and Cohen, 1990; McCarty and Semprini, 1994). Widely used major DNAPLs are trichloroethene (TCE), tetrachloroethene (PCE), carbon tetrachloride (CTC), chloroform, 1,1,1-trichloroethane (TCA), 1,2-dichlorobenzene (DCB), dichloromethane, and polychlorinated biphenyls (PCBs) (Cohen and Mercer, 1993; Shevah and Waldman, 1995; Testa and Winegardner, 2000; U.S. Environmental Protection Agency, 2004; U.S. Environmental Protection Agency, 2018). Their presence in the subsurface leads to further chemical and biological transformation at various rates where a variety of other chlorinated aliphatic hydrocarbons may be produced (Rubin et al., 2013). Most chlorinated solvents are regarded as toxic and many are known to be carcinogenic (Gerstl et al., 1989; Berg et al., 1998; Rubin et al., 2013; Fu et al., 2014).

The majority of NAPLs have considerably low solubility tendencies in water, mostly in the ppm range (Huling and Weaver, 1991; Newell et al., 1995). The direct results of this sparse solubility includes slow and prolonged dissolution of NAPLs into the aqueous phase of aquifers, relocation in the direction of groundwater flow as well as forming a dissolved plume that possess potential threats due to its mobility (Eberhardt and Grathwohl, 2002; Luciano et al., 2010; Falta and Kueper, 2014). Also, most DNAPLs including chlorinated solvents have relatively high vapor pressure, enabling them to partition into the soil gas causing further migration to the vadose zone (Figure 2.2). NAPLs are thought to be able to persist in the subsurface for up to hundreds of years (Johnson and Pankow, 1992).

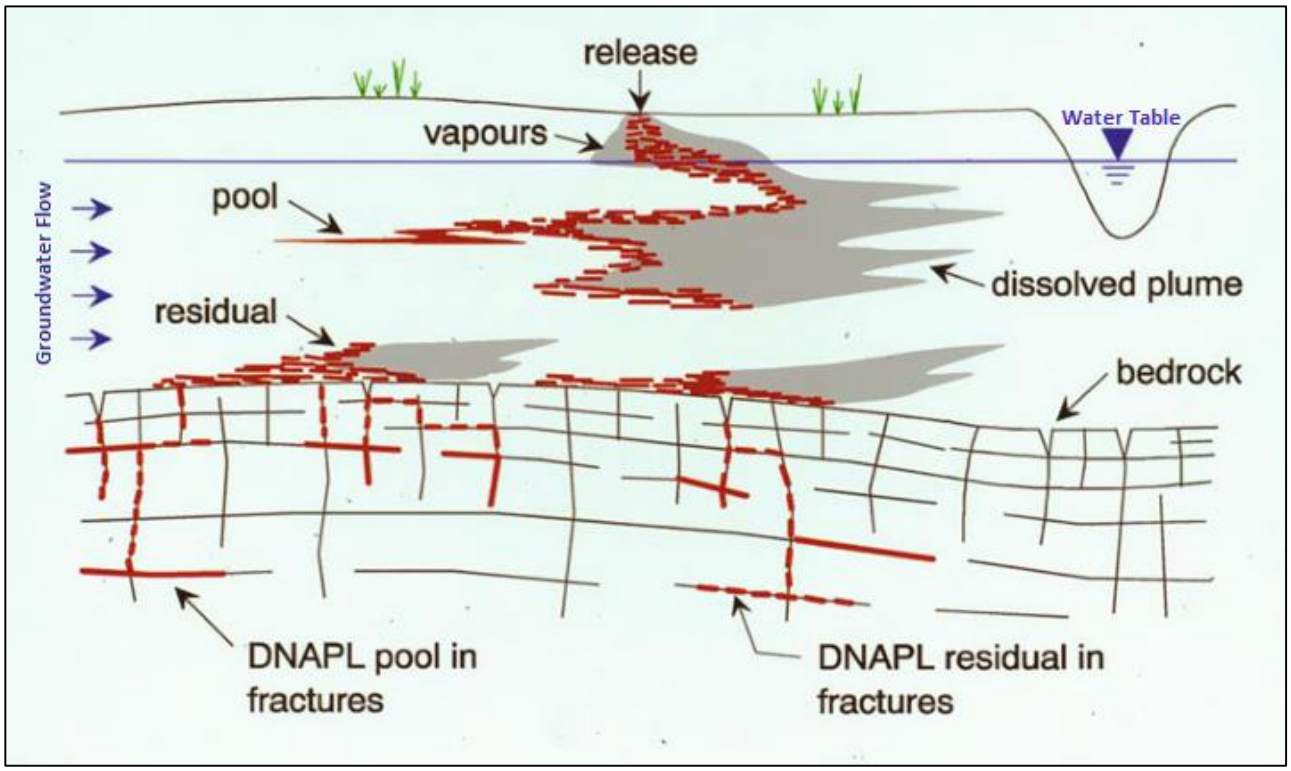

Figure 2.2. Contamination pathways of DNAPLs. Adapted from Figure 1.1(d) of (Kueper et al., 2014b).

2.1.1. Characteristic Properties of Non-aqueous Phase Liquids

It is important to understand the fundamental characteristics of NAPLs in order to cope with the challenges on the pathway of remediation, since the fate of contaminants is affected by them. Altering these characteristics can lead to improved remediation (Pennell et al., 1994; Lunn and Kueper, 1999a; Aydin-Sarikurt et al., 2016). The following parts of this sub-chapter will elaborate the physical and chemical characteristics of NAPLs.

2.1.1.1. Density. Density is a fundamental property of a NAPL as it determines whether it is an LNAPL or a DNAPL. LNAPLs have density values lower than water (997 kg/m^3), as low as up to 750 kg/m^3 (Lowe et al., 1999), whereas chlorinated DNAPLs have much higher densities, in general ranging between 1100 kg/m^3 and 1600 kg/m^3 (Kueper et al., 2003). In remediation methodologies, density of the NAPL should be taken into consideration as – especially for DNAPLs – density manipulation might cause unwanted consequences like further downward migration of blobs (Lunn and Kueper, 1997).

2.1.1.2. Solubility. Equilibrium aqueous concentration of a substance is defined as its solubility. Typically, aqueous solubility for NAPLs are less than 5000 mg/L (on the order of hundreds of mg/L)

for chlorinated solvents, less than 2000 mg/L for most gasoline derivatives, and less than 1.0 mg/L for PCBs (Loop, 2012). Having low aqueous solubility values means that introduced contaminants to the subsurface stay as separate phase liquid, accumulating and migrating as a distinct liquid mass pool or pools (Pankow et al., 1996). The dissolution rate of NAPLs not only depend on its solubility, but also the contact area between groundwater body and contaminant mass as well as the flow regime of groundwater (Park and Parker, 2005). Therefore, the aqueous concentration of NAPL is directly proportional to the interaction between water body and NAPL. Low aqueous solubility is a major limitation of the conventional pump-and-treat NAPL remediation methods as they enable recovery rates at low levels (Grubb and Sitar, 1994) but chemical agent flushing with cosolvents or surfactants help increasing solubility and reduce operation durations (Pennell et al., 2014).

2.1.1.3. Interfacial Tension. When two immiscible liquids are in contact, the surfaces of individual liquids are separately held together with a tensile force called interfacial tension (IFT). Solubility (and therefore, miscibility) of two liquids increases as IFT between them approach to zero. IFT is a function of pressure, temperature and composition of each liquid and is the main control parameter for mobility of DNAPLs (Mercer and Cohen, 1990). Cosolvent and surfactants can lead to a decrease of the IFT between the NAPL and the flushing solution. However, decreasing the IFT for remediation purposes must be conducted with caution and in a controlled way as IFT near zero might cause uncontrolled mobility of NAPL mass (Pennell et al., 1996; Gauthier and Kueper, 2006; Jin et al., 2007).

2.1.1.4. Viscosity. Viscosity is a measure of a liquid's resistance to flow. Viscosity has a great influence on the NAPL mobility as it affects the rate of movement of liquids within the subsurface. Distribution and mobility of DNAPLs are greatly affected by their viscosities (Kueper et al., 2014b) and as a general rule, liquids with lower viscosities have a greater tendency to penetrate downwards through porous media strata. The main factors affecting the viscosity of a liquid are temperature as well as content of the liquid (Davis 1997; González et al., 2007; Khattab et al., 2012).

2.1.1.5. Wettability. Wettability is a measure of a solid surface's affinity to a liquid system and is related to IFT. It is measured via the contact angle (α) which is formed at the liquid-vapor surface, or in the subsurface conditions liquid-liquid surface, contacts a solid surface. For contact angles less than 90°, the liquid is said to be a wetting fluid, where for α more than 90° is considered as a non-wetting fluid (see Figure 2.3).

NAPLs are mostly non-wetting fluids where upon penetration to the groundwater body, water is the wetting fluid of the system (Lowe et al., 1999; Kueper and Davies, 2014). Soils that are initially wet by water tend to remain so, whereas the same affinity is true for NAPL-wet soils (Testa and Winegardner, 2000). In the vadose zone, NAPLs is less wetting than water for most soils but are more wetting than air.

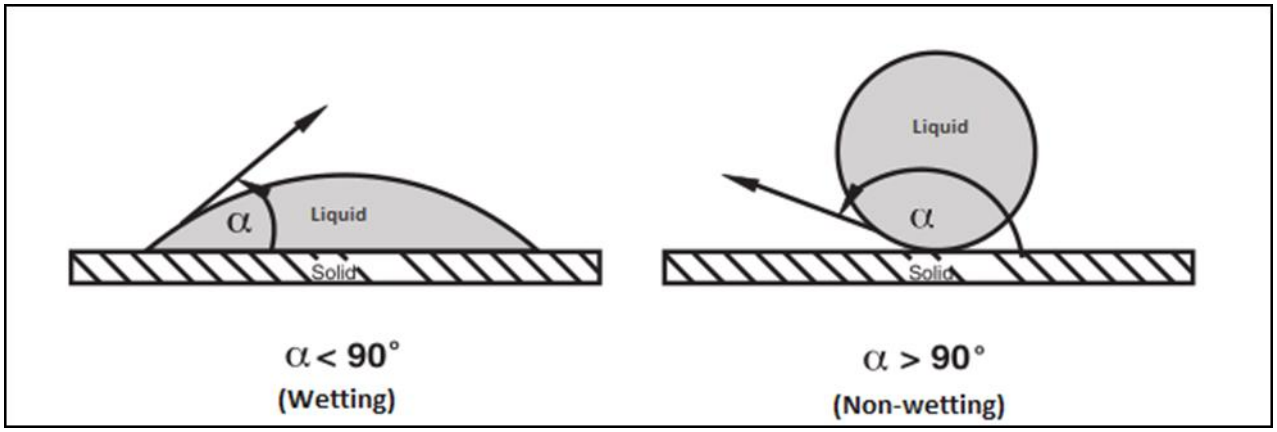

Figure 2.3. Contact angles of wetting and non-wetting liquids. Adapted from Figure 5.7 of (Testa and Winegardner, 2000)

2.1.1.6. Temperature. Although often not considered in remedial activities, temperature is an important external property of NAPL contaminated sites, and can be taken into consideration for enhanced recovery operations (Aydin et al., 2011) despite being out of the scope of this chapter. Its significance results from the fact that all NAPL properties such as solubility, interfacial tension, sorption, and volatility are temperature-dependent.

2.2. In-situ Remediation Methods for Sites Contaminated with Non-aqueous Phase Liquids

Attempts to recover hazardous organics have existed since the beginning of industrialization. The earliest methods to remediate NAPLs included the use of pitcher pumps, and was driven by economic concerns rather than environmental aspects until the labor value exceeded the product value (Testa and Winegardner, 2000). For a long time, inefficient pump-and-treat technologies have been used to recover the NAPLs via extraction from the subsurface and treating ex-situ. NAPLs' insufficient aqueous soluble properties resulted in the contaminant mass to be recovered at relatively low rates (Grubb and Sitar, 1994; U.S. Environmental Protection Agency, 1996; Lowe et al., 1999; Kavanaugh and Rao, 2003). Furthermore, long and costly operational durations and poor NAPL recovery rates caused it to be considered as a "failure" method for the job. Today pump-and-treat is recognized as a means to contain the spread of NAPLs to a particular region of the aquifer but not as

an effective remedial technology for NAPL mass recover. This recognition, including the persistence nature of chlorinated solvents, directed the research to be focused on in-situ remediation (Kueper et al., 2014b).

Several enhanced treatment technologies have since been introduced for improved remediation of NAPLs. In this section, a number of commonly used NAPL remediation methods are presented including chemical agent flushing which is of direct relevance to the present study. Customized methods for specific conditions are suggested to be applied for higher efficiency remediation work as no single remediation technology is universally adequate for all field conditions.

2.2.1. Bioremediation

Bioremediation is a class of remediation methods, which utilizes microbial catabolic abilities in order to degrade, transform or immobilize organics; notably petroleum organics and (Adams et al., 2015) halogenated solvents (Chaudhry and Chapalamadugu, 1991; Shukla et al., 2014; Guerrero-Barajas et al., 2014) under both aerobic and anaerobic conditions. Bioremediation has become more and more prominent starting from the 1980s due to its economic feasibility, high efficiency and eco-friendly nature (Russell et al., 1992; Bradley, 2003; Atlas and Philp, 2005; Schaefer et al., 2017; Sheu et al., 2018), thanks to the recent advances on reductive and oxidative operations. Several case studies by Stroo and colleagues (Stroo et al., 2014) indicate that while in-situ bioremediation is a promising and effective technology; proper long term monitoring and site evaluation is needed, and that long-term treatment impacts are not fully known; hence, setting realistic objectives are of great importance.

2.2.2. Sparging, Venting, and Vacuum-Enhanced Recovery

This set of NAPL recovery methods include venting of contaminated subsurface areas with gas of various content (mostly air for economic reasons). One form of this technology is soil vapor extraction, where volatilization of contaminants is enhanced in vadose zone via creation of an artificial airflow either by vertical extraction wells or horizontal extraction pipes (Suthersan et al., 2017). This method provides convenient remediation of volatile organic compounds, petroleum products and sorbed contaminants (Anwar et al., 2003). Another is air sparging, which aims at the recovery of contaminants in the saturated zones by injecting air below the NAPL zone to promote mass transfer between the liquid phase(s) and the mobile vapor phase. The injected air transfers within artificial continuous air channels (Johnson et al., 1993; Wei et al., 1993) while dispose the contaminants through extraction wells. Air sparging is effective for the remediating BTEX,

chlorinated solvents and various petroleum products (U.S. Environmental Protection Agency, 1995b; Chao et al., 2018; Lee et al., 2019).

2.2.3. In-situ Chemical Treatment

NAPLs entrapped in the subsurface can be treated in-situ to be either oxidized or reduced. Frequently used oxidizing agents are ozone, hydrogen peroxide, potassium permanganate, activated sodium persulfate (Siegrist et al., 2011) and reducing agents are electron donating species of iron, sulphur and natural organic matter (Tratnyek et al., 2014). The processes involve electron transfer between contaminants and treatment agent. Contaminant-based selection has to be made and the stabilities of agents must be taken into consideration. Treating chlorinated solvents with oxidizers in the subsurface is becoming more and more prominent in the recent years (The Interstate Technology and Regulatory Council (ITRC), 2005; Brusseau et al., 2011; Ko et al., 2012; Akyol and Yolcubal, 2013; Akyol, 2018). However, it is important to note that chemical oxidation occurs in the aqueous phase and that low NAPL dissolution rates is often the limiting process. In recent years the use of enhanced dissolution agents along with in-situ chemical treatment is being considered to overcome this limitation (Besha et al., 2018).

2.2.4. Reactive Walls

The use of reactive walls, or permeable reactive barriers (PRBs), is another promising remediation technology for remediating contaminant plumes in the subsurface as an alternative to conventional pump-and-treat approach. It involves placement of a porous reactive structure in the path of contaminant phases, and having them passively undergo chemical, physical or biological alterations while in contact with the reactive barrier (Rivett, 2006). A vertical wall structure is installed for transformation of contaminants in dissolved plume in groundwater (Boshoff and Bone, 2005). For the vapor plume in unsaturated vadose zone, horizontal setups have been proposed (Mahmoodlu et al., 2015; Verginelli et al., 2017). The ease and depths of installations, variety of reactive substances, sustaining long term effectiveness and efficient mass removal rates (up to 90 %) makes this method feasible for various chlorinated DNAPLs and enabled the technology to further develop (O'Hannesin and Gillham, 1998; Rivett, 2006; Obiri-Nyarko et al., 2014; Wilkin et al., 2014; Faisal et al., 2018).

2.2.5. Chemical Agent Flushing

This remediation method, is a promising recovery technique in which entrapped NAPLs are flushed with reagents in the subsurface. As additives are introduced and recovery times shortened, chemical agent flushing differs from conventional and impracticable pump-and-treat methods with promising enhanced recovery rates (U.S. Environmental Protection Agency, 1995a). Surfactant and cosolvent flushing as a remediation method gained attention in the late 80s and early 90s (Nkedi-Kizza et al., 1985; Brusseau et al., 1991) as a result of lack of convenient and effective soil and groundwater treatment (U.S. Environmental Protection Agency, 1991). The method is essentially consists of introducing a mixture of active ingredients, to be forced to circulate between injection and extraction wells to enhance the recovery of contaminants. The remnant mixture of agents and contaminants are extracted and further treated ex-situ. A schematic representation of the basic principle of chemical agent flushing is presented in Figure 2.4. Various compounds can be used as reagent, while cosolvents (alcohols) and surfactants are among the most frequently applied reagents (Imhoff et al., 1995; Mulligan et al., 2001; Zhong et al., 2003; Paria, 2008; Pennell et al., 2014; Agaoglu et al., 2015; Akyol, 2018; Akyol and Turkkan, 2018; Yang and Yanga, 2018).

The usage of surfactants/cosolvents relies on increasing the solubility of NAPLs and reducing their interfacial tensions so that enhanced mobilization can be achieved. For this purpose, single-component reagents can be used as well as multi-component mixtures (various combinations of alcohols and/or surfactants) to maximize the success of a recovery operation. Careful analysis and characterization of sites and reagents should be undertaken in order to achieve successful removal of NAPLs as studies show that marginal mass recovery rates are achievable but their costs-efficiencies were being suppressed by alternative methods (Mulligan et al., 2001; McDade et al., 2005; McGuire et al., 2006).

Surfactant enhanced flushing aims to increase the solubilization of NAPL as well as to reduce the interfacial tension so that the entrapped mass can dissolve into the mobile phase or directly mobilize to extraction wells for collection (Lowe et al., 1999). Surfactant agents present duality in their chemical structures in terms of their affinities to aqueous dissolution; their molecules have both hydrophilic and hydrophobic parts allowing them to exhibit amphiphilic properties. Toxicity should also be evaluated for the surfactant agents to be used (West and Harwell, 1992; Mulligan et al., 2001). Surfactant flushing has been used frequently for the recovery and remediation of both LNAPLs and DNAPLs (Mulligan et al., 2001; Rathfelder et al., 2003; Akyol, 2018).

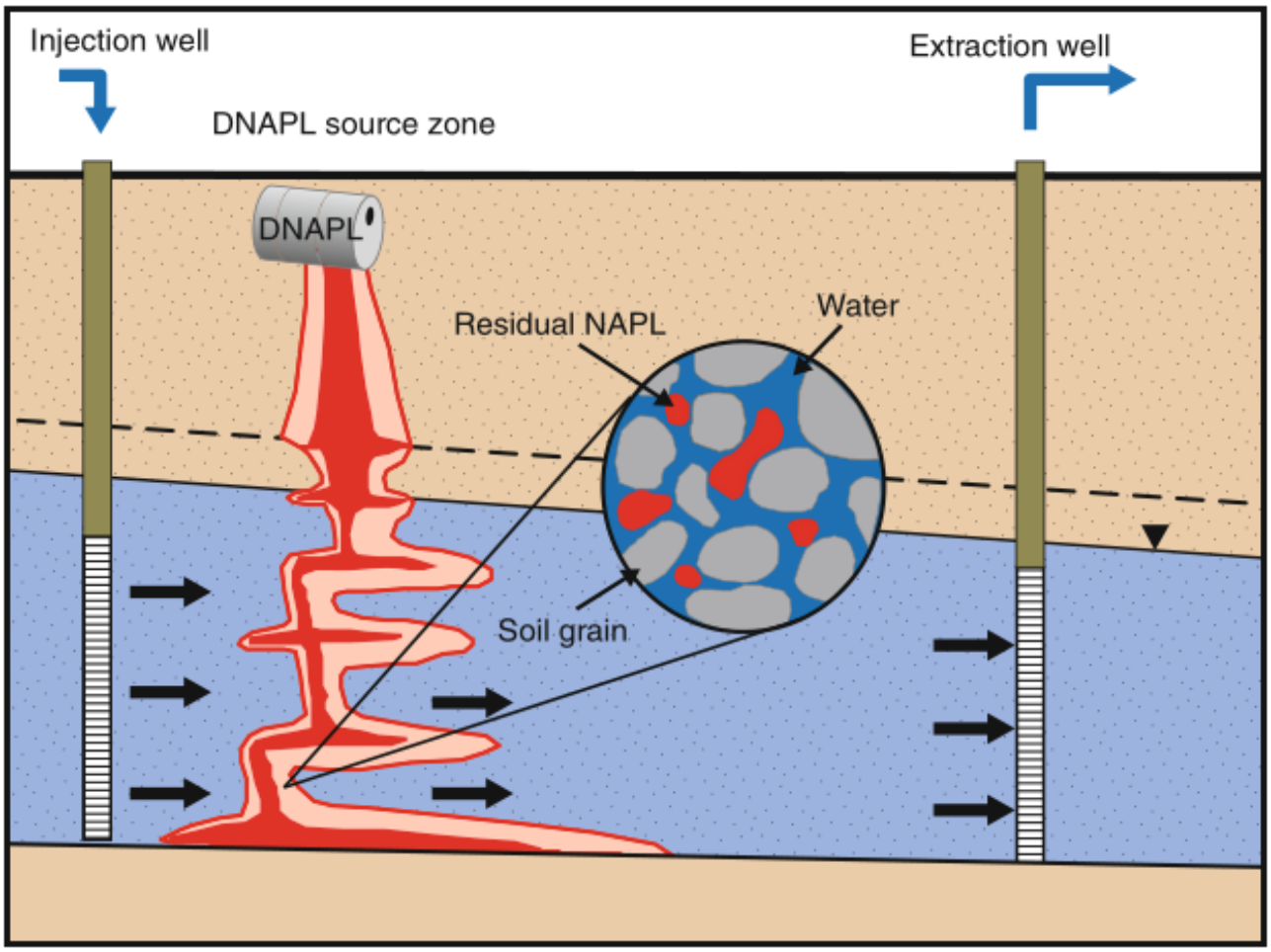

Figure 2.4. Conceptual Schema of an in-situ flushing system (Pennell et al., 2014).

Many researchers have suggested using cosolvents as flushing agents as the method provides convenient, cost-efficient, relatively fast and effective remediation of subsurface environments including soil and groundwater (Lunn and Kueper, 1999a; Jawitz et al., 2000; Brooks et al., 2004; Gauthier and Kueper, 2006; Agaoglu et al., 2012; Pennell et al., 2014; Agaoglu et al., 2015). Various agents can be used as cosolvents like alcohols, humic acid and cyclodextrins while earlier studies investigating cosolvent effects mainly focused on low molecular weight alcohols due to their miscibility properties both in water and various other synthetic organics (Morris et al., 1988; Brusseau et al., 1991). A pioneering alcohol flushing operation of a site contaminated mixture of jet fuel and waste solvents was reported with successful recovery rates (Rao et al., 1997) and another with a spill of perchloroethylene (PCE) followed by a successful recovery (Jawitz et al., 2000), both mainly using ethanol as the primary cosolvent ingredient. Post-recovery remnant alcohols (ethanol) reportedly serve as electron donors which contributes further to the elimination of remaining DNAPLs via reductive dehalogenation (McCarty P. L., 2010). Ethanol is a frequently used cosolvent agent due to its abundance as an industrial solvent, low cost, non-toxic nature and effectiveness (Pennell et al., 2014).

In-situ cosolvent flushing can be used for removal of NAPLs via mobilization of bulk entrapped masses as well as enhancing solubility to promote continuous mass transfer. While solubilization is amplified with the help of cosolvent agents, the possibility of uncontrolled downward migration of entrapped DNAPL mass should be regarded (Lunn and Kueper, 1999b; Van Valkenburg and Annable, 2002). Therefore, keeping the density equilibrium balanced and well-adjusted is necessary for preventing any unwanted mobilization.

Many studies showed that the recovery efficiency is dependent on the depth of entrapped contaminant mass. Since most chlorinated solvents are DNPALs and thus moving downgradient until reaching impermeable layers, flushing deeply penetrated contaminants remains as a problem. Hydrodynamic heterogeneity is also arising as a challenging problem in in-situ cosolvent flushing as liquids follow the least resisting paths through their movement in porous media, potentially bypassing DNAPL (Brooks and Corey, 1966; Pennell et al., 1993; Lunn and Kueper, 1999a; Christ et al., 2005; Childs et al., 2006; Mateas et al., 2017) therefore complete recovery of NAPLs is almost never possible.

2.3. Interphase Mass Transfer

Interphase mass transfer can be defined as mobility of material from one phase to another across a phase-separating interface; mass transfer such as dissolution and volatilization is the responsible process that causes the introduction and spread of contaminant into surface, subsurface environment and the atmosphere. A simplified schema representing the interphase mass transfer of a NAPL is shown in Figure 2.5. In recent years, numerous studies have focused on the interphase mass transfer in relation to NAPL contamination and remediation (Miller et al., 1998; Yoon et al., 2002; Cho et al., 2005; Willingham et al., 2010; Liu et al., 2014; Agaoglu et al., 2015; Aydin-Sarikurt et al., 2016; Agaoglu et al., 2016; Aydin-Sarikurt et al., 2017; Shafieiyoun and Thomson, 2018; Yang et al., 2018; Balseiro-Romero et al., 2018). Initial attempts to model interphase mass transfer have assumed that equilibrium conditions between the NAPL and aqueous phase exists. However, it became evident that the dissolution process is a slow process and that a rate-limiting expression is needed for realistic representation of interphase mass transfer (Aydin-Sarikurt et al., 2016).

Much of the published works have defined interphase mass transfer expressions via relations that were empirically generated from experimental data (Miller et al., 1990; Powers et al., 1992). One significant downside of these expressions is that they are mostly valid for the experimental conditions existing during their generation. This has prevented the accurate modeling of the interphase mass

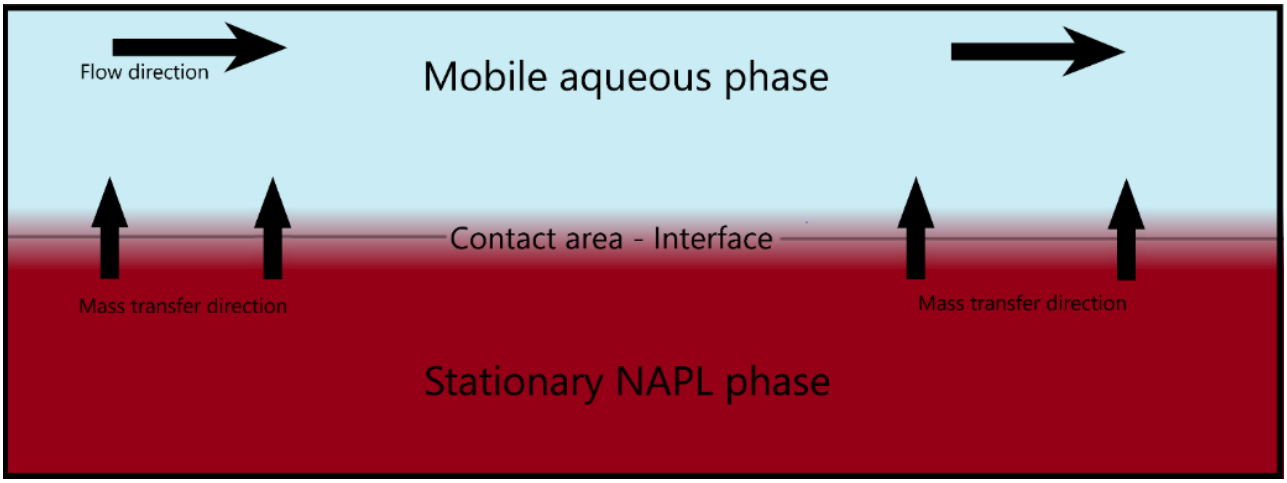

Figure 2.5. Interphase mass transfer of NAPLs.

transfer at the field scale. The factor most responsible for this limitation is the heterogeneity of the subsurface environments which leads to complex NAPL distribution and flow fields which in turn leads to the bypassing of NAPL mass and reduced interphase mass transfer (Kokkinaki et al., 2013; Agaoglu et al., 2015).

Generally, transfer of mass between a stationary NAPL mass and a flowing aqueous phase is defined with the following expression (Miller et al., 1990; Powers et al., 1994a):

$$\frac{\partial M}{\partial t} = k_f \times A \times (C_s - C) \tag{2.1}$$

where

$\frac{\partial M}{\partial t}$: rate of mass transfer from the NAPL to aqueous phase [M/T]

k_f: interphase mass transfer coefficient [L/T]

A: area of interface, separating the two immiscible phases [L^2]

C_s: aqueous solubility of contaminant [M/L^3]

C: the composition of contaminant in the aqueous medium [M/L^3]

Equation 2.1 can also be expressed in terms of contaminant mass flux to aqueous phase:

$$J = k_f \times a \times (C_s - C) \tag{2.2}$$

where

J: the mass flux due to NAPL dissolution per unit volume of porous media [M/L^3-T]

a: contact area per unit volume of porous media $\left(a = \frac{A}{V}\right)$ [L^2/L^3]

Sherwood number is commonly used for relating the interphase mass transfer coefficients to flow conditions and porous media properties. The Sherwood number is a dimensionless parameter that is a measure of interphase mass transfer to the rate of diffusive mass transport. Sherwood number is expressed as:

$$Sh = \frac{k_f \times d_m}{D_m} \tag{2.3}$$

where

d_m: mean grain diameter of porous media [L]

D_m: molecular diffusion coefficient [L^2/T]

In the area of studying and modeling interphase mass transfer, precise determination of interfacial area, *"a"*, between the phases is a difficult, if not impossible, task (Nambi and Powers, 2000). NAPL distribution systems in the subsurface is a result of various forces (capillary, density and hydrodynamic forces) that are function of both soil and fluid properties, making it nearly impossible to accurately observe and calculate the interfacial area. Up to the present, there are only three studies that have developed Sherwood expressions for idealized NAPL placements (Pfannkuch, 1984; Powers et al., 1994b; Aydin-Sarikurt et al., 2017). The lack of such studies stems from the difficulty of defining the interfacial area between the aqueous and NAPL phases.

To overcome this challenge, many researchers have proposed incorporating the interfacial area into the mass transfer coefficient (Imhoff et al., 1994):

$$K_L = k_f \times a = k_f \times \frac{A}{V} \tag{2.4}$$

Where K_L is referred to as the lumped interphase transfer coefficient. This lumped coefficient can thus be integrated into related mass transfer expressions in (Equation 2.2):

$$J = K_L \times (C_s - C) \tag{2.5}$$

This "lumped" approach to interphase mass transfer coefficient can also be applied to Sherwood number, enabling the expression of "lumped Sherwood number", or "modified Sherwood number" (*Sh'*):

$$Sh' = \frac{K_L \times {d_m}^2}{D_m} \tag{2.6}$$

A growing number of researchers have investigated the phase and medium properties using lumped mass transfer coefficient and lumped Sherwood number (Miller et al., 1990; Powers et al., 1992; Imhoff et al., 1994; Goldstein and Cho, 1995; Saba and Illangasekare, 2000; Chu et al., 2007; Agaoglu et al., 2015). Fluid properties that have been considered in these studies include Péclet number (*Pe*), NAPL saturation, mean grain diameter of the medium, Reynolds number (*Re*), and Schmidt number (*Sc)*. Péclet number is a dimensionless number that relates the advective flux to the diffusive flux:

$$Pe = \frac{v \times d_m}{D_m} \tag{2.7}$$

Where *v* is velocity of the mobile phase [L/T]. Péclet number is proportional to the effectiveness of advection and inversely proportional to the effectiveness of diffusion in mass transfer phenomena.

Schmidt number is a dimensionless number that represents the ratio of viscous diffusion to mass diffusion. It is the ratio of momentum diffusivity (kinematic viscosity) to mass diffusivity and is expressed as:

$$Sc = \frac{\mu_w}{\rho_w \times D_m} \tag{2.8}$$

where

μ_w: dynamic viscosity of the aqueous phase in Pa×s [M/L-T]

ρ_w: density of the aqueous phase in kg/m^3 [M/L^3]

Reynolds number is a dimensionless number that represents the ratio of inertial forces to viscous forces within a fluid, and expressed as:

$$Re = \frac{v \times d_m}{\mu} \tag{2.9}$$

where μ is the aqueous phase kinetmatic viscosity [L^2/T].

Table 2.1 shows a set of selected interphase mass transfer correlations in the form of lumped Sherwood numbers from the literature. Using the modified Sherwood correlations and working with lumped interphase mass transfer coefficients can be a desirable approach, particularly where precise estimation of contact area (interface) between phases is unavailable. Yet, lumping the interfacial area term reduces the validity and applicability of results and correlations to conditions similar to those present during the experiments. Studies show that predictions made while developing such correlations may vary widely from each other and from real data observed in the field. This is mostly credited to the complex distribution of NAPLs, the hydrodynamics of the systems, and heterogeneity of soil structures (Powers et al., 1994b; Maji and Sudicky, 2008; Roudet et al., 2017). Such restrictions inevitably limit incorporation of these expressions to field conditions.

Table 2.1. Lumped Sherwood correlation specimens from the literature. Adapted from Table 2.1 of (Aydin-Sarikurt, 2018) and Table 1 of (Kokkinaki et al., 2013).

***Sh'* Correlations**	**Valid conditions**	**Reference**
$12\ Re^{0.75}{\theta_n}^{0.6}Sc^{0.5}$	Steady-state flow, glass bead column experiments for $0.016 \leq \theta_n \leq 0.07$ $0.0015 \leq Re \leq 0.1$	(Miller et al., 1990)
$150\ {\theta_n}^{0.79}Re^{0.87}$ $340\ {\theta_n}^{0.87}Re^{0.71}\left(\frac{x_d}{d_m}\right)^{-0.31}$	Steady-state flow, sand column $0 \leq \theta_n \leq 0.04$ $0.0025 \leq Re \leq 0.021$ $1.4 \leq \frac{x_d}{d_m} \leq 180$	(Imhoff et al., 1995)
$11.34\ Sc^{0.33}\ Re^{0.2767}\ \left(\frac{d_m\,\theta_n}{\tau\,L}\right)^{1.037}$	2D cell experiments for NAPL pools $0.0015 < Re < 0.1$ $\tau = 2$, L = dx	(Saba and Illangasekare, 2000)
$37.15\ Re^{0.61}S_n^{1.24}$	Uniformly distributed NAPL ganglia $0.01 < S_n < 0.35$; $0.0048 < \theta_n < 0.168$ $0.018 < Re < 0.134$	(Nambi and Powers, 2003)

Re is the Reynolds number, θ_n is saturation of the organic phase, S_c is the Schmidt number, x_d is the travel distance into the region of residual organic phase, and d_m is the mean grain diameter; S_n is the initial NAPL saturation.

While there are numerous Sherwood expressions that have been developed for the lumped mass transfer coefficient, Sherwood correlations for the non-lumped mass transfer are quite few. In fact there are only three such relations that can be found in the literature: the work presented by Pfannkuch (Pfannkuch H. O., 1984), Powers and colleagues (Powers et al., 1994a) and Aydın-Sarıkurt and

colleagues (Aydin-Sarikurt et al., 2017). The lack of Sherwood correlations for the non-lumped mass transfer stems from the difficulty of accurately estimating the interfacial area. The abovementioned studies were for well-defined conditions where the interfacial area between the NAPL and aqueous phases can be estimated. The Sherwood correlation developed by Pfannkuch, which relied on the experimental data from Bernhard Hoffmann's work on 1969 (Hoffmann, 1969), relates to the dissolution of pooled NAPL into the aqueous phase. The correlation by Powers et al. (1994) on the other hand is for the dissolution of spheres embedded in porous media into the aqueous phase. The study by Aydın-Sarıkurt and colleagues (Aydin-Sarikurt et al., 2017) is similar in experimental setup to that of Pfannkuch but covering a wider range of velocities. Moreover, they used a two-dimensional transport model for the interpretation of the results yielding more robust Sherwood number expressions. All of these correlations are for NAPL dissolution into pure aqueous phase with no cosolvents present in the flushing solution.

In most experimental work for the determination of the interphase mass transfer coefficients, pure aqueous phase was used with the absence of any cosolvent agents. It has generally been assumed by researchers and modelers that the same mass transfer coefficient of the aqueous phase is also valid when cosolvent is present. However, very limited number of studies have rigorously examined this assumption.

3. PURPOSE

As discussed in the previous chapters, contamination of soil and groundwater bodies with NAPLs is still a challenging problem of the industrialized world. The focus of this thesis is on the estimation and development of interphase mass transfer expressions for multiphase systems in porous media in the presence of cosolvents, which is lacking in the academic literature. Specifically, the purpose of this study is to:

I. Conduct dissolution experiments for different flushing solution compositions to assess the impact of the presence of cosolvents, as well as the velocity of water flow, on the interphase mass transfer.
II. Develop interphase mass transfer expressions for multiphase mixtures in a porous media when cosolvents are present.
III. Use modeling tools (1D analytic solution and 2D pore network model, written in Fortran language) to investigate and generate interphase mass transfer expressions, referred to as Sherwood number correlations, for comparison and reliability test for experimental and theoretical results.

The goals will be achieved through flow cell experiments for a range of controlled input parameters including composition of the flushing solution, grain diameter of the porous media and velocity of the flushing solutions. The experimental data will be interpreted using two tools: a 1D analytic solution and a 2D contaminant transport model. The results of the two models will be used to investigate the effect of cosolvents on mass transfer phenomena. The NAPL used in the dissolution experiments is 1,2-dichlorobenzene (DCB) due to its low evaporation rate and low aqueous solubility properties. DCB is a chlorinated benzene ring, a DNAPL widely used in the chemical and agrochemical industry as an industrial solvent, washing fluid and softening agent. The cosolvent selected for this purpose is ethanol. The flushing solutions consisted of various compositions of ethanol with water to investigate the effect of cosolvents in the remediation process. The outcomes of this study are expected to provide a basis or support future laboratory-scale, field-scale and modeling works aiming to evaluate the application of cosolvents for the enhanced remediation of groundwater contaminated with NAPLs.

4. MATERIALS AND METHODS

In this chapter, the experimental methodology and modeling used to interpret the data are presented. The first section of this chapter describes the batch experiments conducted to measure the solubility values of various DCB-water-cosolvent (ethanol) systems and the calibration curve for concentration analysis, respectively. In the following section, the flow cell experiments (in which the dissolution of DCB took place) are described in detail. Following these procedures, the analytical relations and parameters between mass transfer coefficients among multiphase systems are further evaluated. Finally, the modeling work of the study is elaborated.

4.1. Batch Experiments

Batch tests have been performed in order to obtain;

I. Calibration curve of DCB-water systems for a specific dynamic range and
II. The solubility values of DCB in different water-ethanol systems.

In all operations that required the usage of pure DCB, a dyed DCB stock (0.01 % Sudan IV by weight, purchased from Sigma Aldrich) was prepared prior for better visualizing the injected liquid DCB.

The obtained results were also substituted to the relevant parameters at the modeling work of this study, which is further described at Section 4.4.

4.1.1. Calibration Curve

For a reliable measurement of DCB concentrations in samples, a calibration curve was generated with a dynamic range between 1 – 30 ppm. A stock solution of 30 ppm DCB was first prepared in bulk, then carefully diluted to 25 ppm, 20 ppm, 15 ppm, 10 ppm, 5 ppm, 2 ppm and 1 ppm respectively; later measured using a UV-VIS spectrophotometer (Shimadzu UV-160A UV-Visible Recording Spectrophotometer) at the wavelength of 220 nm (Aydin-Sarikurt, 2018). The absorbance values were corrected with a blank sample (deionized water) to eliminate potential background signals.

Further analysis with DCB throughout the study was carried out in accordance with the calibration curve generated, adhering to the corresponding dynamic range.

4.1.2. Solubility Measurements

Solubility tests were conducted in order to measure the solubility of DCB in various water-ethanol compositions. DCB solubility in deionized water was also measured for comparison with the literature value of 155.82 ppm (Banerjee et al., 1980). The ethanol contents considered are: 0 %, 10 %, 20 %, 30 % and 40 % of ethanol-water solutions by volume. Higher ethanol contents were not considered as they may cause significant suppression of the IFT. This in turn can lead to DNAPL mobilization which would complicate the interpretation of the experimental data. Deionized water and ethanol (purchased from Merck) for synthesis was used for eliminating contaminants at the analysis.

40 mL vials were used to prepare the mixture systems, of which 8 mL of pure DCB (providing excess amount of solute) and 30 mL of corresponding ethanol-water solution to the desired percentage. 2 mL of headspace was allowed for the ease of mix to the components of the system. After some rigorous shaking by hand, the vials were sealed and anchored in an IKA “KS130 Control” model orbital shaker, adjusted to 360 rpm shaking in room temperature. After 48 hours of constant shaking, with ambient temperature adjusted to 22°C, the vials were centrifuged to 3500 rpm for 30 minutes to separate the organic and aqueous phase in the emulsions. The aqueous phase of the samples was then diluted and analyzed using a UV-VIS spectrophotometer (Shimadzu UV-160A UV-Visible Recording Spectrophotometer) at the wavelength of 220 nm. The absorbance values were corrected with a blank sample (deionized water) to eliminate potential background signals.

4.2. Flow Cell Experiments

For evaluating the impact of flushing solution content on the interphase mass transfer, flow cell experiments were conducted. The flow cell was designed with the length 10 cm, height 4 cm and width 4 cm. The main skeleton of the tank is stainless steel, integrated with a glass front which allows visualization of DCB injection and placement. The tank has three main ports; inlet and outlet ports for the flow of deionized water and collection of contaminated water and a tertiary port at the bottom center of the flow cell, sealed with a silicon rubber for inserting DCB with the help of a syringe needle (Figure 4.1).

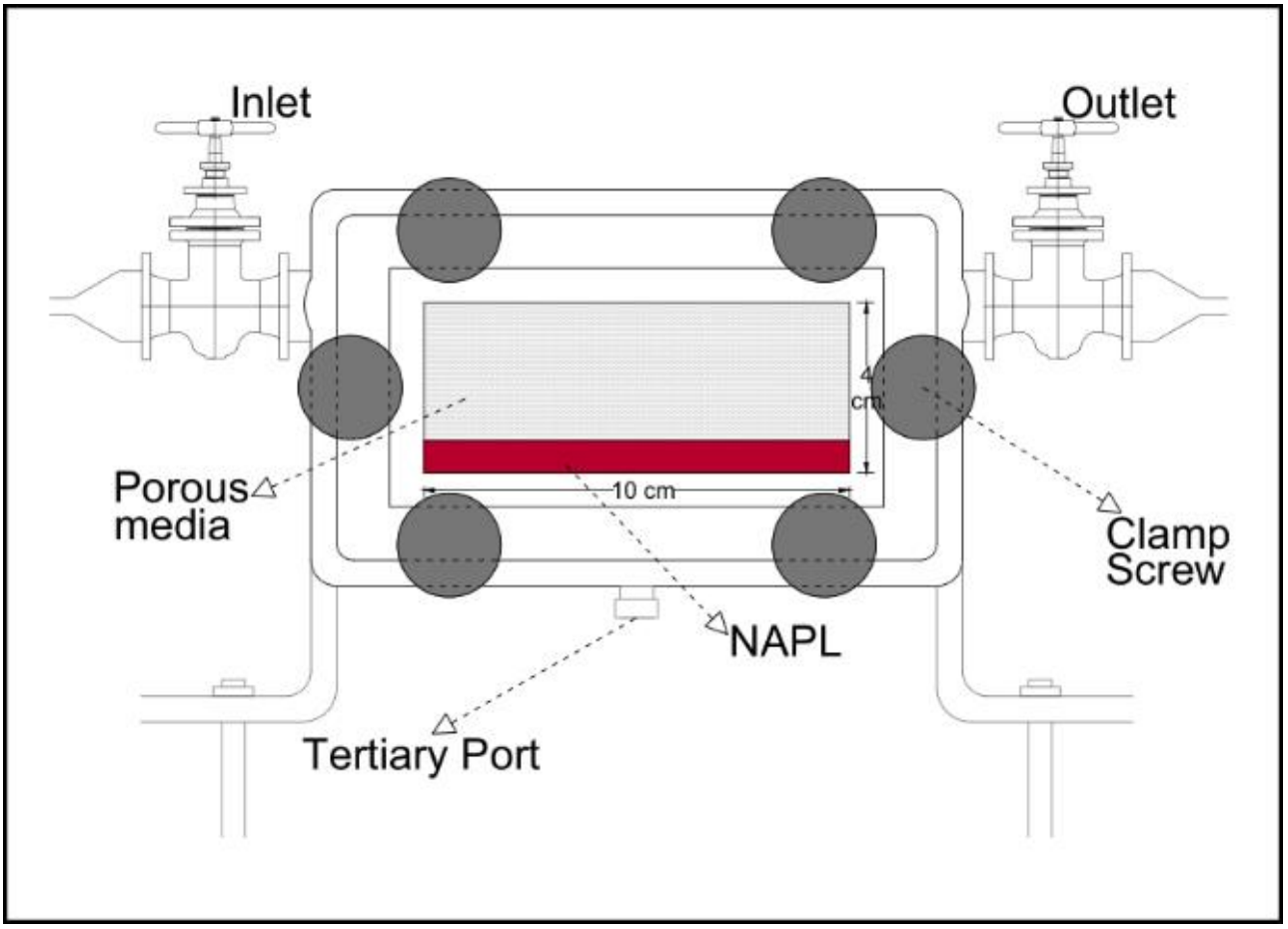

Figure 4.1. A sketch of the tank/flow cell.

Two types of porous media were used throughout the experimental work, namely sand and glass beads. Mean grain diameter were 1 mm for glass beads and 0.2 mm for sand, while the porosity 0.34 for glass beads and 0.36 for sand, respectively (Aydin-Sarikurt et al., 2017).

The main challenge for preparing the desired experimental conditions was the entrapment of DCB to the lower end of the flow cell, so that mobile aqueous phase flow horizontally over the DCB emplaced in the lower section of the tank. That contact area was aimed to be prepared as evenly and orderly as possible for the ease of interpretation of the results and the accurate estimation of the mass transfer coefficient (in other words, knowing the exact contact area between the two phases which requires having an undisrupted, plain surface area). For the first set of experiments, the tank was filled with glass beads. Then the glass front was sealed and DCB was injected from the tertiary port very slowly (11 mL of DCB was introduced over a period of one hour, with the help of a thin glass syringe and needle). The injection flow rate was kept low to prevent bubble formation and to better saturate the media. Further suggestions to prevent bubble formation can be found in (Lewis and Sjöstrom, 2010). Deionized water was then introduced to saturate the media completely, again very slowly for the same reason, from the inlet and outlet ports sequentially. With the pump adjusted to 0.7 mL/min,

deionized water was introduced alternatingly from each of the two ports over 2 minute intervals. The setup was then kept waiting for 12 hours for the NAPL/water to settle across the entire bottom of the flow cell.

For the silica sand experiments a modified method was applied for the entrapment of the NAPL because of the higher capillarity of the sand due to its smaller size compared to that of the glass beads (fact of 5 or smaller). The entrapment method described in the study of Phenrat and colleagues (Phenrat et al., 2011) was used in order to trap the DNAPL in desired pool form. To start, a layer of glass beads with height of 0.6 cm was placed at the bottom of the tank. Then, slightly wetted sand was packed firmly till the tank was completely filled. A uniform packing of sand was aimed to be achieved. The porosity values from the tracer tests of the study by Aydin-Sarikurt and colleagues are used (Aydin-Sarikurt et al., 2017) as well as the sand packing. The screws were then tightened and the whole tank was saturated with deionized water with slow flow rates. Then the liquid DCB was injected from the tertiary port of the tank (5.9 mL of DCB was introduced over a 1 hour period). Because of the larger pores within the glass beads and due to the wetted surface of the sand the DNAPL remained in pool format at the bottom of the flow cell. This was confirmed visually. The setup was then kept waiting for 12 hours to settle as in the case of the glass beads.

For all the experiments involving both porous media, the tank was washed with at least 2 PV (pore volume) of deionized water prior to performing each dissolution experiment). Flushing the system with deionized water in between the different dissolution experiments eliminates any residual ethanol and hence any enhanced dissolved DCB from the resident aqueous phase inside the flow cell. This enabled obtaining a relatively consistent concentration average for pre-dissolution states of the system and thus better determining of the concentration change.

Each experiment sample cover 2 – 2.5 PV of solvent system and 25-30 samples. The collection of the samples was started at t = 0 PV and ended at the desired PV flushing. 0 PV was set as a reference corresponding to the time when the solvent-cosolvent system started to be introduced from the inlet port of the flow cell.

The experiments performed were planned in a way to test all the parameters upon variation, including grain size (type of the media), flushing flow rate and cosolvent content of the flushing solution. Flow was kept at steady rates throughout each experiment.

The mobility of DNAPL as a separate phase liquid was avoided because of its interference with the estimated dissolution rates. Collecting liquid DCB instead of dissolved DCB as effluent would significantly change the analysis results as the effluent concentrations ranged between 15 to 1500 ppm. This issue prevented performing some experiments at higher ethanol contents, which is further explained in the Results section (Chapter 5) of the thesis.

To avoid exceeding the dynamic range of the calibration curve produced, proper dilutions were done at the time of sampling (usually 1/14 and 1/28). The samples collected from the outlet port (effluent) were brought to analysis immediately in order to prevent error raised by evaporation of the analyte. The samples were then diluted and analyzed using a UV-VIS spectrophotometer (Shimadzu UV-160A UV-Visible Recording Spectrophotometer) at the wavelength of 220 nm. The absorbance values were corrected with a blank sample (deionized water) to eliminate potential background signals.

The tested parameters (flow rates, cosolvent compositions, etc.), performed experiments and encountered issues are further discussed in Chapter 5.

4.3. Estimation of the Mass Transfer Coefficients & Sherwood Correlations

Assuming advection as the dominant transport mechanism of the dissolved NAPL (i.e. neglecting dispersion) (Powers et al., 1992), 1D steady-state NAPL dissolution equation can be expressed as (Agaoglu et al., 2015):

$$nv\frac{\partial C}{\partial x} = k_f a(C_s - C) \tag{4.1}$$

where

n: porosity of the porous media [-]

v: velocity of the mobile (aqueous) phase [L/T]

x: length coordinate in the direction of flow [L]

k_f: interphase mass transfer coefficient [L/T]

a: contact area per unit volume of porous media [1/L]

C_s: aqueous solubility of NAPL [M/L^3]

C: composition of NAPL in the aqueous medium [M/L^3]

It can be noted that the concentration of NAPL in the aqueous phase is a function of *x*, therefore varies longitudinally. Integrating Equation (4.1) enables the back calculation of interphase mass transfer coefficient analytically:

$$k_f = -\left(\frac{nv}{La}\right) \times ln\left(1 - \frac{C_{eff}}{C_s}\right) \tag{4.2}$$

where

C_{eff} is the steady-state effluent concentration of NAPL at the position $x=L$, obtained from the flow cell experiments [M/L^3]

L is the length of the flow cell, 0.1 m for the experiments of this study [L]

For the ease of calculations, the contact area between the phases is assumed to be flat throughout the tank. Thus, the specific interfacial area term "*a*" is computed as:

$$a = \frac{nL}{HL} = \frac{n}{H} \tag{4.3}$$

where H stands for the height of the aqueous phase [L].

Flow velocities (in m/s) of aqueous phases in porous media are calculated with the following expression:

$$v = \frac{Q}{n \times A_{tank}} \tag{4.4}$$

where

Q: flow rate [L^3/T]

A_{tank}: the cross sectional area of the aqueous phase [L^2]

The flow cell experiments are performed to obtain the effluent DCB concentrations in order to calculate the interphase mass transfer coefficients, k_f for each conducted experiment, using Equation 4.2. Aqueous solubility of DCB in the expression, C_s, is substituted with experimentally calculated solubility values for various DCB-ethanol compositions. For the aqueous solubility of DCB (where ethanol % is zero in the experimental setting) the literature value of 156 mg/L (Yalkowsky et al., 2010) was used both for the experimental and the modeling calculations, which is indicating consistency for the experimentally measured value of 151 mg/L.

The analytical results of interphase mass transfer values are then used to calculate the corresponding Sherwood numbers, for further correlating with Péclet and Schmidt Numbers:

$$Sh = \frac{k_f \times d_m}{D_m} \tag{4.5}$$

$$Pe = \frac{v \times d_m}{D_m} \tag{4.6}$$

$$Sc = \frac{\mu_w}{\rho_w \times D_m} \tag{4.7}$$

Including the Schmidt number within the correlations is attractive features because it relates to the fluid properties and ethanol content of flushing solutions. All three numbers are unitless, thus provides an ease of use in calculations. Using the Schmidt number instead of some other parameter such as the ethanol content has another attractive feature: the logarithm of the Schmidt number can be computed in the regression analysis (Section 5.4), whereas this would not be possible with the ethanol content for the case when pure water (i.e., zero ethanol content) is used as the flushing solution. Also, building these correlations with a normalized expression as Schmidt number allows application and comparison with potential further studies, using different cosolvent agents, since it is not compound specific.

4.4. Modeling of the Interphase Mass Transfer Coefficients

In this study, in addition to the 1-D analytical expressions presented in Section 4.3, a two-dimensional pore network model written in Fortran language is used to generate interphase mass transfer coefficients. The model was adopted from a previous study with similar experimental setup (Aydin-Sarikurt, 2018). The model essentially simulates the transfer of mass from a stationary NAPL mass placed at the bottom of a cell to the aqueous phase through a uniform flow. The pore network model relies on the principle that chambers representing individual pores are connected to each other to form a network of passages (Lenormand et al., 1988). A theoretical sketch of the network model that has been used to simulate dissolution experiments is shown in Figure 4.2.

The experiments are modeled in the form of “regular structured network”; uniform grain size and spatial arrangement, with a pore body (chamber) is connected to 4 others via tubes (in another words, the coordination number is 4). It should be noted that real subsurface media can be composed

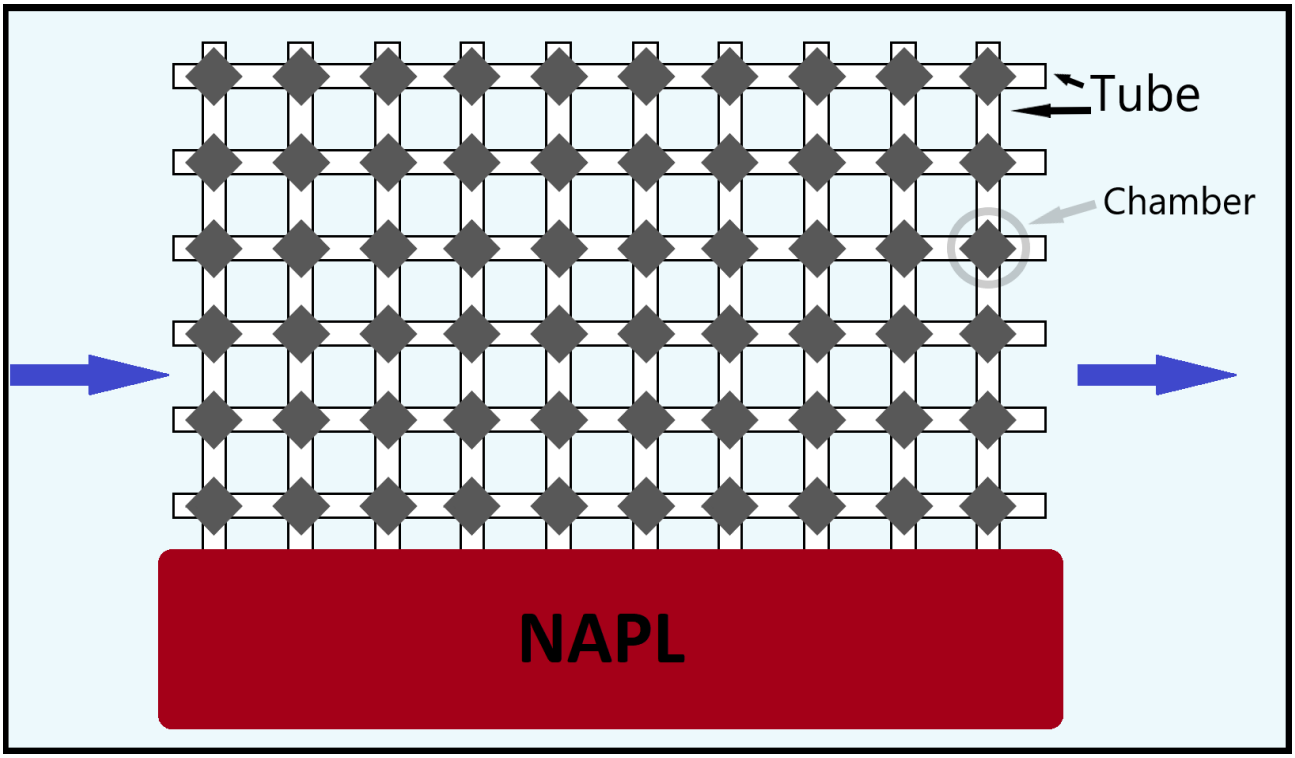

Figure 4.2. Representative sketch of the pore network model.

of various structures covering diverse grain sizes, coordination numbers and spatial arrangements (Joekar-Niasar and Hassanizadeh, 2012).

The following expression describes solute transport via the pore network model in which time dependent change in concentration of chamber *i*, based on the model developed by Jia and colleagues (Jia et al., 1999):

$$V_s \frac{\partial C_i}{\partial t} = \sum_{m=1}^{M} \{Q_m C_m\} + \sum_{m=1}^{M} \left\{ DA \frac{\Delta C_{im}}{l} \right\} + k_f A (C_s - C_i) \tag{4.8}$$

where

i: chamber index

V_s: volume of chamber i [L^3]

C_i: aqueous-phase concentration in chamber i [M/L^3]

M: number of adjacent chambers

Q_m: flow rate into/out of chamber i to adjacent chambers [L^3/T]

C_m: concentration associated with Q_m [M/L^3]

D: dispersion coefficient [L^2/T]

ΔC_{im}: difference in concentration between chamber i and adjacent chambers m [M/L^3]

k_f: mass transfer coefficient along the water-NAPL interface [L/T]

C_s: aqueous phase solubility [M/L^3]

l: length of the tube connecting chamber i to adjacent chambers [L]

A: cross-sectional area of the tube connecting chamber i to adjacent chambers [L^2]

This model processes the spatial arrangements of individual pore bodies through the chamber volumes and tube length parameters; and is consistent with the relevant literature (Dillard et al., 2000; Agaoglu et al., 2016; Aydin-Sarikurt et al., 2017).

The model is used to generate mass transfer coefficients, k_f, in a way to substitute the best fitting values in accordance with the analytically calculated coefficients which are derived from the experimental data. The model output is sequential effluent concentrations for specified experimental properties. The k_f values are substituted to match the equilibrium effluent concentrations (i.e. reaching steady state conditions) to the experimentally measured effluent concentrations of the flow cell experiments. The input parameters of the simulations are presented in Table 4.1. The chambers in the model were assumed to be cubical shaped, corresponding the uniform porous media used in the dissolution experiments, and the tubes connecting the chambers were assumed to have a square cross sectional area (Aydin-Sarikurt, 2018).

The initial concentration in the model was assumed to be equal to zero. Along the boundary of NAPL and pore network structure, dissolution process defined at Equation 2.2 was enforced. The model was solved explicitly in time until steady-state concentrations are acquired. The mobile phase flow was assumed to be uniform over the NAPL mass similar to the experimental conditions. The NAPL mass was also assumed to be remained unchanged with time. The latter assumption is considered to be a safe one as DCB has low solubility properties and flushed pore volumes did not exceed 3.

Table 4.1. Input parameters of the pore network model for simulation.

Input parameters	Glass beads	Sand	Notes
Porosity	0.34	0.36	In consistency with the flow cell experiments.
Longitudinal dispersivity (m)	0.002	0.002	From the experimental work of (Aydin-Sarikurt, 2018)
Mean grain diameter (m)	0.001	0.0002	In consistency with the flow cell experiments.
Chamber dimensions (m)	0.0007	0.00014	Defined as $L_c = 0.7\ d_m$
Chamber volume (m^3)	3.43×10^{-10}	2.74×10^{-12}	Volume = $L_c^3 = (0.7\ d_m)^3$
Length of tube (m)	0.0003	0.00006	Assumed to be 30 % of the mean grain diameter $L = 0.3\ d_m$
Area of tube (m^2)	2.5×10^{-7}	1×10^{-8}	Cross-sectional area of the tube $A = (0.5\ d_m)^2$

5. RESULTS AND DISCUSSIONS

In this chapter, the results of the batch tests and controlled flow cell experiments are presented first. Subsequently, the calculation of the mass transfer coefficients using the 1D analytic solution and the numerical 2D model are described. The regression analysis used for the development of the mass transfer expressions and the correlations between them are subsequently discussed in detail. Also, the statistical reliability of all the data is evaluated.

5.1. Dense Non-aqueous Phase Liquid Emplacement and Flow Cell Saturation

The ultimate goal of preparing the flow cell to the experiments was to place DCB to the bottom of the tank as evenly and uniformly as possible as the contact area between the aqueous phase and DCB phase needed to be known for calculation of interphase mass transfer coefficients. Several failed attempts were performed for glass beads media (Figure 5.1) until reaching the desired displacement state (Figure 5.2).

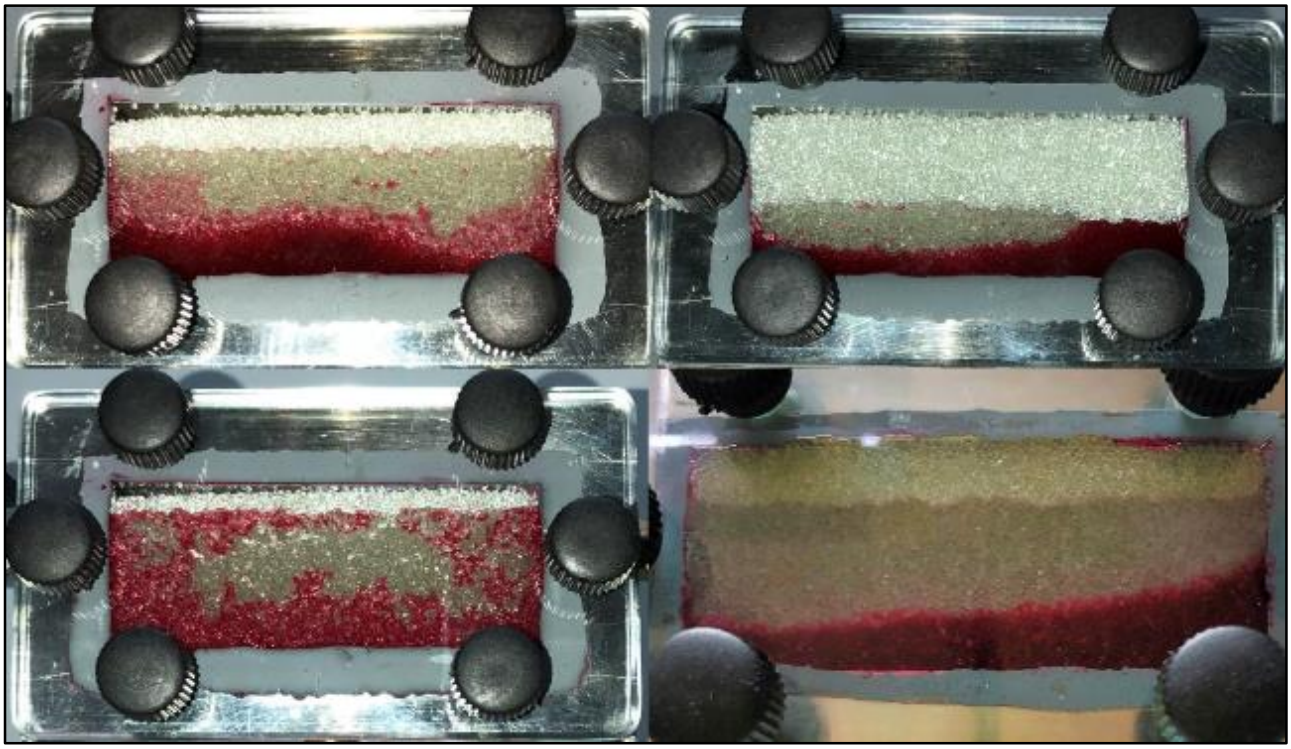

Figure 5.1. Photographs of failed attempts to setup the flow cell for glass beads.

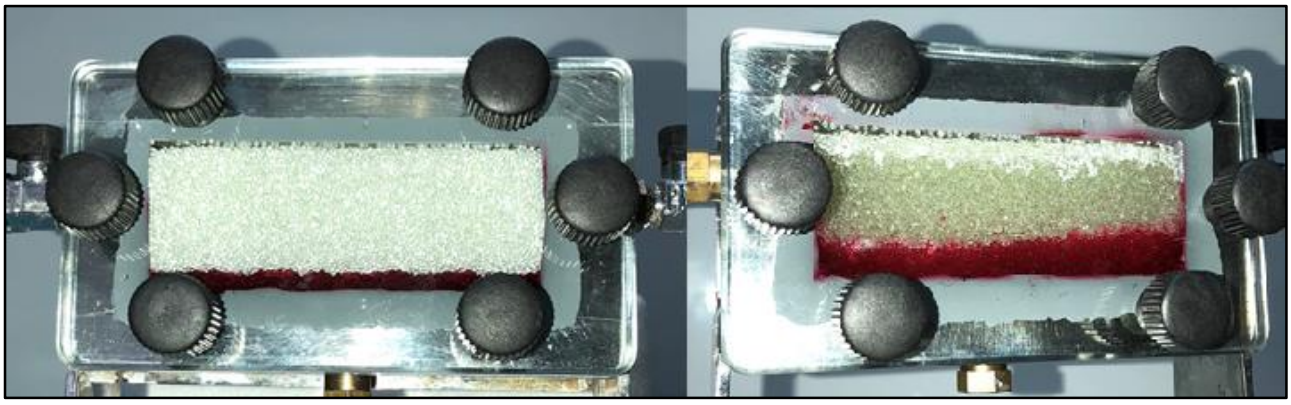

Figure 5.2. Photographs of the tank for glass beads, before and after the saturation with deionized water.

Saturation velocity of the glass beads media with deionized water was the critical parameter during this stage as DCB tends to move physically upon the applied pressure of aqueous phase during saturation.

For the case of sand experiments, it was trickier to prepare the flow cell as the diameter of sand grains was relatively small. Hence, the larger capillary forces prevented the DCB pool to form an ordered geometrical form (i.e. it spreads all over the media randomly). Therefore, introducing DCB to the bottom of the tank first and introducing deionized water later was not feasible. Figure 5.3 clearly shows some unsuccessful examples.

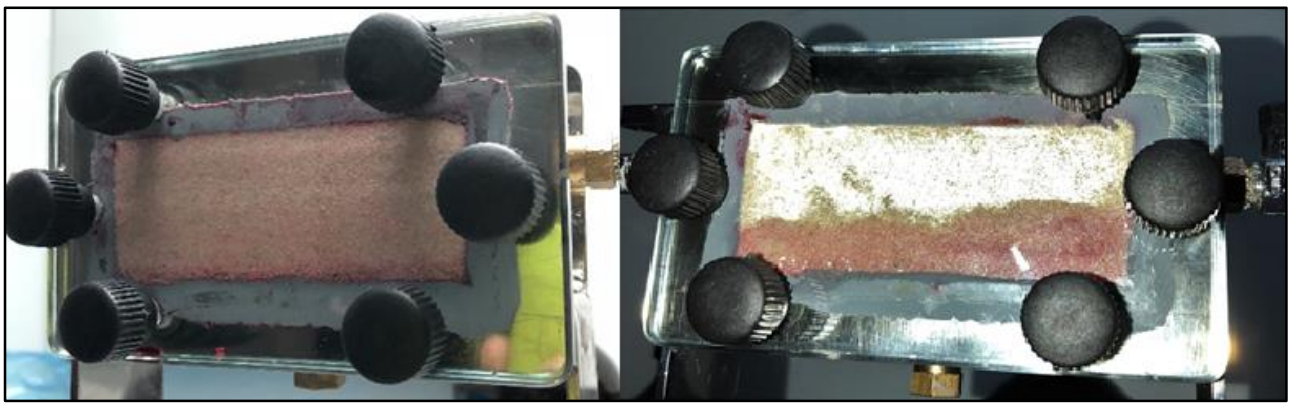

Figure 5.3. Photographs of the failed attempts to setup the tank with sand.

Because the sand grain diameter was much smaller than that of the glass beads, the capillarity was higher which prevented the placement of the DNAPL pool within the dry sand. As noted in the Materials and Method chapter, to overcome this problem, a method described in the publication of Phenrat and colleagues (Phenrat et al., 2011) was used and modified to achieve a proper placement of DCB. The key factor at this point was to pack the sand carefully so that the upper layer of the glass

beads would not be disrupted, thus, having a decent interface for mass transfer between the phases. Figure 5.4 shows the final state of entrapped DCB for conducting sand experiments.

NAPL saturation of the systems were 0.27 for glass beads and 0.12 for sand.

Figure 5.4. Photographs of the tank packed and saturated for sand experiments.

5.2. Experimental Parameters

Considering the flow rate was kept steady for all the experiments, the variables in the conducted experiments were diameter of the porous media (glass beads (d_m = 1 mm) and sand (d_m = 0.2 mm)), ethanol content (10 %, 20 %, 30 % and 40 %) and flow rates (0.5>, 1, 2, 5, 25 in mL/min).

Because the emphasis of this study was on the dissolution from immobile DNAPL, avoiding the physical mobility of entrapped DCB was crucial throughout the experimental work. Two parameters contribute towards mobility of liquid DCP; increasing the flow rate and high ethanol content. Experiments with lower ethanol contents and lower velocities were conducted first. Conducting experiments with 40 % ethanol content was not possible for glass beads as droplets of DCB were being observed in the effluent from the flow cell. For the case of 30 % ethanol composition and 25 mL/min experiment, no DCB droplets were detected at the end of the experiments. The same precautions was taken for sand experiments. Although the set of experiments enabled introducing 40 % ethanol as cosolvent, adjusting flow rate to 25 mL/min was not possible as it promoted DCB mobility right away. Instead, 11 mL/min was the maximum flow rate considered.

In total 15 dissolution experiments were conducted with the glass beads and 17 experiments with the sand. Although it was not possible to test all cosolvent composition - flow rate combinations, the results were sufficient to develop the Sherwood correlations. Table 5.1 shows the parameters that were tested with the dissolution experiments.

Table 5.1. Performed experiments and parameters.

Type of porous media	**Ethanol Content (% Volume)**	**Flow rate of the flushing liquid (mL/min)***
Glass beads (d_m = 1 mm)	10 %, 20 %, 30 %	0.232, 1, 2, 5, 25
Sand (d_m = 0.2 mm)	10 %, 20 %, 30 %, 40 %**	0.156, 0.187, 1, 2, 5, 11***

**: Flow rates are calculated as volume accumulated per minute.*
***: Not in higher flow rates. See Table 5.5.*
****: Mobility of DNAPL was observed above this flow rate.*

5.2.1. Calibration Curve of 1,2-dichlorobenzene

For measuring the concentration of DCB for the following experiment sets, a calibration curve with a conversion function is generated covering the absorbance values of UV-vis spectrophotometer at a wavelength of 220 nm (Figure 5.5). The intercept is set at (0,0) point to include blank correction. (The blank sample was corrected at all times during all the measurements with the UV instrument).

A high correlation coefficient (R^2) value of 0.9992 ensures the linearity of the trend, providing a high reliability. All the succeeding DCB measurements with the instruments were done within the dynamic range of this curve, which is 1- 30 ppm, via proper dilutions.

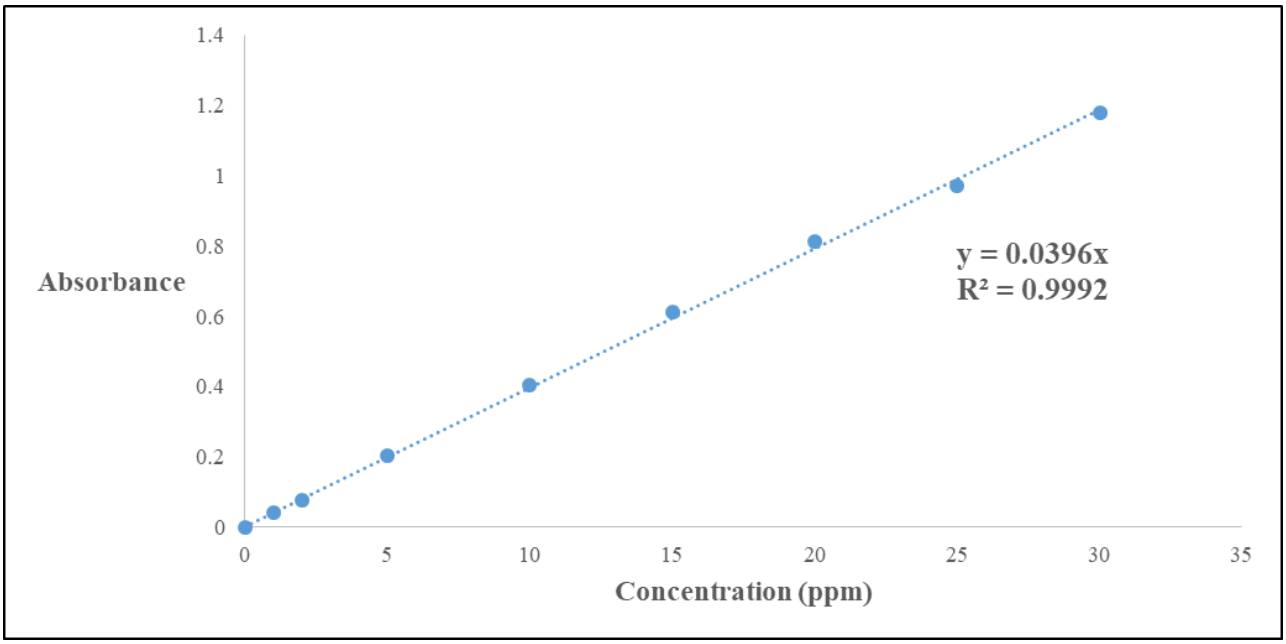

Figure 5.5. Calibration curve of DCB for UV-vis Spectrophotometer.

5.2.2. Solubility Measurements of 1,2-dichlorobenzene

The results in Table 5.2 are obtained from the solubility measurements of DCB. It is noted that more than one solubility tests were performed for 30 % and 40 % ethanol contents to reduce error and the average is used in the modeling. The standard error normalized by the average is 3.55 % for the 40 % ethanol solubility measurements.

Table 5.2. Solubility measurements for DCB.

Ethanol volume (%)	Absorbance	Dilution Factor	DCB Concentration (ppm)
0	0.597	1/10	151
10	0.077	1/100	194
20	0.150	1/100	378
30	0.037	1/1000	934
30	0.400	1/100	1009
40	0.405	1/500	5114
40	0.427	1/500	5391
40	0.781	1/250	4931
40	0.696	1/250	4394
40	0.942	1/200	4758
40	0.852	1/200	4303

Table 5.3 summarizes the solubility values of DCB used in the calculation of the mass transfer coefficients. The measured solubility of DCB in deionized water (i.e. 0 % ethanol) is consistent with the literature value of 156 ppm (Yalkowsky et al., 2010) is used throughout the study.

Table 5.3. DCB solubility values.

Ethanol volume (%)	DCB Concentration (ppm)
0	151*
10	194
20	378
30	972
40	4815

*: *Literature value is 156 ppm* (Yalkowsky et al., 2010).

The curve indicating the solubility trend of DCB with increasing ethanol content is shown in Figure 5.6. Lower ethanol content had relatively smaller effect on the solubility of DCB while for ethanol contents greater than 20 %, the solubility decreased rapidly.

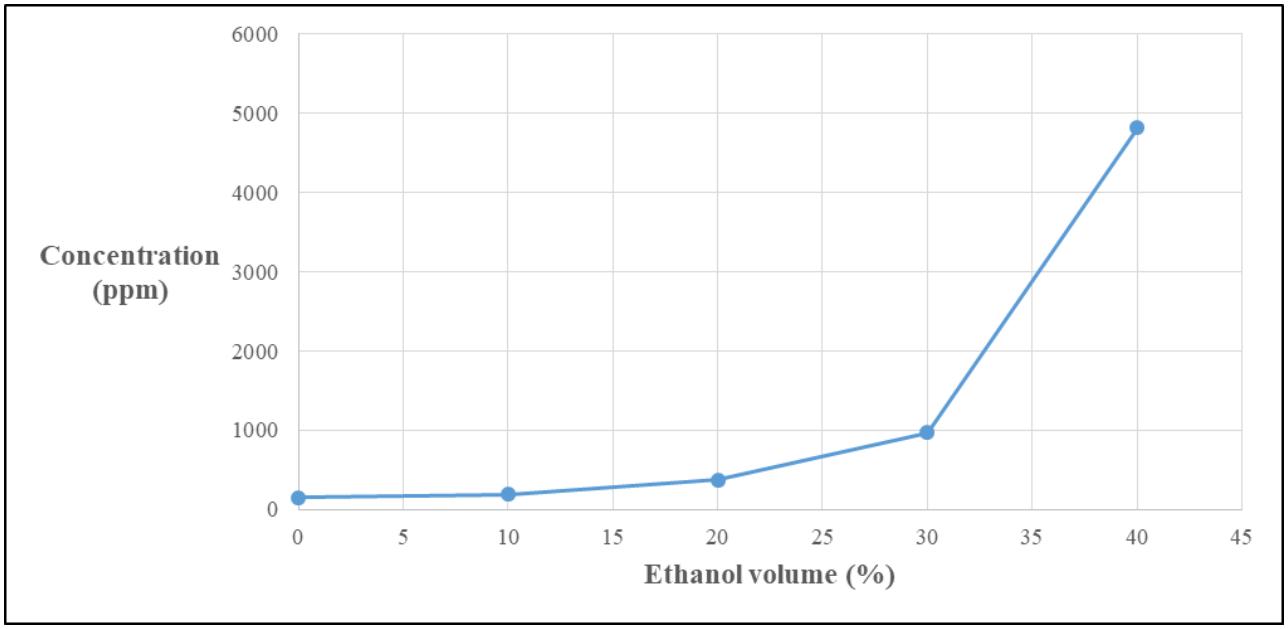

Figure 5.6. Solubility of DCB as a function of ethanol content.

5.3. Computation of the Interphase Mass Transfer Coefficients

5.3.1. One-dimensional (1-D) analytical solution

The experimental results of the dissolution experiments, consisting of the aqueous phase ethanol content, flow rates, velocities, steady-state effluent concentrations and their standard errors are presented in Table 5.4 for the glass beads set and Table 5.5 for the sand set. The velocity ranges in the experiments are 9.49×10^{-6} - 1.02×10^{-3} m/s for the glass beads set and 5.32×10^{-6} - 3.74×10^{-4} m/s for the sand set.

Plots of the effluent concentration as a function of the flow rate are shown in Figure 5.7 for the glass beads experiments and Figure 5.8 for the sand experiments. Similar plots showing the variation of the effluent concentration as a function of ethanol content are shown in Figure 5.9 for the glass beads experiments and Figure 5.10 for the sand experiments. Data for the ethanol content above 40 % for the glass beads set, and for flow rates above 11 mL/min for the sand set are not shown because NAPL mobility occurred during these experiments. Moreover, because the low flow rates ($Q<1$ ml/min) were very close to each other, their average is shown in Figure 5.10.

Table 5.4. Experimental data from the glass beads dissolution experiments.

Ethanol volume (%)	Flow rate (mL/min)	Velocity (m/s)	Steady-state effluent concentration (ppm)	Standard error of effluent concentration (%)
0	0.232	9.49×10^{-6}	44	3.8
10	0.232	9.49×10^{-6}	53	2.5
20	0.232	9.49×10^{-6}	62	2.6
30	0.232	9.49×10^{-6}	82	1.9
0	1	4.08×10^{-5}	28	2.0
10	1	4.08×10^{-5}	30	1.5
20	1	4.08×10^{-5}	32	3.0
30	1	4.08×10^{-5}	77	1.6
0	2	8.17×10^{-5}	24	2.1
10	2	8.17×10^{-5}	45	3.9
20	2	8.17×10^{-5}	41	1.2
30	2	8.17×10^{-5}	82	2.0
0	5	2.04×10^{-4}	26	3.3
10	5	2.04×10^{-4}	30	1.8
20	5	2.04×10^{-4}	47	2.4
30	5	2.04×10^{-4}	67	3.2
0	25	1.02×10^{-3}	18	2.3
10	25	1.02×10^{-3}	23	5.0
20	25	1.02×10^{-3}	32	2.6
30	25	1.02×10^{-3}	63	2.0

A general trend of decrease in effluent concentrations with increasing flow rate is observed, resulting from the shorter contact time between the phases as velocity increases. On the other hand, increased ethanol content significantly increased the solubilization of DCB, as expected. The trends in Figure 5.9 and Figure 5.10 are consistent with the overall increase in the solubility with ethanol content in Figure 5.6. It can be noted that 10 % ethanol content had very little effect on solubility, the change in effluent concentration, thus, mass transfer of DCB.

Table 5.5. Experimental data from the sand dissolution experiments.

Ethanol volume (%)	Flow rate (mL/min)	Velocity (m/s)	Steady-state effluent concentration (ppm)	Standard error of effluent concentration (%)
0	0.156	5.32×10^{-6}	61	6.3
40	0.156	5.32×10^{-6}	844	2.1
0	0.187	6.37×10^{-6}	43	4.4
10	0.187	6.37×10^{-6}	46	3.5
20	0.187	6.37×10^{-6}	56	3.1
30	0.187	6.37×10^{-6}	177	4.4
0	1	3.40×10^{-5}	83	2.1
10	1	3.40×10^{-5}	96	3.6
20	1	3.40×10^{-5}	129	4.3
30	1	3.40×10^{-5}	370	3.1
40	1	3.40×10^{-5}	1500	2.6
0	2	6.81×10^{-5}	49	2.8
10	2	6.81×10^{-5}	77	3.5
20	2	6.81×10^{-5}	105	2.1
30	2	6.81×10^{-5}	298	1.8
40	2	6.81×10^{-5}	1073	3.8
0	5	1.70×10^{-4}	58	2.3
10	5	1.70×10^{-4}	86	1.6
20	5	1.70×10^{-4}	118	1.8
30	5	1.70×10^{-4}	213	2.6
40	5	1.70×10^{-4}	1022	2.0
0	11	3.74×10^{-4}	20	4.2
10	11	3.74×10^{-4}	25	2.7

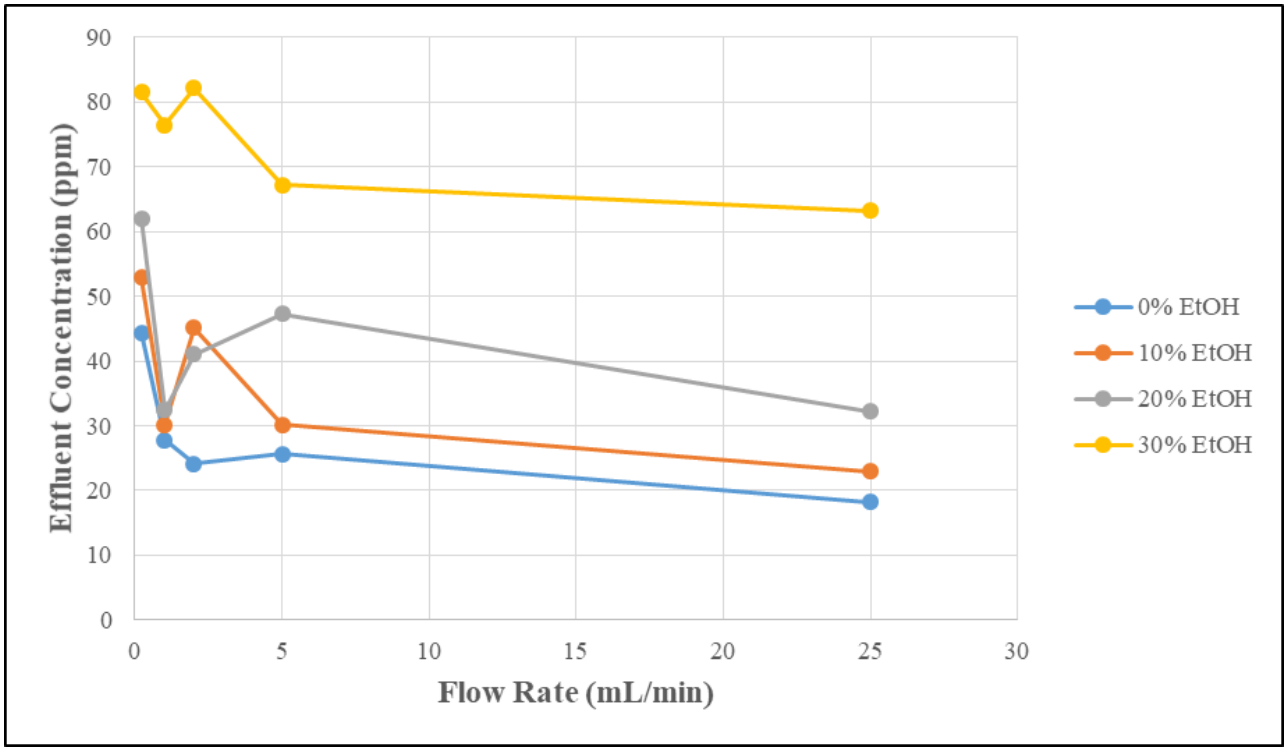

Figure 5.7. Effluent concentration as a function of flow rate for glass beads experiments.

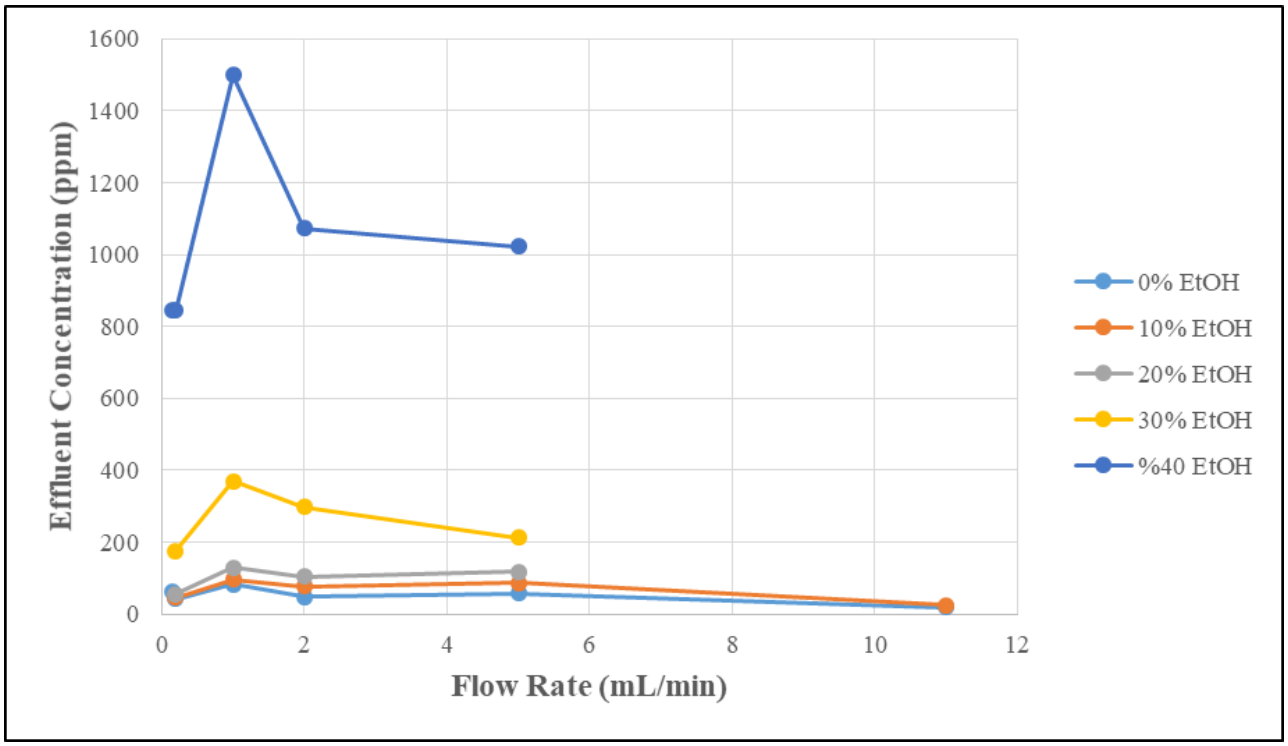

Figure 5.8. Effluent concentration as a function of flow rate for sand experiments.

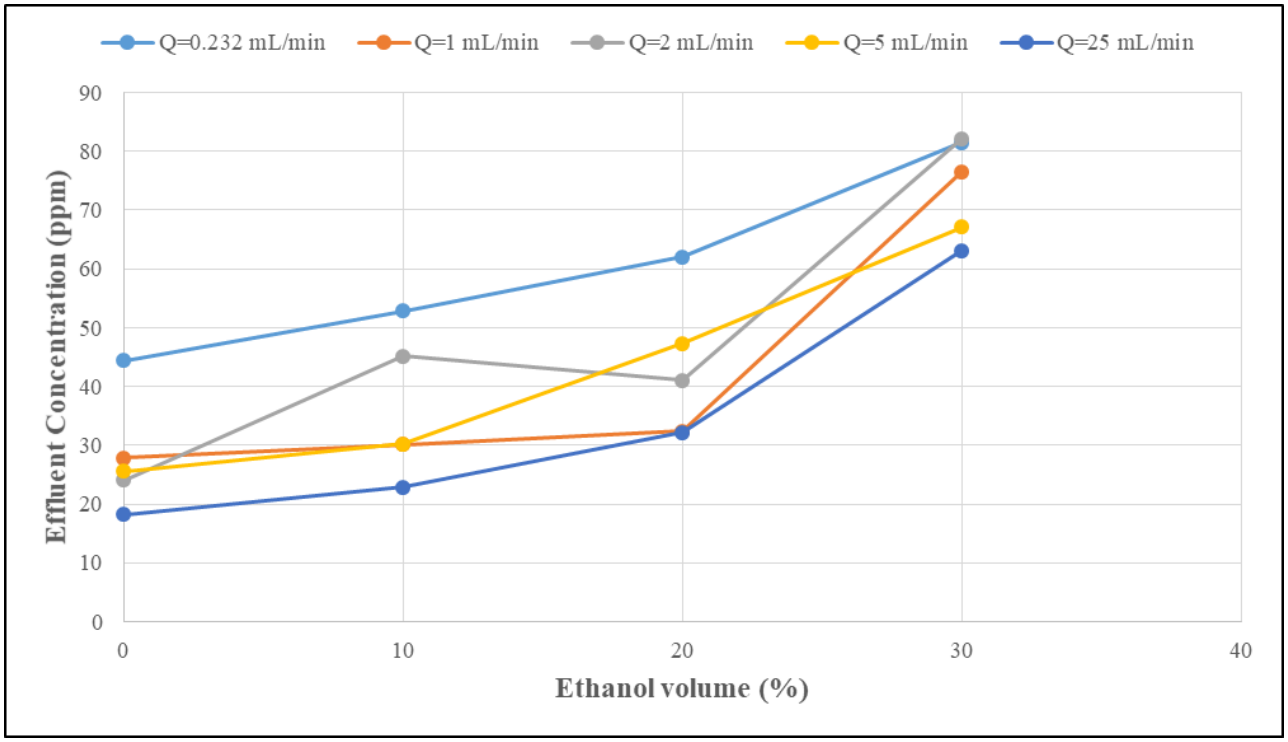

Figure 5.9. Effluent concentration as a function of ethanol content for glass beads experiments.

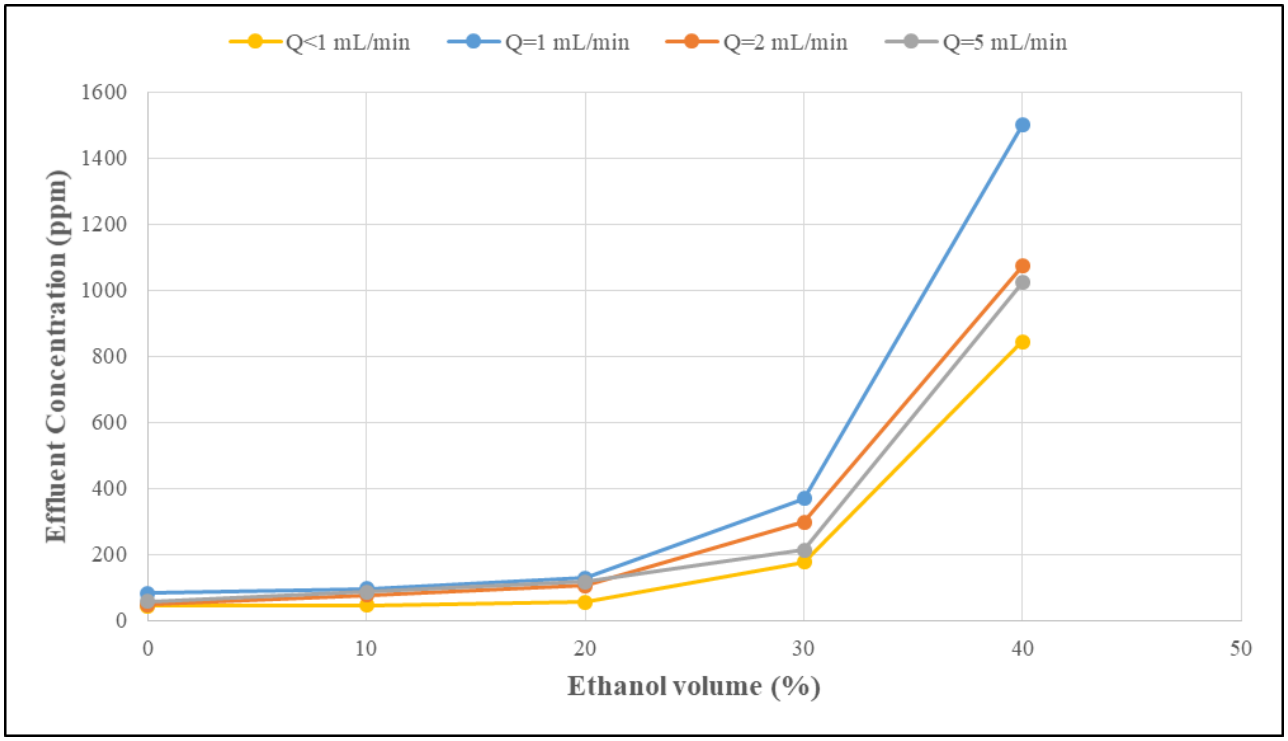

Figure 5.10. Effluent concentration as a function of ethanol content for sand experiments.

For 0 % ethanol values, average effluent concentrations from the pure water injection stage are used in calculations (i.e. samples until reaching 1 PV of effluent volume). Figure 5.7 and Figure 5.8 show that even though the cross-sectional area of the aqueous phase is relatively small, the effluent concentrations are still well below the aqueous solubility concentrations of the NAPL, indicating that

the system is at non-equilibrium conditions and effective solubility has not been reached. In other words, a kinetic expression is needed for the definition of the interphase mass transfer which is consistent with what is reported in the literature (Kokkinaki et al., 2013; Aydin-Sarikurt et al., 2017).

For the glass beads experiments, results for above 30 % ethanol content were excluded as the mobilization of the NAPL mass was observed visually both in the tank and in the collected effluent. To avoid similar issues with the sand experiments, ethanol contents up to 30 % are tested first for flow rates up to 5 mL/min. Mobility of the NAPL mass is observed for 11 mL/min flow rate and 20 % ethanol, therefore no further data are obtained.

Velocities of the mobile phases are calculated using Equation 4.4. The area of the tank is taken as the cross-sectional plane where aqueous phase was allowed to flow which is the total cross-sectional area of the tank excluding the part filled with the NAPL. The height of the water level was 3 cm for the glass beads experiments and 3.4 cm for the sand experiments (i.e. the height of the NAPL level was 1 cm for the glass beads experiments and 0.6 cm for the sand experiments).

The average standard error values for all glass beads and sand experiments are 2.5 % and 3.1 % respectively, indicating a slightly higher degree of error for sand experiments. However, both numbers are relatively small.

The data from Table 5.4 and Table 5.5 are then used to calculate interphase mass transfer coefficients analytically, using Equation 4.2. The results are shown in Table 5.6 for the glass beads experiments and Table 5.7 for the sand experiments. Solubility values indicated in Table 5.3 are used in the analytical solution. The results show an increasing trend for interphase mass transfer coefficients as the aqueous phase flow rate increases, which can be visualized in Figure 5.11 and Figure 5.12. This trend can be associated with the increased concentration gradients away from the NAPL-aqueous phase interphase (the driving force consisting of the concentration difference in Equation 2.1 and 2.2) resulting from the increase in velocity. An exception is the sand experiments performed with 11 mL/min flow rate where the overall rising trend is disrupted. This issue will be further evaluated in Section 5.4.

As the trends suggest in Figure 5.11 and Figure 5.12, increasing ethanol content is inversely proportional to the value of mass transfer coefficients. This relation can be linked with the diminishing effect of viscosity over liquid mass transfer coefficients (Song et al., 2014), since increasing the ethanol content of a pure aqueous solution within the range of our work increases the

viscosity property of the liquid (Khattab et al., 2012). The experimental data presented by Khattab and colleagues are gathered in Figure 5.13 to represent how viscosity changes with increasing ethanol content of pure water.

Table 5.6. Mass transfer coefficients of glass beads experiments determined with the 1D analytical equation.

Ethanol volume (%)	**Velocity (m/s)**	**Mass transfer coefficient (m/s)**
0	9.49×10^{-6}	9.53×10^{-7}
10	9.49×10^{-6}	9.03×10^{-7}
20	9.49×10^{-6}	5.11×10^{-7}
30	9.49×10^{-6}	2.49×10^{-7}
0	4.08×10^{-5}	2.41×10^{-6}
10	4.08×10^{-5}	2.06×10^{-6}
20	4.08×10^{-5}	1.10×10^{-6}
30	4.08×10^{-5}	1.00×10^{-6}
0	8.17×10^{-5}	4.12×10^{-6}
10	8.17×10^{-5}	6.48×10^{-6}
20	8.17×10^{-5}	2.82×10^{-6}
30	8.17×10^{-5}	2.17×10^{-6}
0	2.04×10^{-4}	1.10×10^{-5}
10	2.04×10^{-4}	1.03×10^{-5}
20	2.04×10^{-4}	8.20×10^{-6}
30	2.04×10^{-4}	4.39×10^{-6}
0	1.02×10^{-3}	3.80×10^{-5}
10	1.02×10^{-3}	3.84×10^{-5}
20	1.02×10^{-3}	2.73×10^{-5}
30	1.02×10^{-3}	2.06×10^{-5}

Table 5.7. Mass transfer coefficients of sand experiments determined with the 1D analytical equation.

Ethanol volume (%)	**Velocity (m/s)**	**Mass transfer coefficient (m/s)**
0	5.32×10^{-6}	8.98×10^{-7}
40	5.32×10^{-6}	3.49×10^{-7}
0	6.37×10^{-6}	7.02×10^{-7}
10	6.37×10^{-6}	5.89×10^{-7}
20	6.37×10^{-6}	3.49×10^{-7}
30	6.37×10^{-6}	4.35×10^{-7}
0	3.40×10^{-5}	8.74×10^{-6}
10	3.40×10^{-5}	7.89×10^{-6}
20	3.40×10^{-5}	4.83×10^{-6}
30	3.40×10^{-5}	5.54×10^{-6}
40	3.40×10^{-5}	4.32×10^{-6}
0	6.81×10^{-5}	8.68×10^{-6}
10	6.81×10^{-5}	1.17×10^{-5}
20	6.81×10^{-5}	7.52×10^{-6}
30	6.81×10^{-5}	8.45×10^{-6}
40	6.81×10^{-5}	5.84×10^{-6}
0	1.70×10^{-4}	2.71×10^{-5}
10	1.70×10^{-4}	3.39×10^{-5}
20	1.70×10^{-4}	2.16×10^{-5}
30	1.70×10^{-4}	1.43×10^{-5}
40	1.70×10^{-4}	1.38×10^{-5}
0	3.74×10^{-4}	1.75×10^{-5}
10	3.74×10^{-4}	1.74×10^{-5}

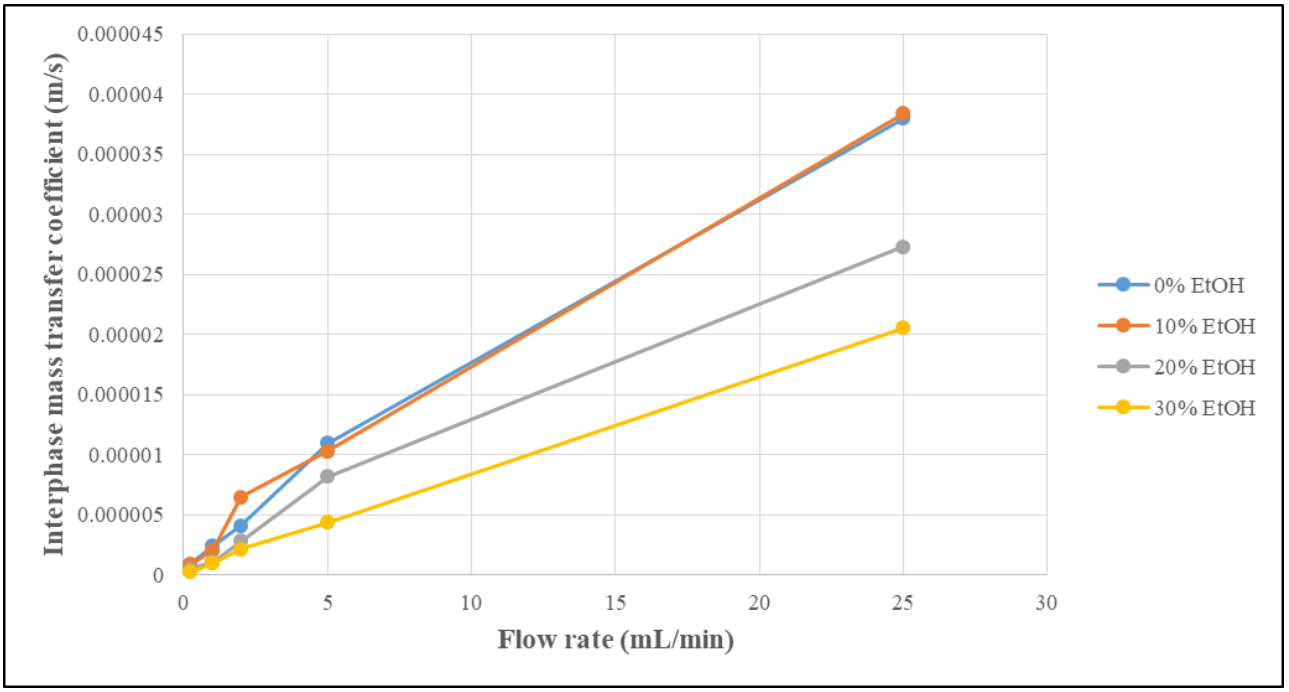

Figure 5.11. Mass transfer coefficient (estimated with the 1D analytical solution) as a function of flow rate for glass beads experiments.

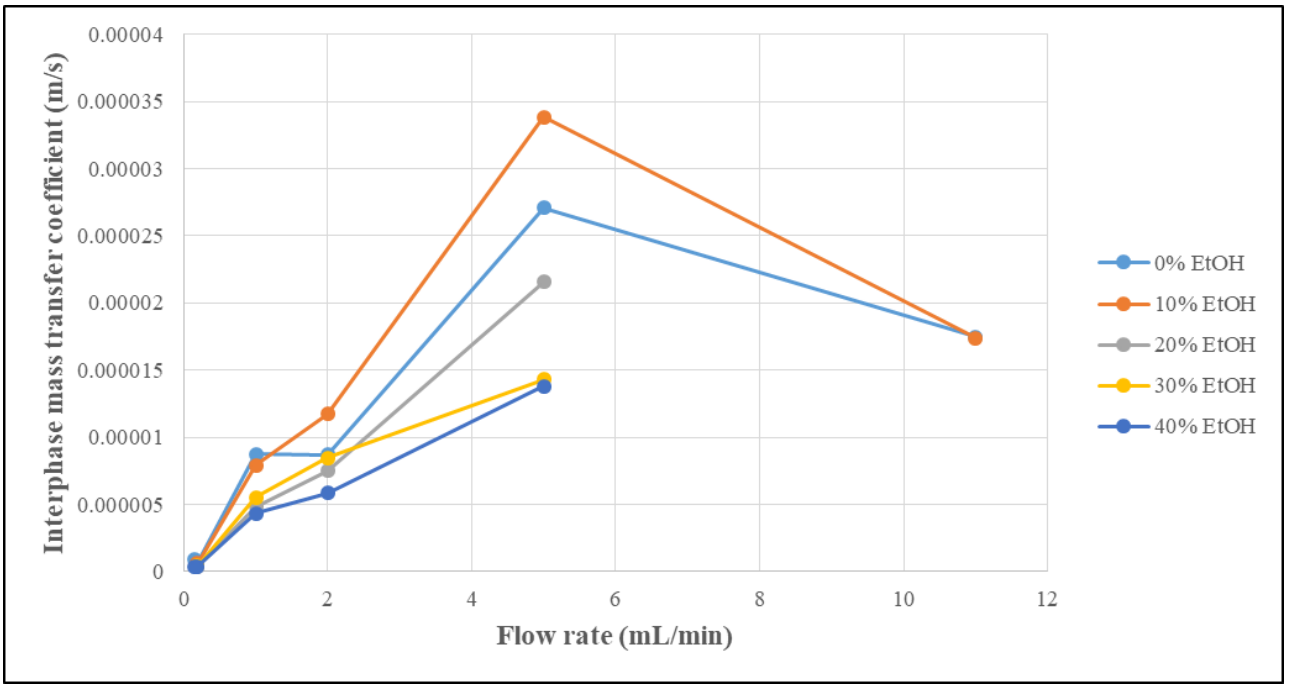

Figure 5.12. Mass transfer coefficient (estimated with the 1D analytical solution) as a function of flow rate for sand experiments.

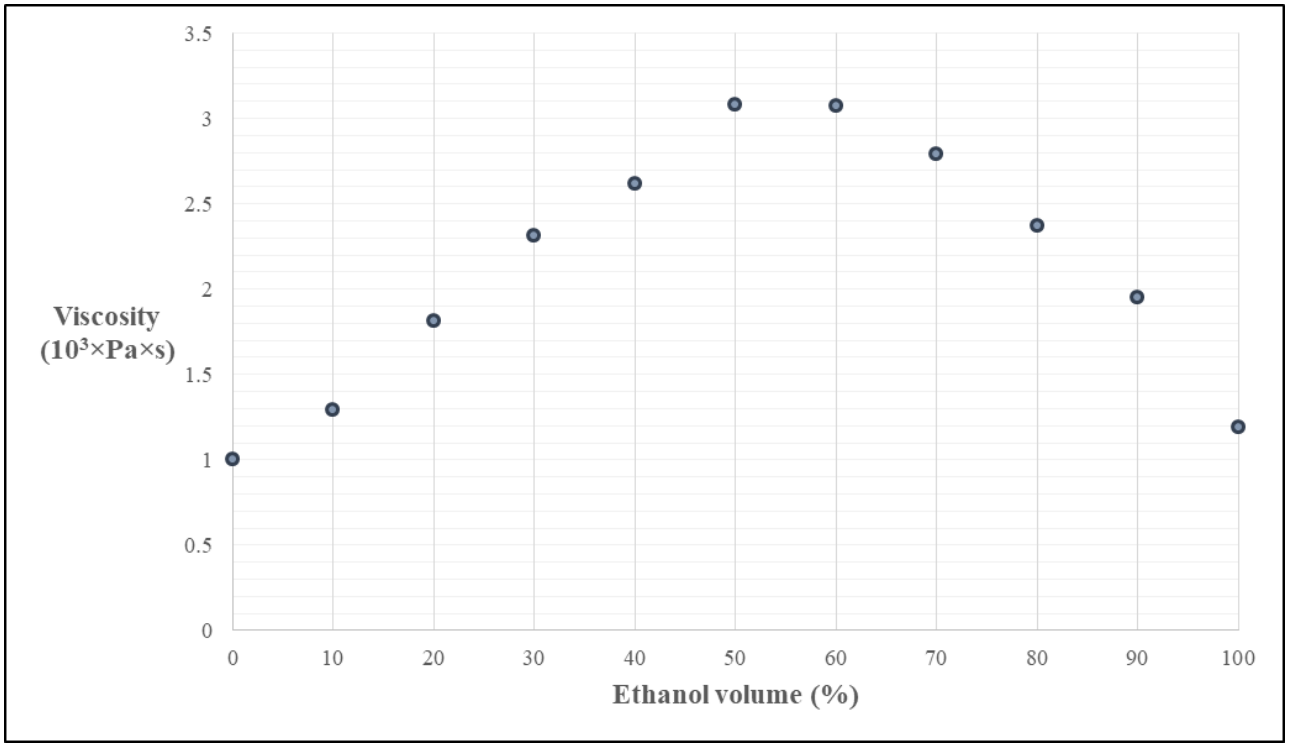

Figure 5.13. Viscosity of water with various ethanol compositions at 293 Kelvin. Adapted from Table 1 and Figure 2 of (Khattab et al., 2012).

5.3.2. Two-dimensional (2-D) numerical model

While the interphase mass transfer coefficient can directly be calculated through 1D analytical equation, the mass transfer coefficient is an input parameter for the 2D pore network model used in simulations. Therefore, the best fitting mass transfer coefficients are predicted via a trial and error procedure until the output concentrations calculated with the model match the experimentally measured effluent concentrations. The modeling results are presented in Table 5.8 and Table 5.9, along with comparison to the results of 1D analytical equation.

The parameters appearing in the 2D transport equation (Equation 4.8), such as the flow rates, dimensions of aqueous and NAPL phases and aqueous solubility values of DCB are adjusted for each model simulation. The velocities are calculated from the flow rates, porosity and cross-sectional area of the flow. Similar to the analytical solution, solubility values indicated in Table 5.3 are used in the model.

Since the model outputs are dependent on the input parameters used in the simulation (flow dimensions, flow rate, solubility, etc.), errors will also propagate from the input parameters based on the experimental properties. For a better visualization of comparison of mass transfer coefficients,

Table 5.8. Mass transfer coefficients of glass beads experiments determined with the 2D pore network model and the 1D analytical equation.

Ethanol volume (%)	Flow rate (mL/min)	Mass transfer coefficient (2D Pore network) (m/s)	Mass transfer coefficient (1D Analytical) (m/s)
0	0.232	1.54×10^{-6}	9.53×10^{-7}
10	0.232	1.43×10^{-6}	9.03×10^{-7}
20	0.232	7.50×10^{-7}	5.11×10^{-7}
30	0.232	3.47×10^{-7}	2.49×10^{-7}
0	1	3.56×10^{-6}	2.41×10^{-6}
10	1	3.00×10^{-6}	2.06×10^{-6}
20	1	1.53×10^{-6}	1.10×10^{-6}
30	1	1.40×10^{-6}	1.00×10^{-6}
0	2	6.00×10^{-6}	4.12×10^{-6}
10	2	1.01×10^{-5}	6.48×10^{-6}
20	2	4.00×10^{-6}	2.82×10^{-6}
30	2	3.02×10^{-6}	2.17×10^{-6}
0	5	1.62×10^{-5}	1.10×10^{-5}
10	5	1.51×10^{-5}	1.03×10^{-5}
20	5	1.18×10^{-5}	8.20×10^{-6}
30	5	6.05×10^{-6}	4.39×10^{-6}
0	25	5.45×10^{-5}	3.80×10^{-5}
10	25	5.48×10^{-5}	3.84×10^{-5}
20	25	3.80×10^{-5}	2.73×10^{-5}
30	25	2.84×10^{-5}	2.06×10^{-5}

corresponding values of the same system properties computed by both methods are presented in individual graphs in Figure 5.14 for glass beads medium and Figure 5.15 for sand medium. A higher degree of deviation for higher velocities can be noted as a general trend.

The coefficients predicted by the model are higher than the analytically calculated values for both glass beads and sand media. Specifically, the ratios of values by the model to the values by the analytical solution range from 1.38 to 1.61 with an average of 1.45 for glass beads media. For the sand, ratios range from 1.83 to 4.81 with an average of 2.47. This indicates a higher degree of deviation for values calculated in the sand media.

Table 5.9. Mass transfer coefficients of sand experiments determined with the 2D pore network model and the 1D analytical equation.

Ethanol volume (%)	Flow rate (mL/min)	Mass transfer coefficient (2D Pore network) (m/s)	Mass transfer coefficient (1D Analytical) (m/s)
0	0.156	2.41×10^{-6}	8.98×10^{-7}
40	0.156	6.65×10^{-7}	3.49×10^{-7}
0	0.187	1.53×10^{-6}	7.02×10^{-7}
10	0.187	1.22×10^{-6}	5.89×10^{-7}
20	0.187	6.49×10^{-7}	3.49×10^{-7}
30	0.187	8.38×10^{-7}	4.35×10^{-7}
0	1	4.20×10^{-5}	8.74×10^{-6}
10	1	3.15×10^{-5}	7.89×10^{-6}
20	1	1.21×10^{-5}	4.83×10^{-6}
30	1	1.51×10^{-5}	5.54×10^{-6}
40	1	1.02×10^{-5}	4.32×10^{-6}
0	2	2.05×10^{-5}	8.68×10^{-6}
10	2	3.37×10^{-5}	1.17×10^{-5}
20	2	1.68×10^{-5}	7.52×10^{-6}
30	2	1.98×10^{-5}	8.45×10^{-6}
40	2	1.20×10^{-5}	5.84×10^{-6}
0	5	7.30×10^{-5}	2.71×10^{-5}
10	5	1.11×10^{-4}	3.39×10^{-5}
20	5	5.10×10^{-5}	2.16×10^{-5}
30	5	2.91×10^{-5}	1.43×10^{-5}
40	5	2.80×10^{-5}	1.38×10^{-5}
0	11	3.20×10^{-5}	1.75×10^{-5}
10	11	3.19×10^{-5}	1.74×10^{-5}

Similar trends can be observed in modeled mass transfer coefficients as the experimental ones, meaning the values are proportional to the velocity of the mobile phase and inversely proportional to the ethanol content. One important factor for the deviations between the two computing approach is the exclusion of dispersion in the 1D analytical computation. The 2D model can account for dispersion in the vertical and horizontal directions, providing an important benefit for the usage of 2D pore network model.

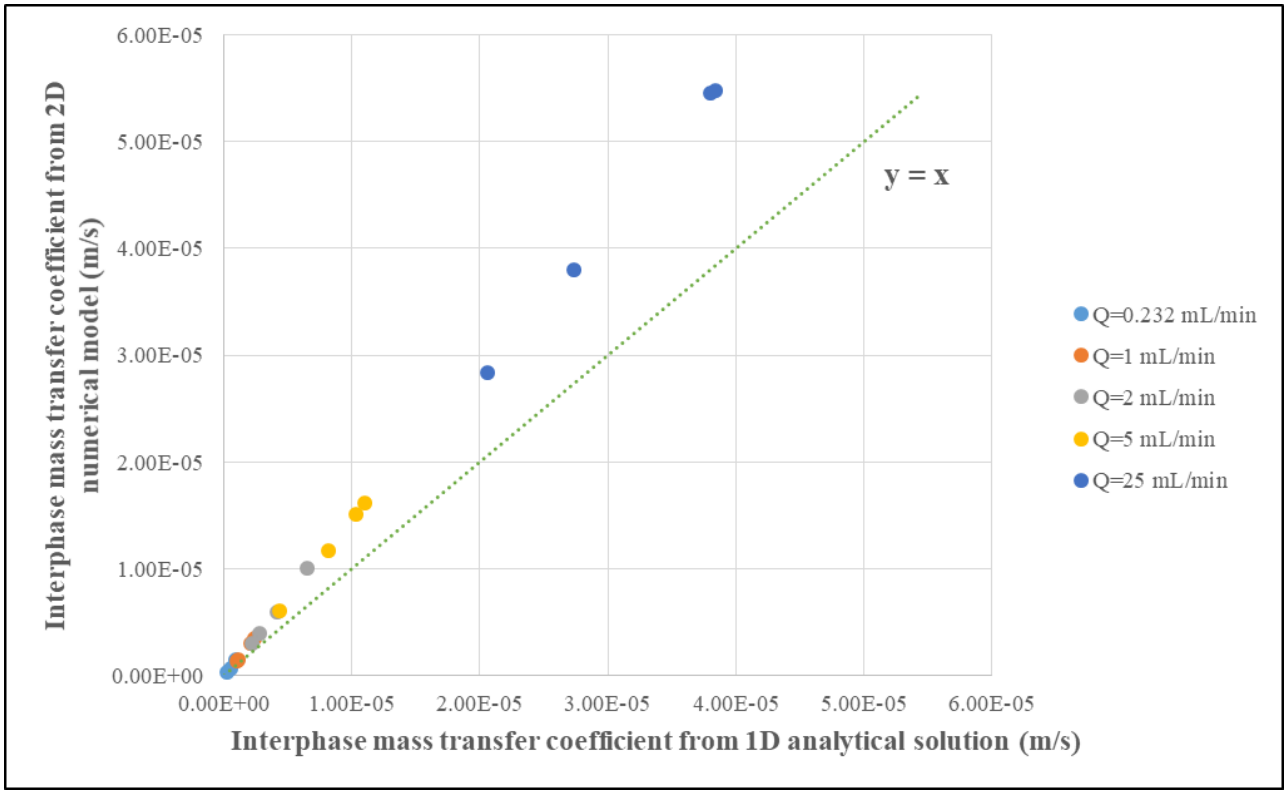

Figure 5.14. Comparison of interphase mass transfer values for glass beads media.

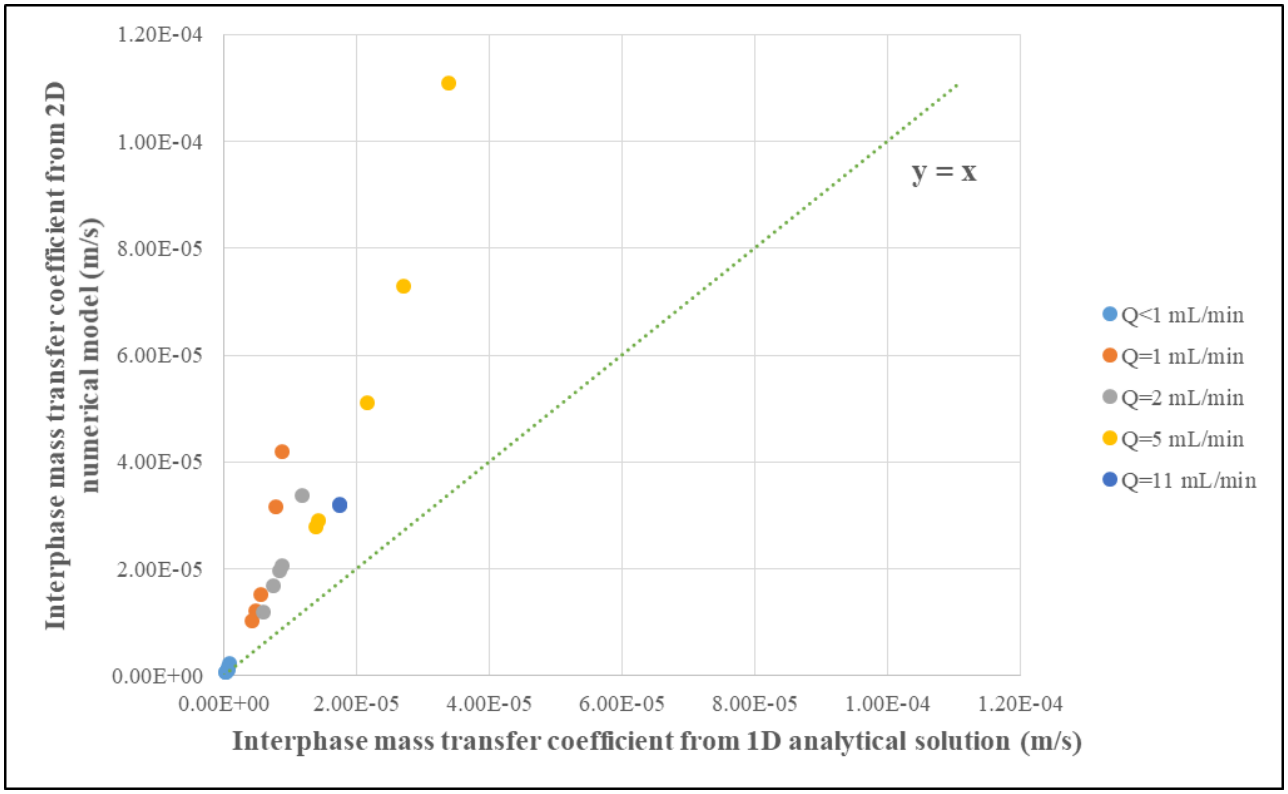

Figure 5.15. Comparison of interphase mass transfer values for sand media.

While addition of chemical agents change a complex set of phase behaviors, the only parameter changed in the model to implement ethanol presence was to modify the aqueous phase concentration

of DCB. Mixing pure water with ethanol (or any other solvent, in that matter) changes a number of properties of the aqueous phase; most notably the viscosity, density and interfacial tension between the phases. The effect of these parameters is particularly important during the transient stage of the experiments when the flushing solution is displacing the resident pure water in the flow cell. However, it is important to recall that steady-state concentrations (after 2-3 pore volumes of injected solution) were used in the 2D model, the impact of viscosity and especially density effects are not decisive.

Figure 5.16 – Figure 5.58 show contour plots of DCB concentration values for each of the experiments simulated with the 2D pore network model. The total number of plots is 43 (20 for glass beads and 23 for sand). Each individual plot illustrates the cross-sectional DCB distribution over the pore network for particular system properties, namely the porous media (sand or glass beads), flow rates (Q) and ethanol composition. The concentrations are normalized by the corresponding DCB solubility values (i.e. 156 for 0 %, 194 for 10 %, 378 for 20 %, 972 for 30 % and 4815 for 40 % ethanol contents). Each graph should be evaluated individually as the scales and grid intervals are adjusted condition-specific. As expected, the highest concentration grids are accumulated at the lower edge of pore network systems where the mass transfer with NAPL takes place. Concentrations also increase with travel distance.

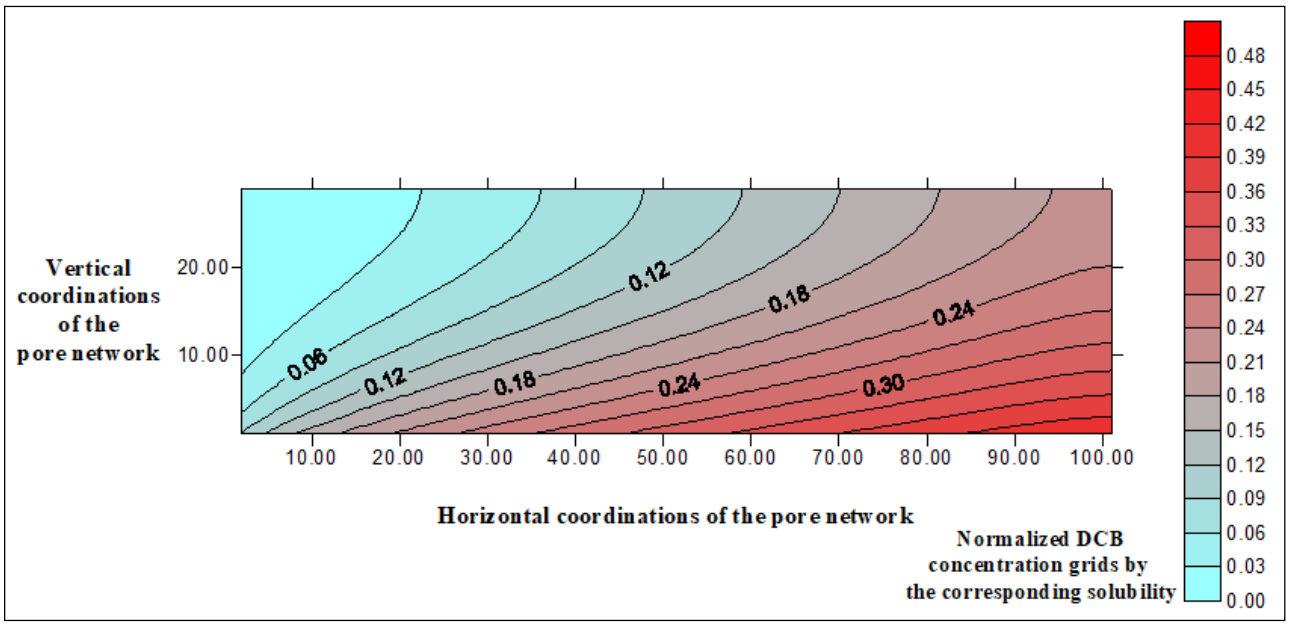

Figure 5.16. Contour plot of the normalized DCB distribution computed with the pore network model for Q = 0.232 mL/min, EtOH = 0 % (glass beads).

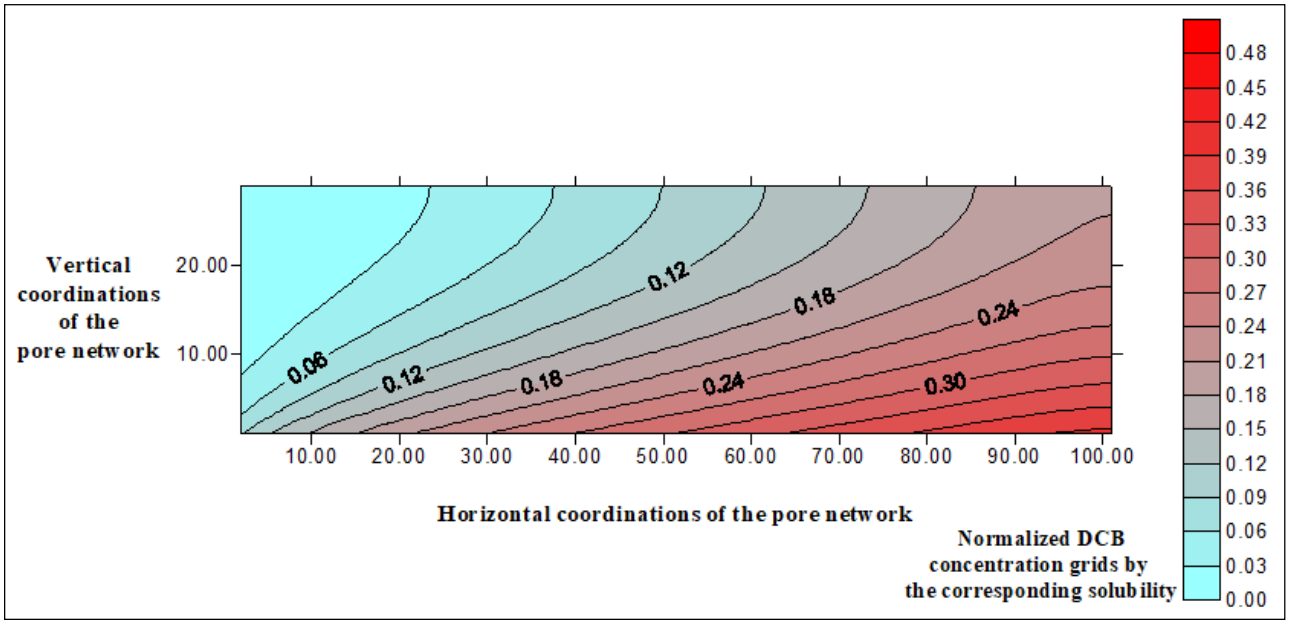

Figure 5.17. Contour plot of the normalized DCB distribution computed with the pore network model for Q = 0.232 mL/min, EtOH = 10 % (glass beads).

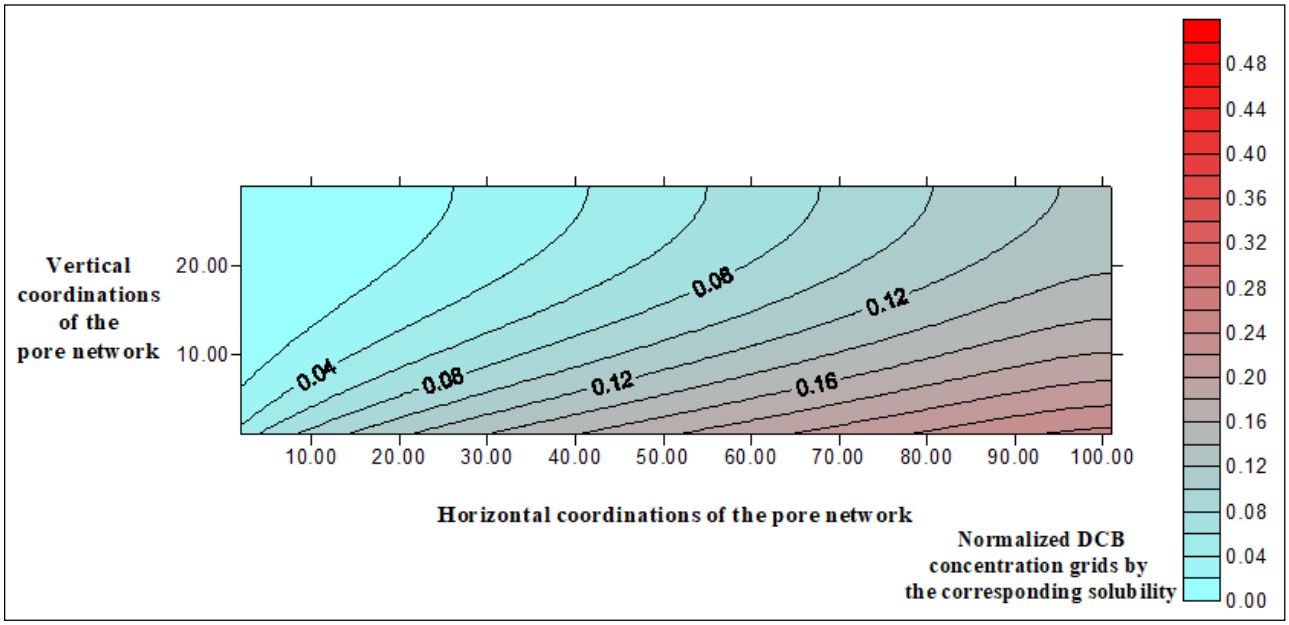

Figure 5.18. Contour plot of the normalized DCB distribution computed with the pore network model for Q = 0.232 mL/min, EtOH = 20 % (glass beads).

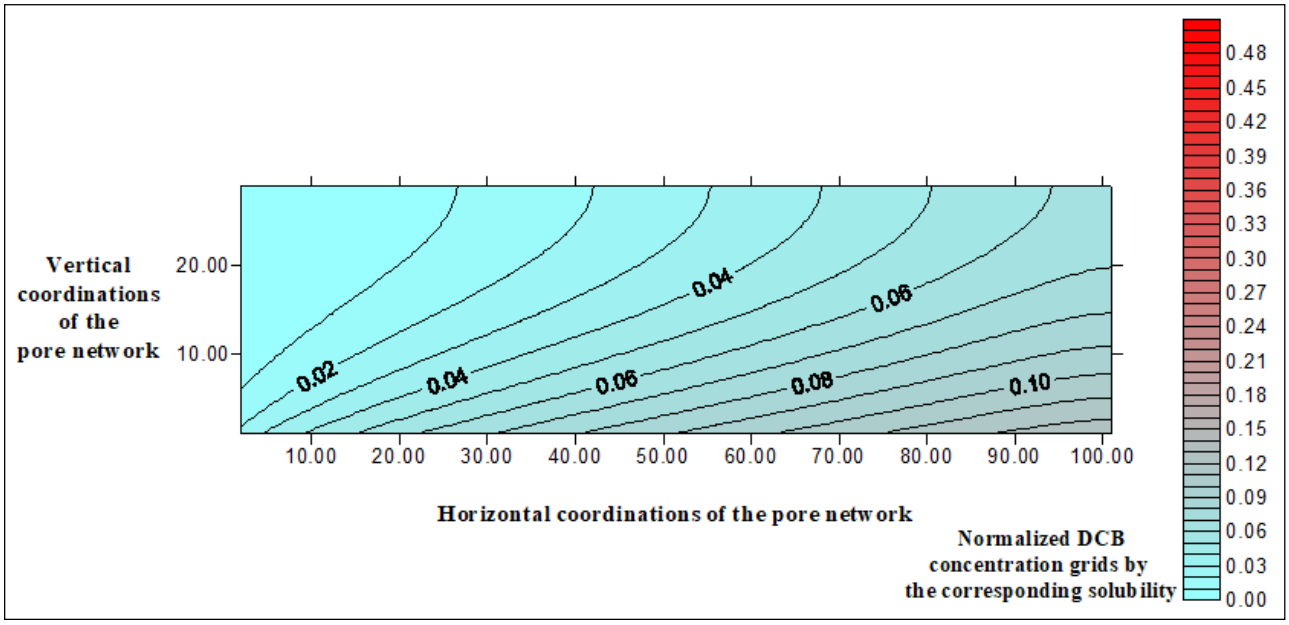

Figure 5.19. Contour plot of the normalized DCB distribution computed with the pore network model for Q = 0.232 mL/min, EtOH = 30 % (glass beads).

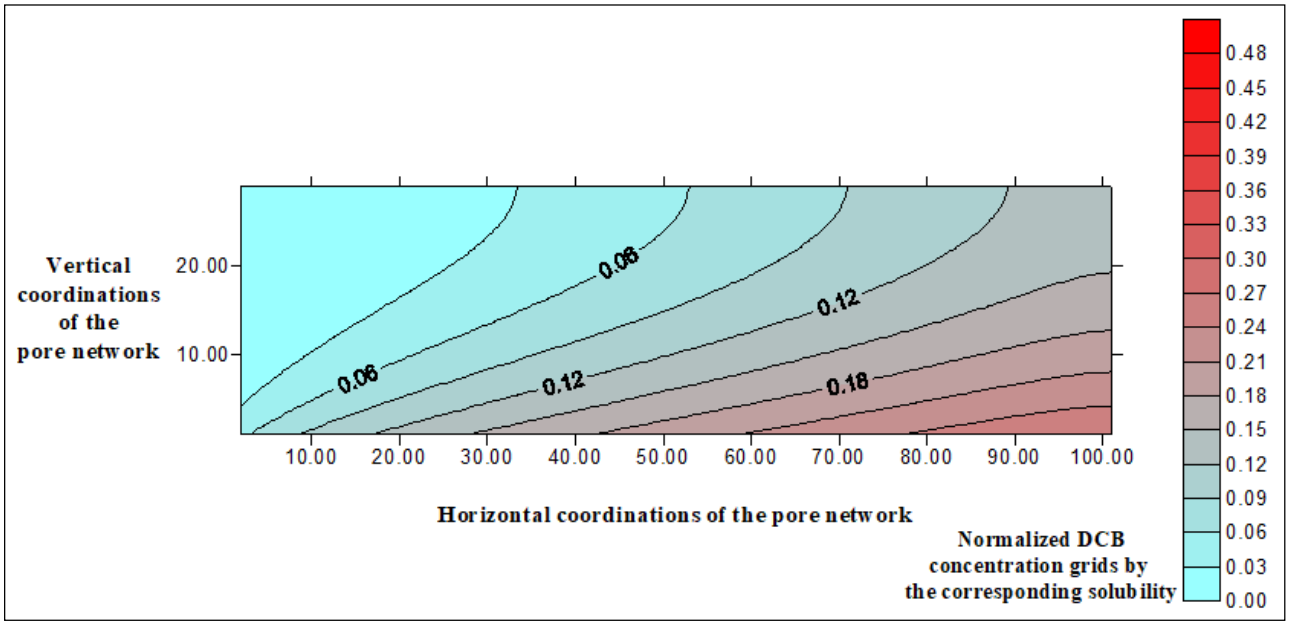

Figure 5.20. Contour plot of the normalized DCB distribution computed with the pore network model for Q = 1 mL/min, EtOH = 0 % (glass beads).

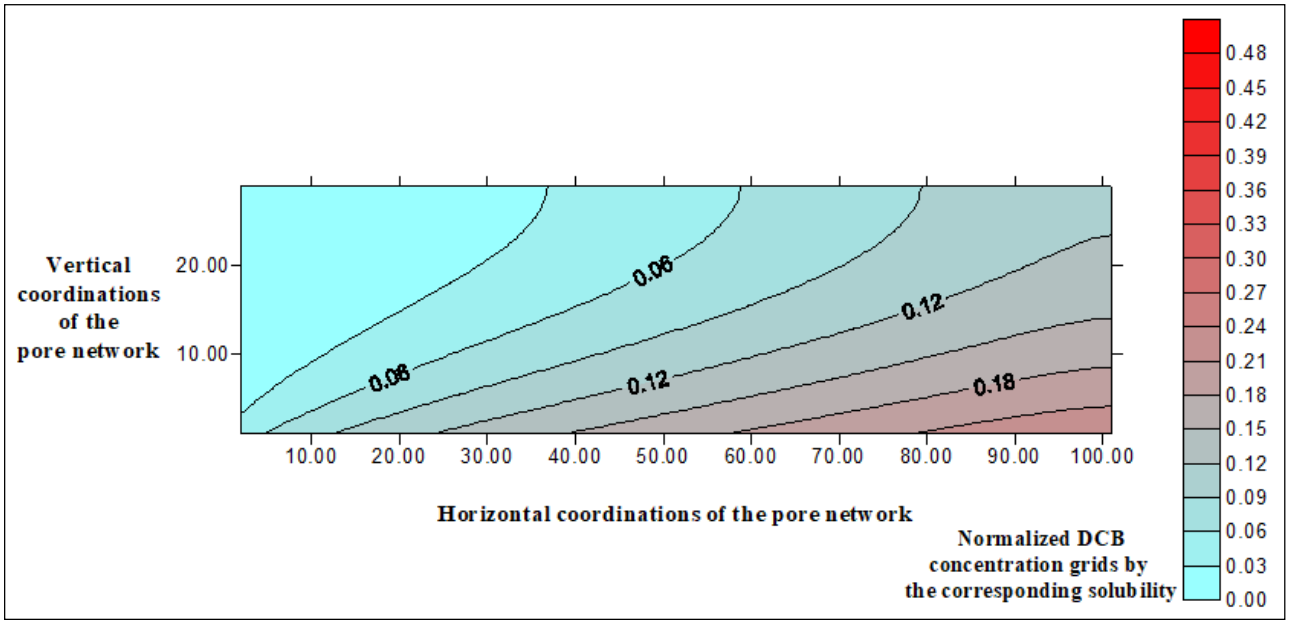

Figure 5.21. Contour plot of the normalized DCB distribution computed with the pore network model for Q = 1 mL/min, EtOH = 10 % (glass beads).

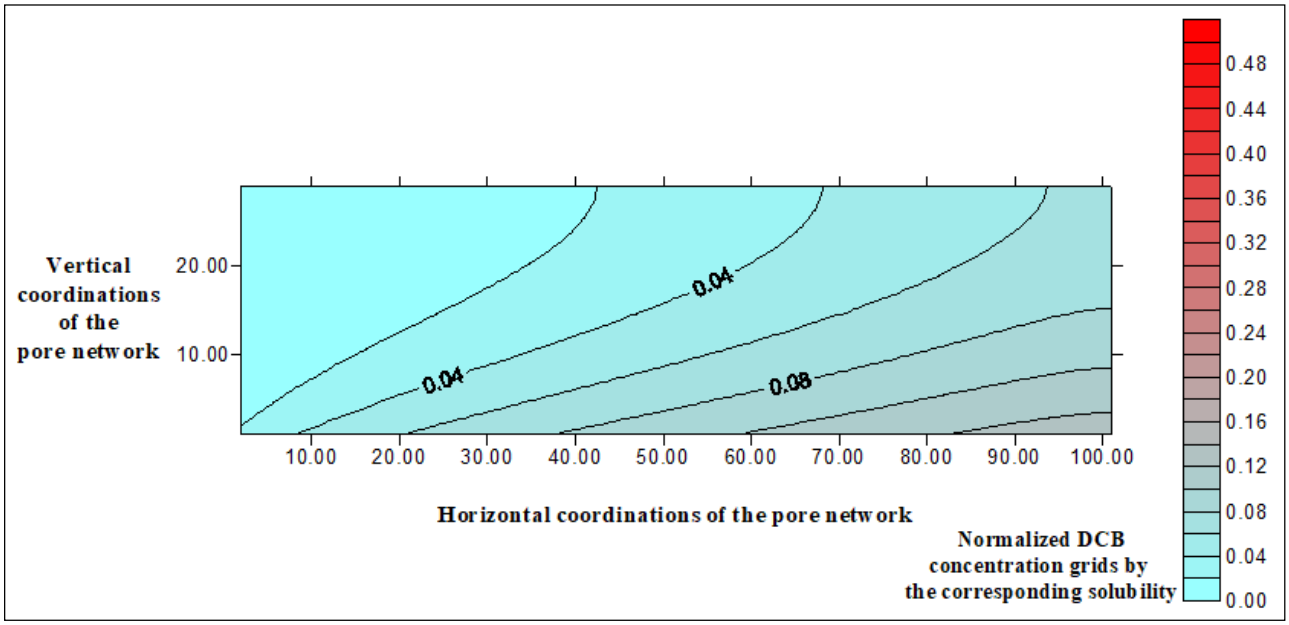

Figure 5.22. Contour plot of the normalized DCB distribution computed with the pore network model for Q = 1 mL/min, EtOH = 20 % (glass beads).

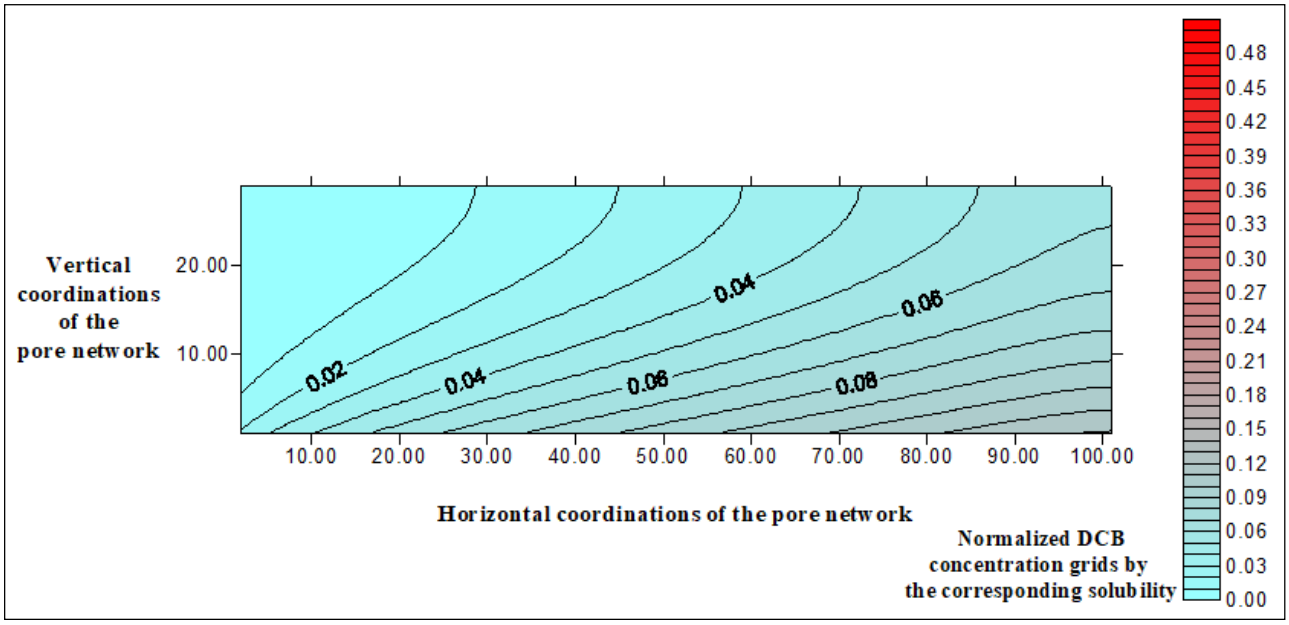

Figure 5.23. Contour plot of the normalized DCB distribution computed with the pore network model for Q = 1 mL/min, EtOH = 30 % (glass beads).

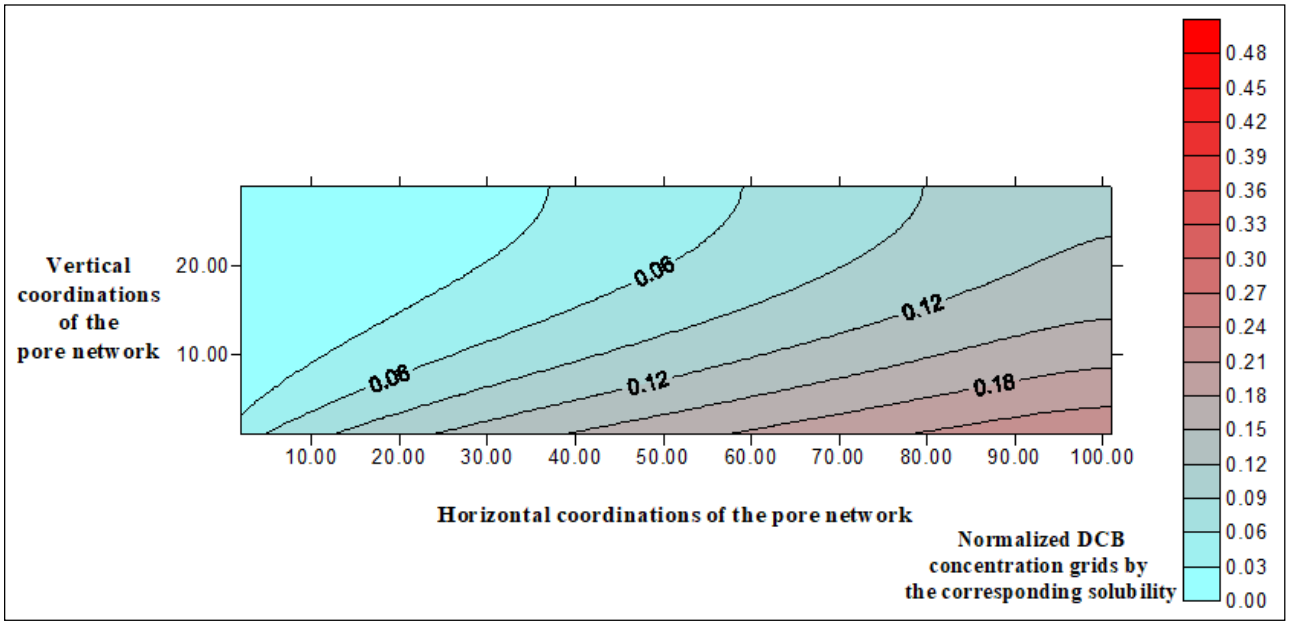

Figure 5.24. Contour plot of the normalized DCB distribution computed with the pore network model for Q = 2 mL/min, EtOH = 0 % (glass beads).

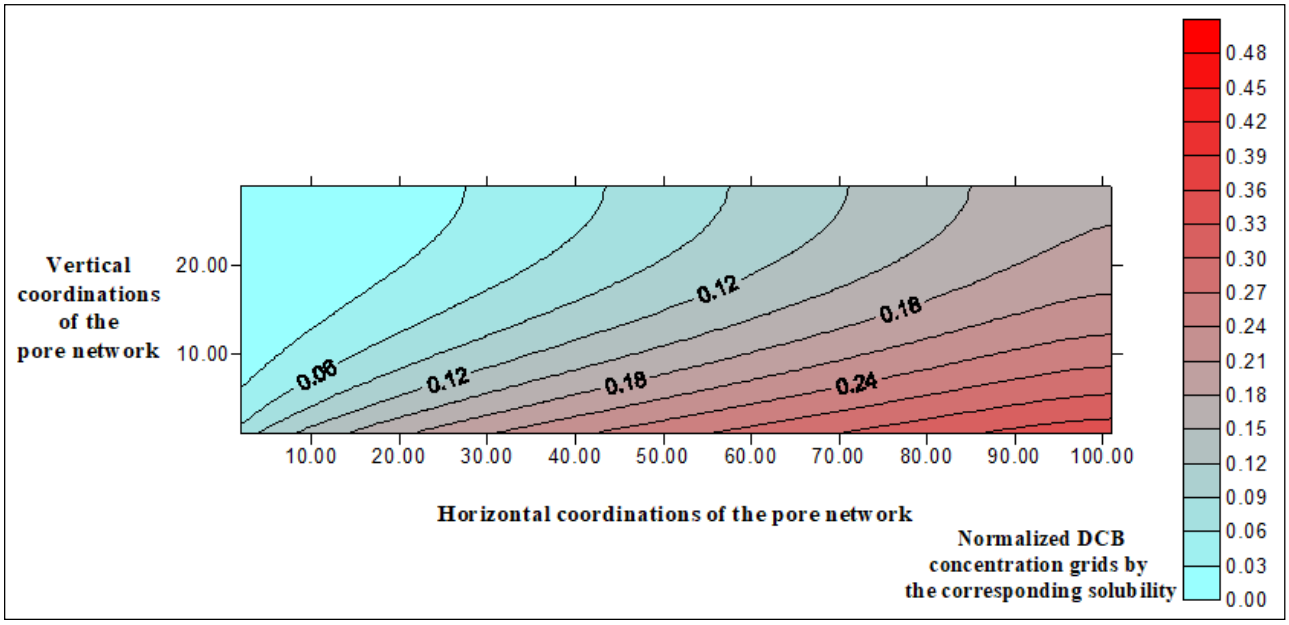

Figure 5.25. Contour plot of the normalized DCB distribution computed with the pore network model for Q = 2 mL/min, EtOH = 10 % (glass beads).

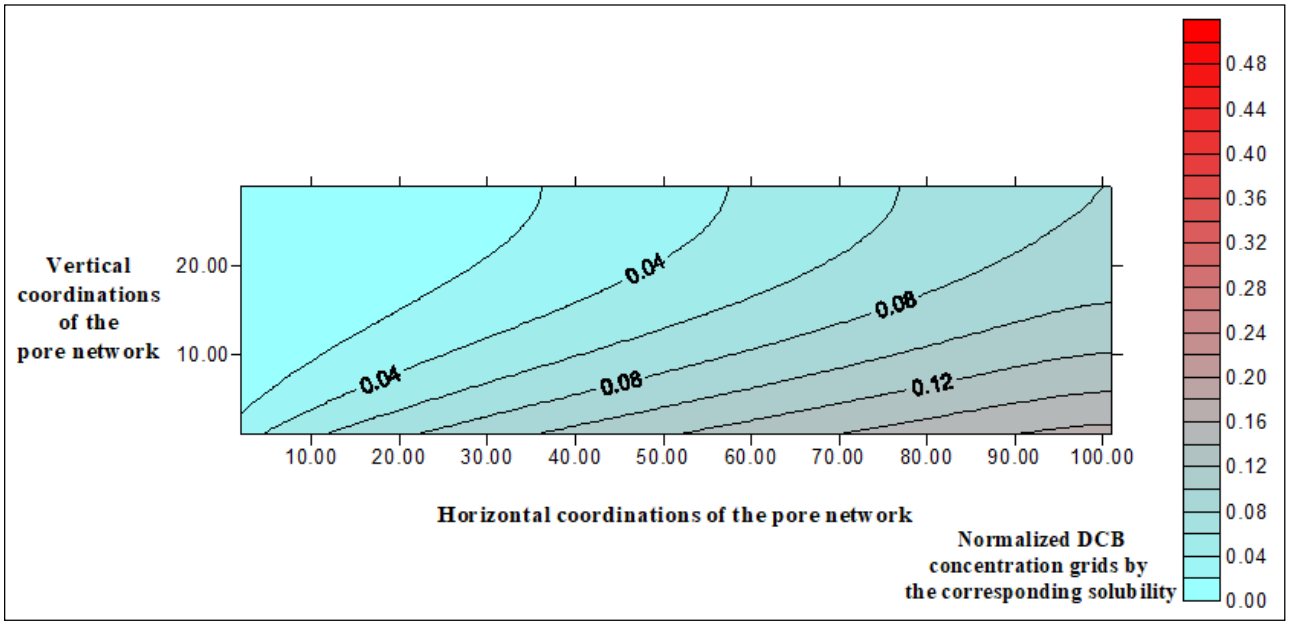

Figure 5.26. Contour plot of the normalized DCB distribution computed with the pore network model for Q = 2 mL/min, EtOH = 20 % (glass beads).

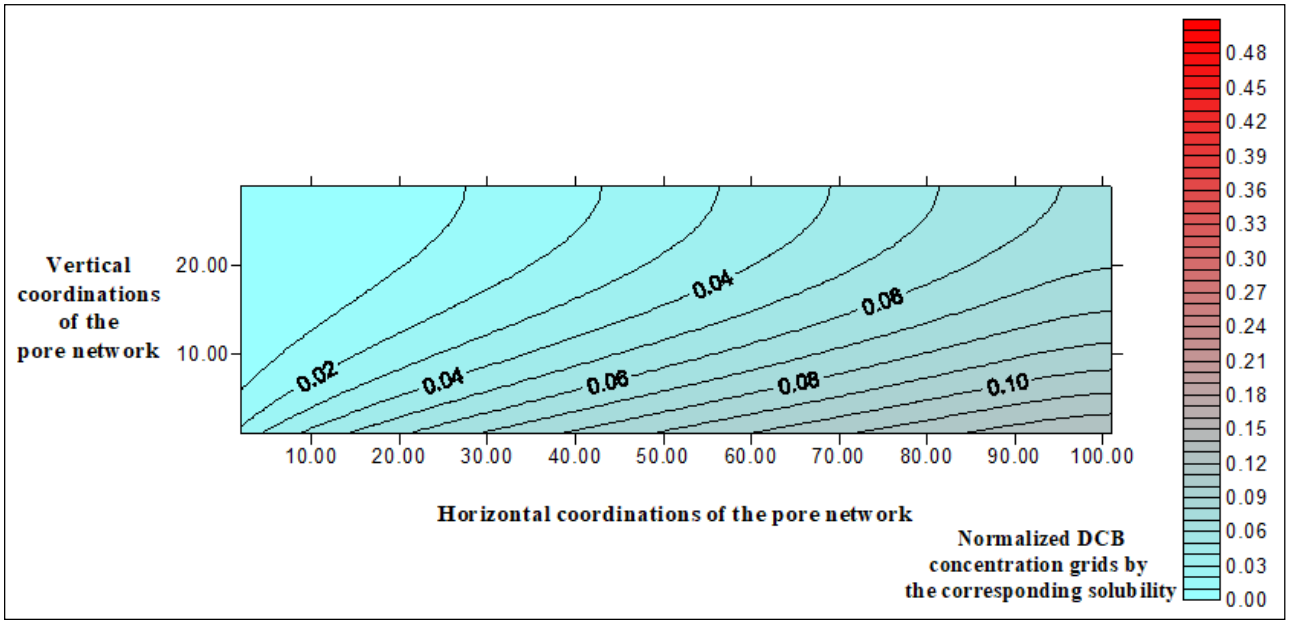

Figure 5.27. Contour plot of the normalized DCB distribution computed with the pore network model for Q = 2 mL/min, EtOH = 30 % (glass beads).

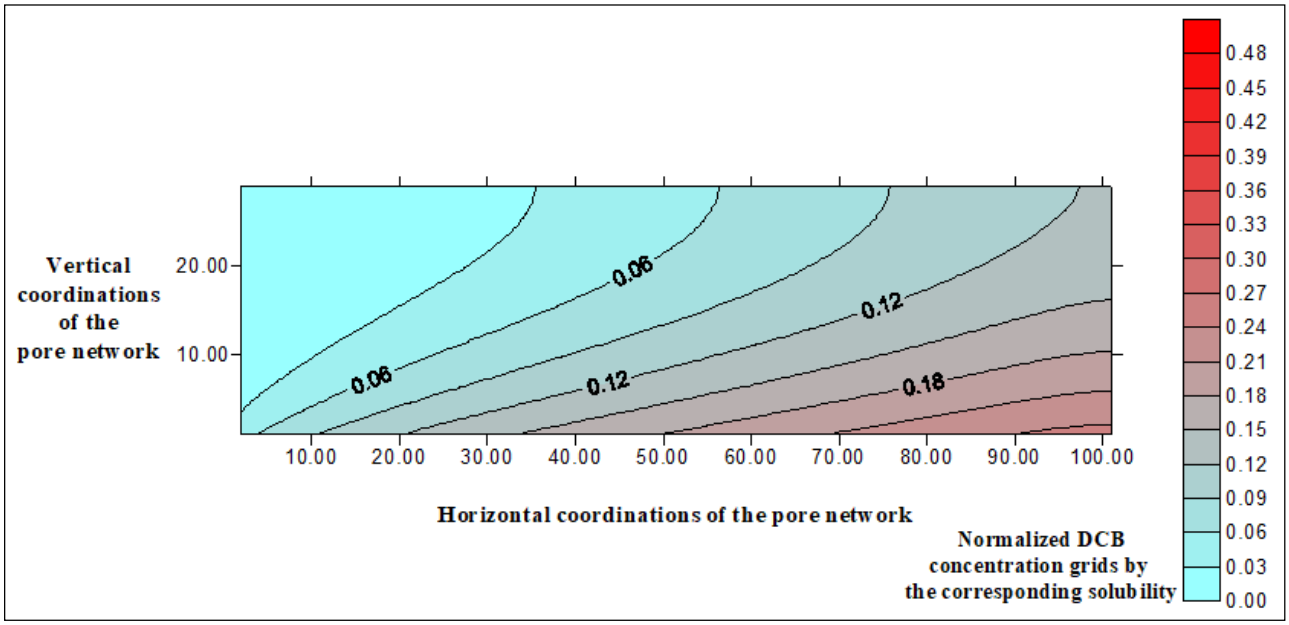

Figure 5.28. Contour plot of the normalized DCB distribution computed with the pore network model for Q = 5 mL/min, EtOH = 0 % (glass beads).

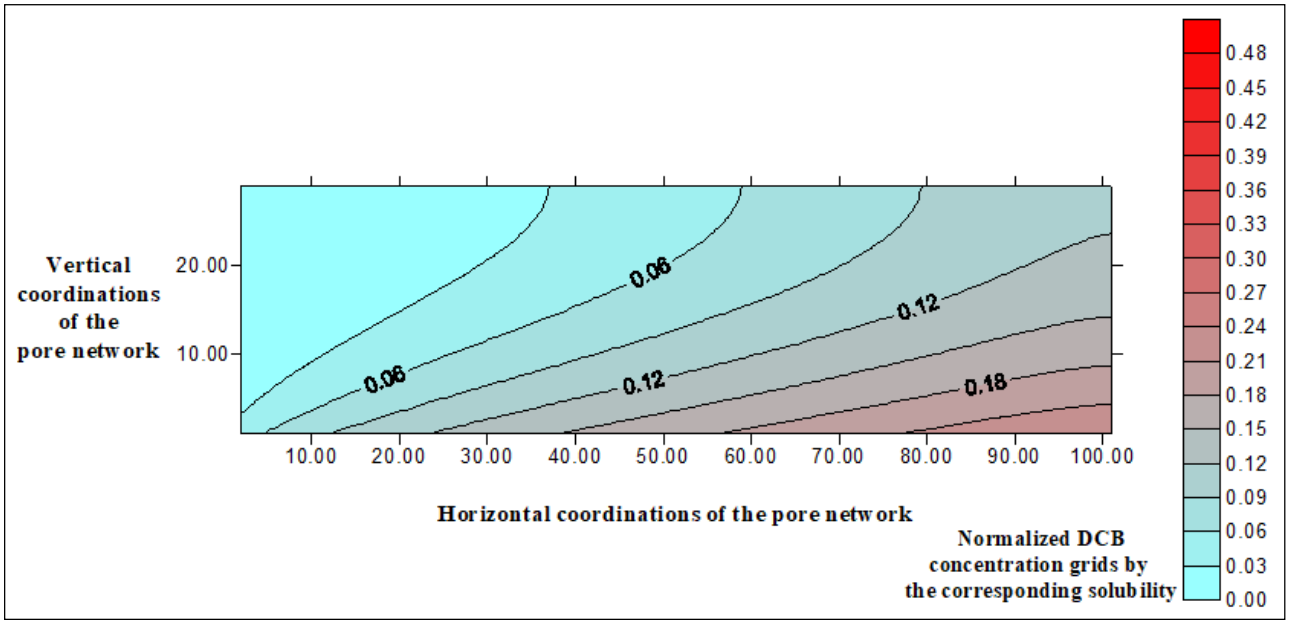

Figure 5.29. Contour plot of the normalized DCB distribution computed with the pore network model for Q = 5 mL/min, EtOH = 10 % (glass beads).

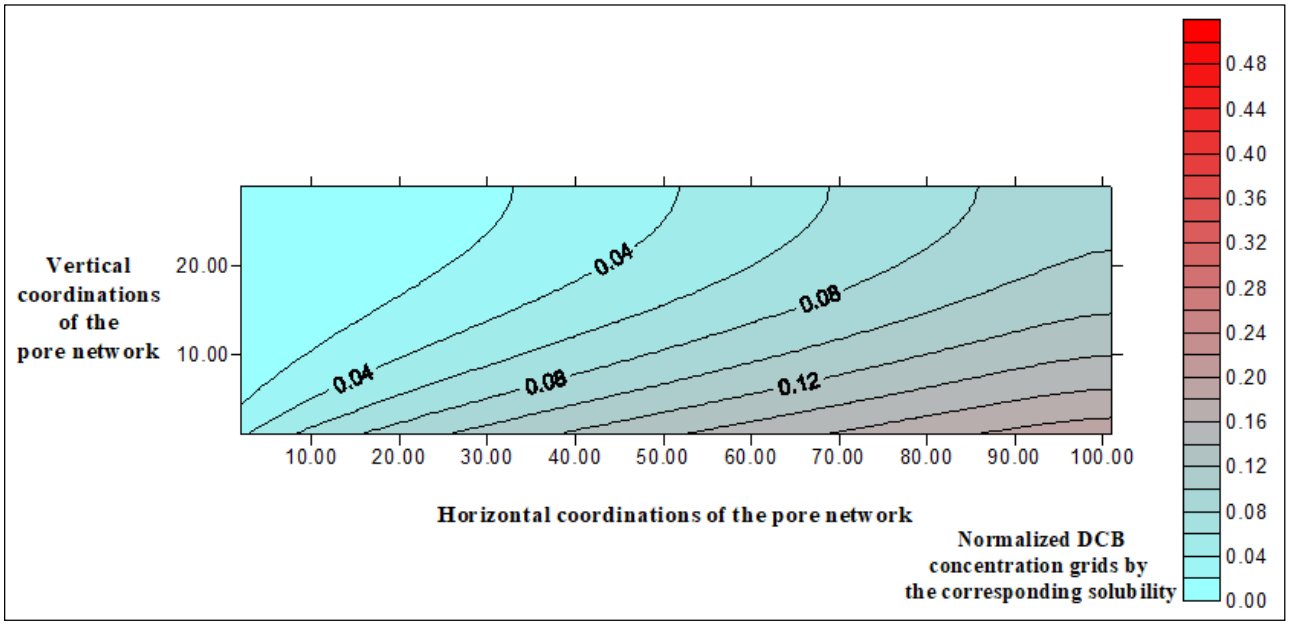

Figure 5.30. Contour plot of the normalized DCB distribution computed with the pore network model for Q = 5 mL/min, EtOH = 20 % (glass beads).

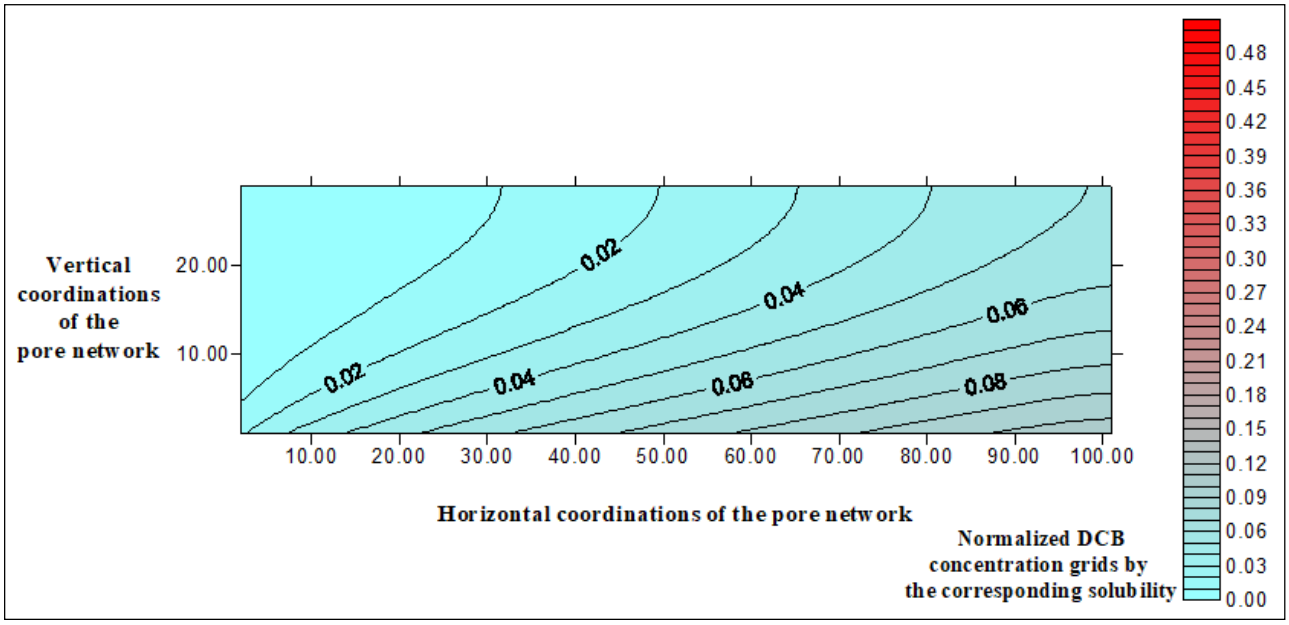

Figure 5.31. Contour plot of the normalized DCB distribution computed with the pore network model for Q = 5 mL/min, EtOH = 30 % (glass beads).

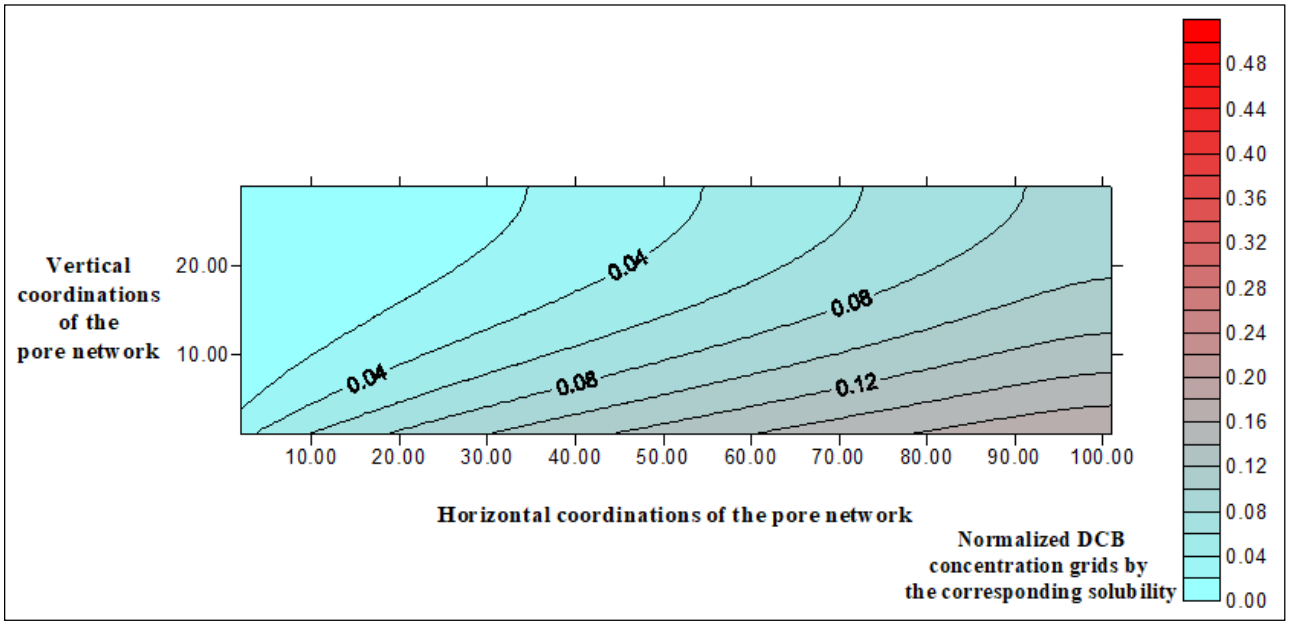

Figure 5.32. Contour plot of the normalized DCB distribution computed with the pore network model for Q = 25 mL/min, EtOH = 0 % (glass beads).

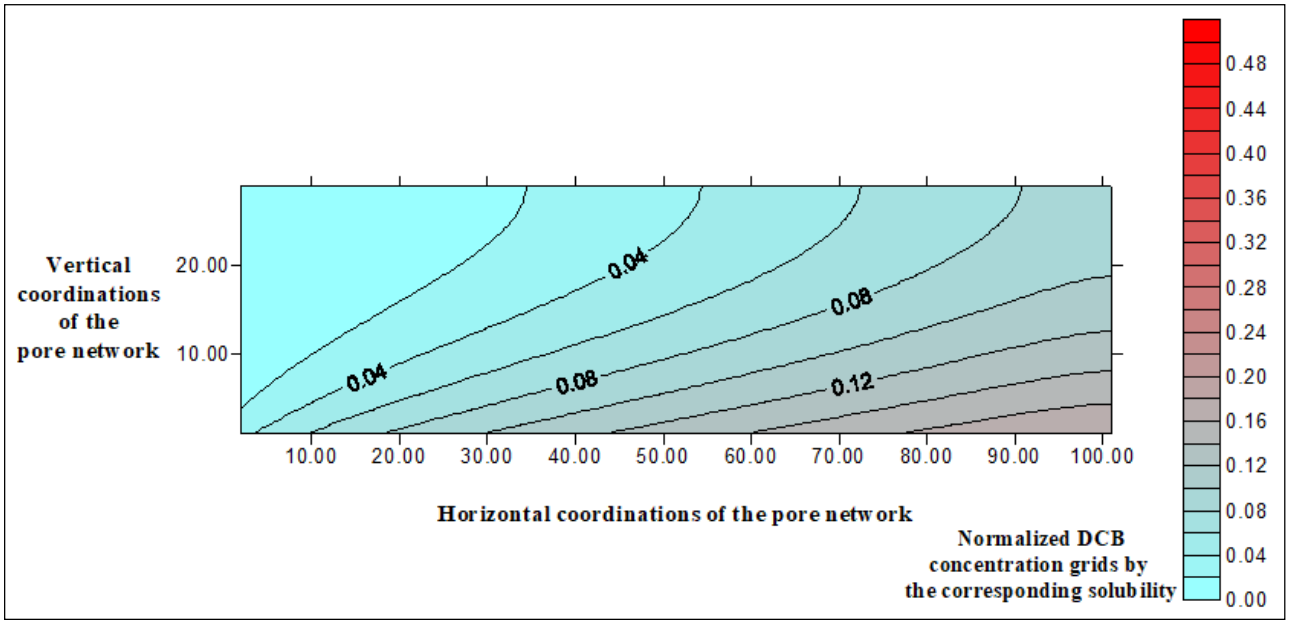

Figure 5.33. Contour plot of the normalized DCB distribution computed with the pore network model for Q = 25 mL/min, EtOH = 10 % (glass beads).

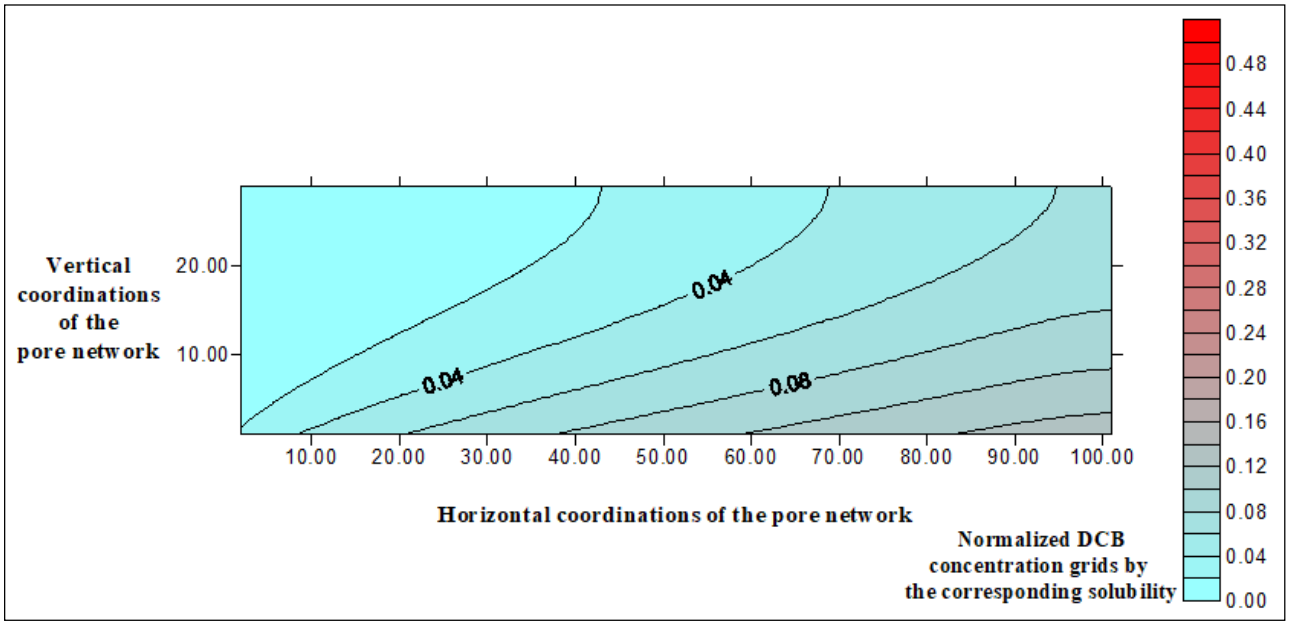

Figure 5.34. Contour plot of the normalized DCB distribution computed with the pore network model for Q = 25 mL/min, EtOH = 20 % (glass beads).

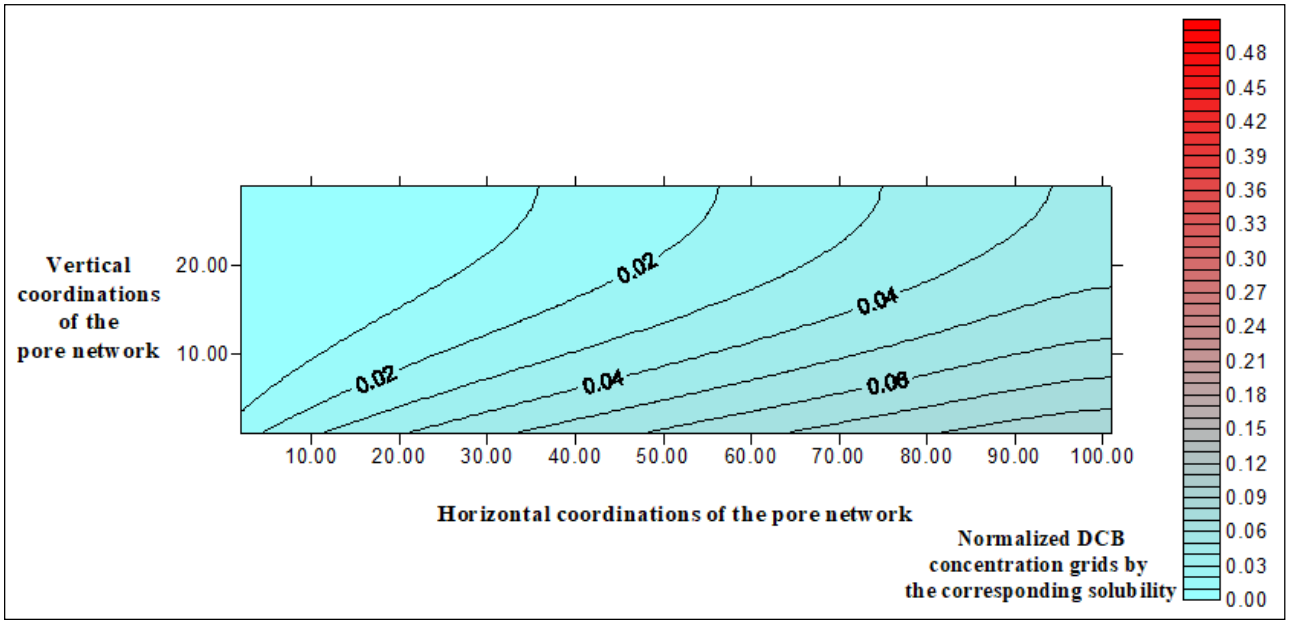

Figure 5.35. Contour plot of the normalized DCB distribution computed with the pore network model for Q = 25 mL/min, EtOH = 30 % (glass beads).

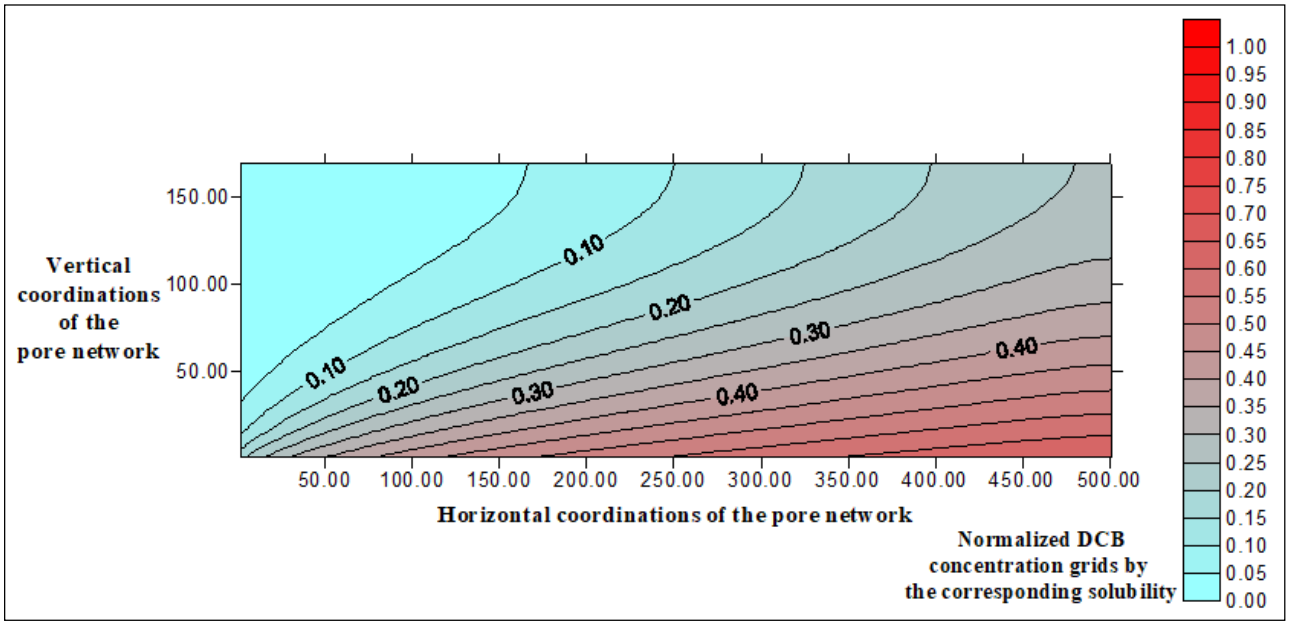

Figure 5.36. Contour plot of the normalized DCB distribution computed with the pore network model for Q = 0.156 mL/min, EtOH = 0 % (sand).

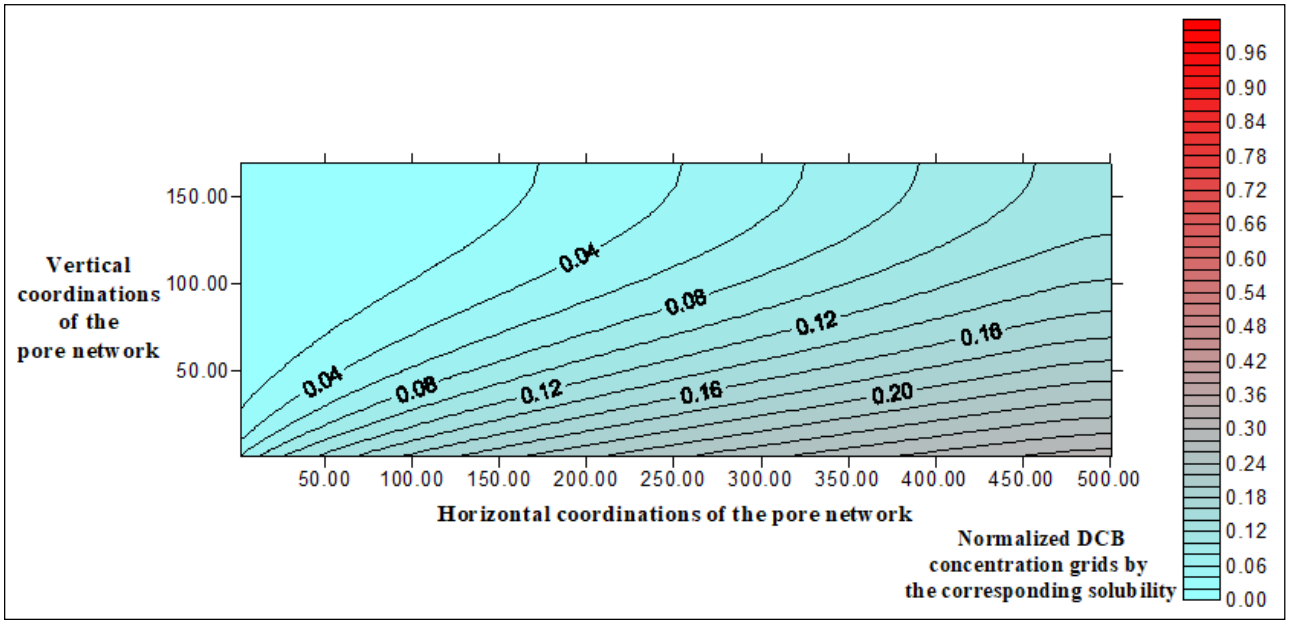

Figure 5.37. Contour plot of the normalized DCB distribution computed with the pore network model for Q = 0.156 mL/min, EtOH = 40 % (sand).

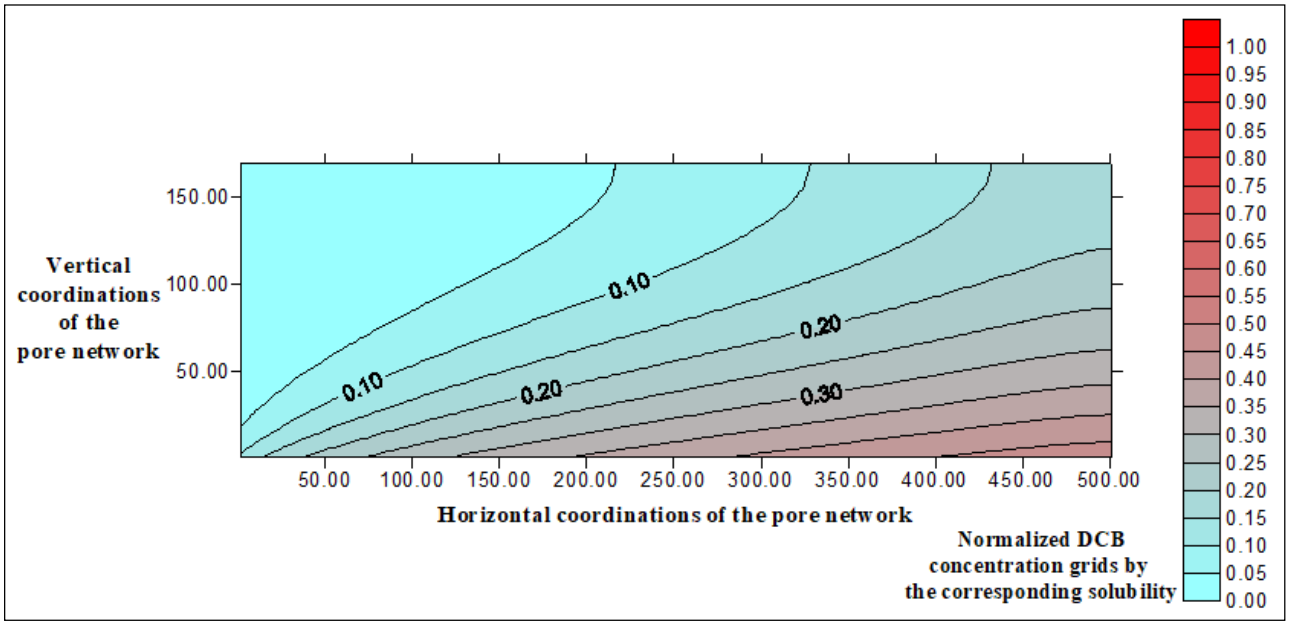

Figure 5.38. Contour plot of the normalized DCB distribution computed with the pore network model for Q = 0.187 mL/min, EtOH = 0 % (sand).

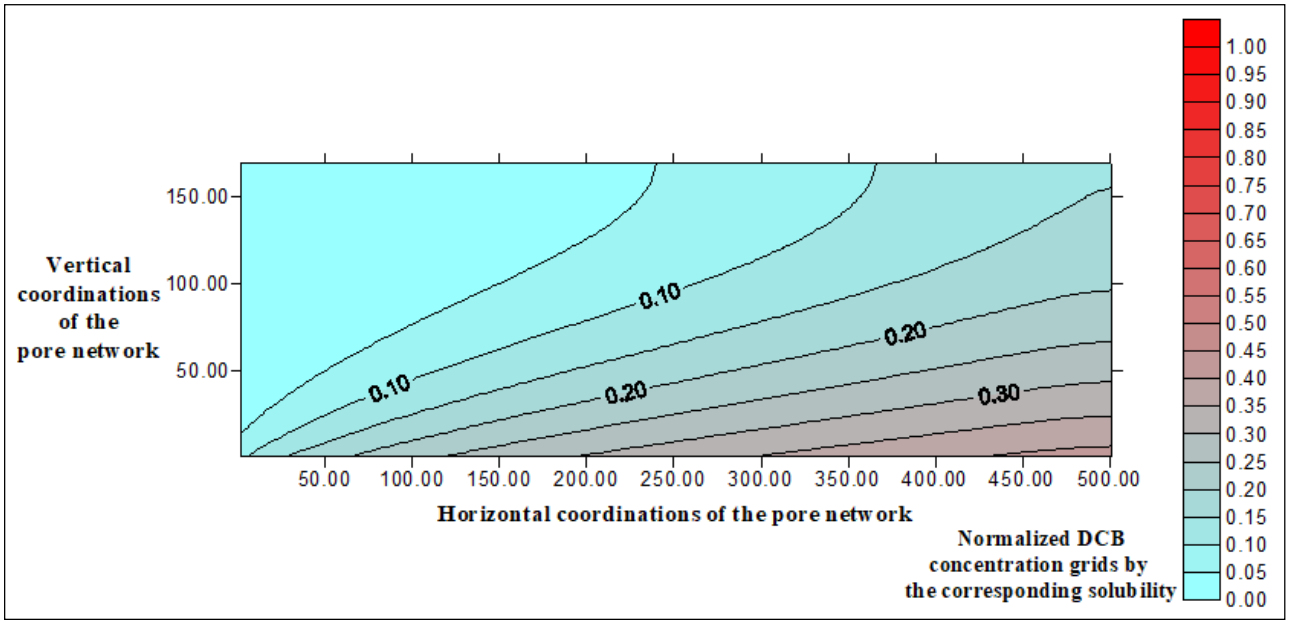

Figure 5.39. Contour plot of the normalized DCB distribution computed with the pore network model for Q = 0.187 mL/min, EtOH = 10 % (sand).

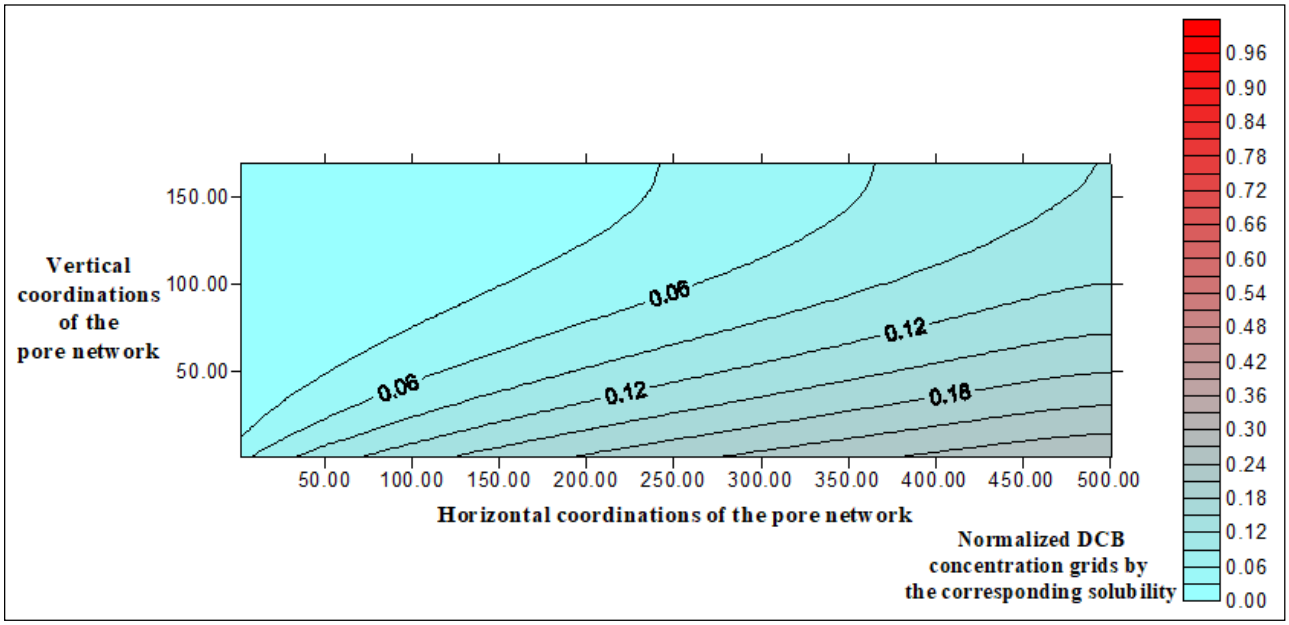

Figure 5.40. Contour plot of the normalized DCB distribution computed with the pore network model for Q = 0.187 mL/min, EtOH = 20 % (sand).

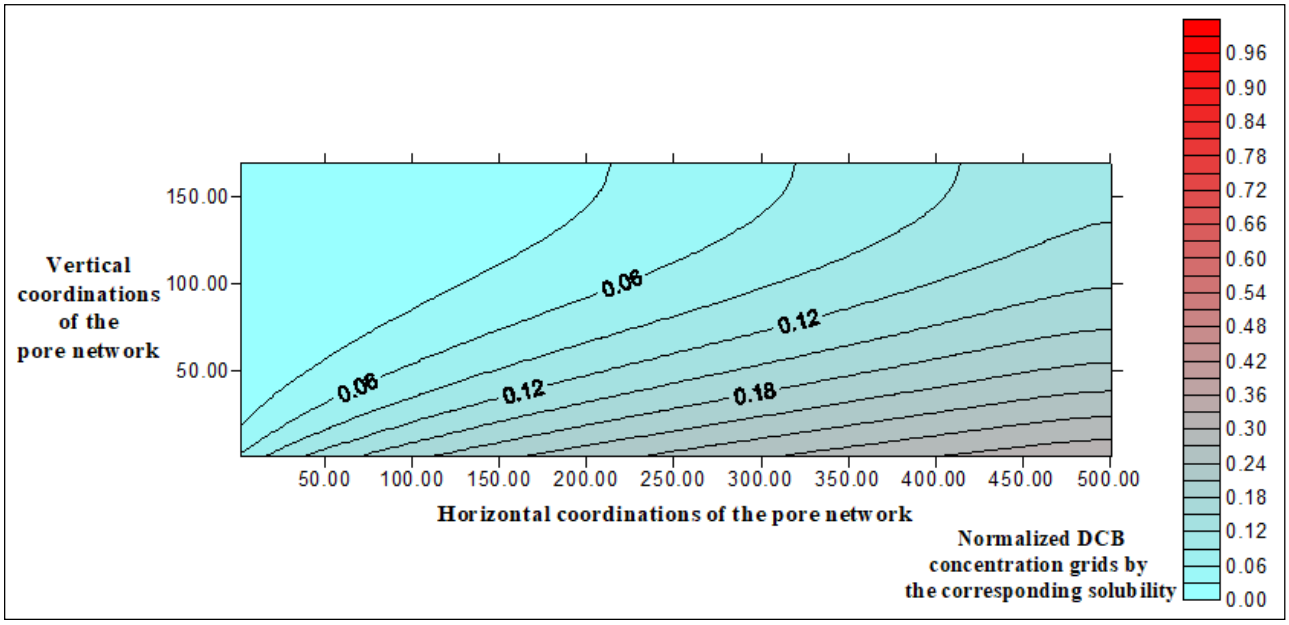

Figure 5.41. Contour plot of the normalized DCB distribution computed with the pore network model for Q = 0.187 mL/min, EtOH = 30 % (sand).

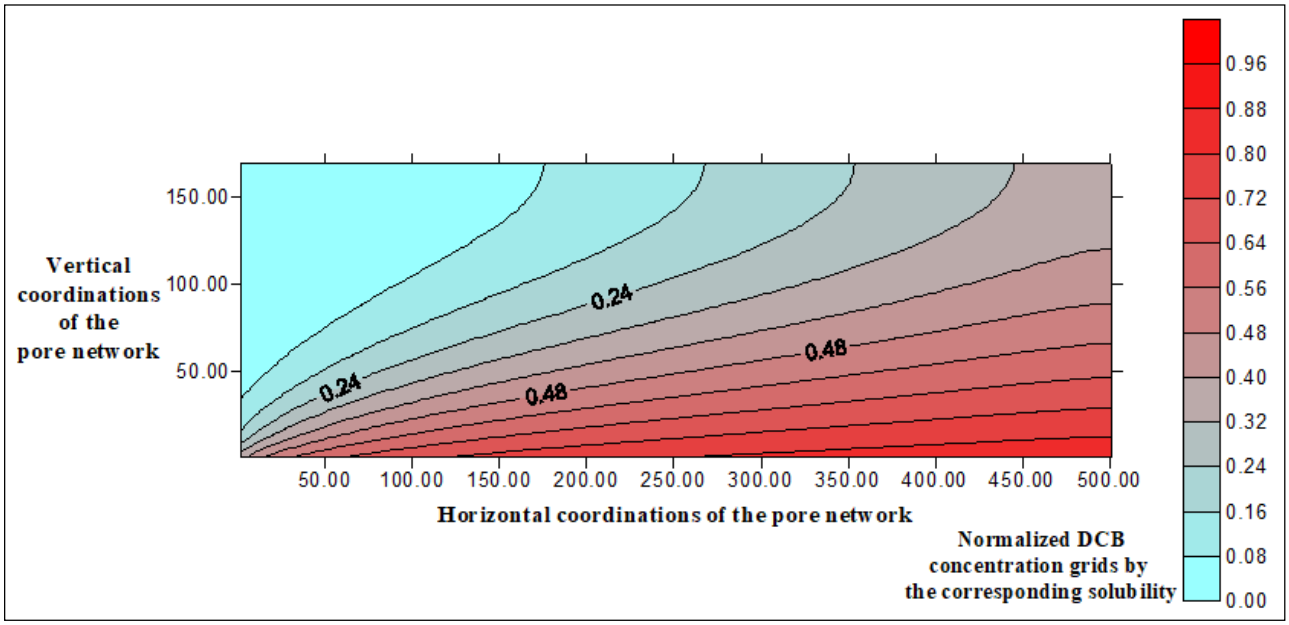

Figure 5.42. Contour plot of the normalized DCB distribution computed with the pore network model for Q = 1 mL/min, EtOH = 0 % (sand).

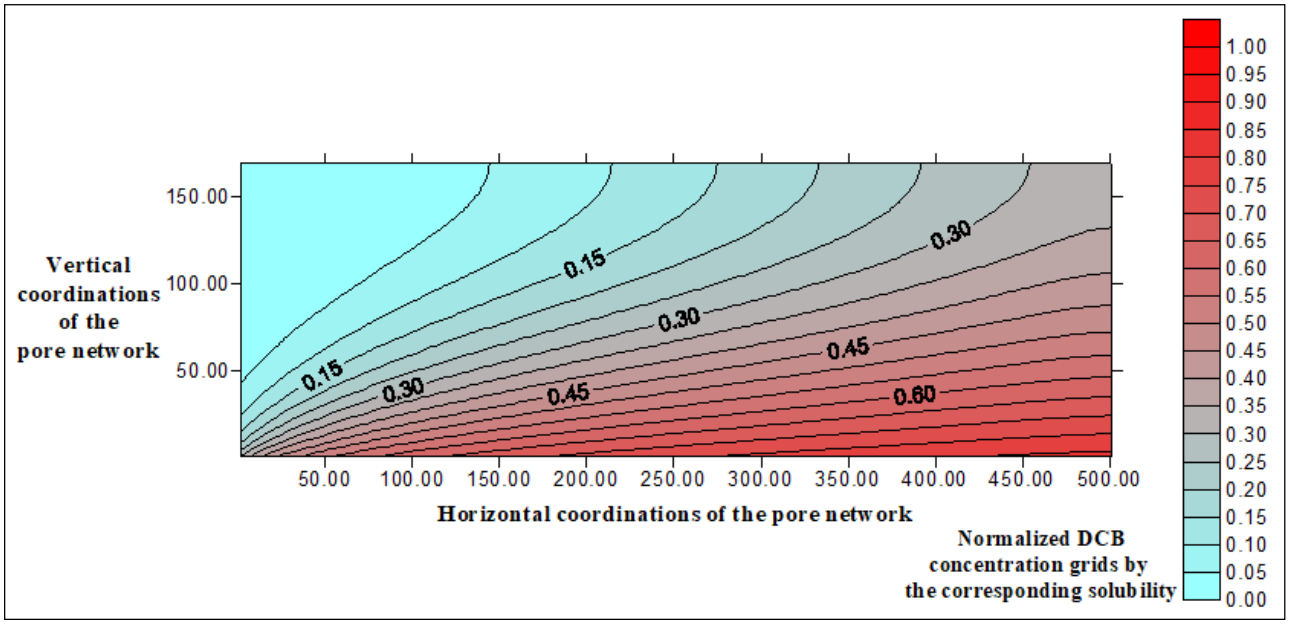

Figure 5.43. Contour plot of the normalized DCB distribution computed with the pore network model for Q = 1 mL/min, EtOH = 10 % (sand).

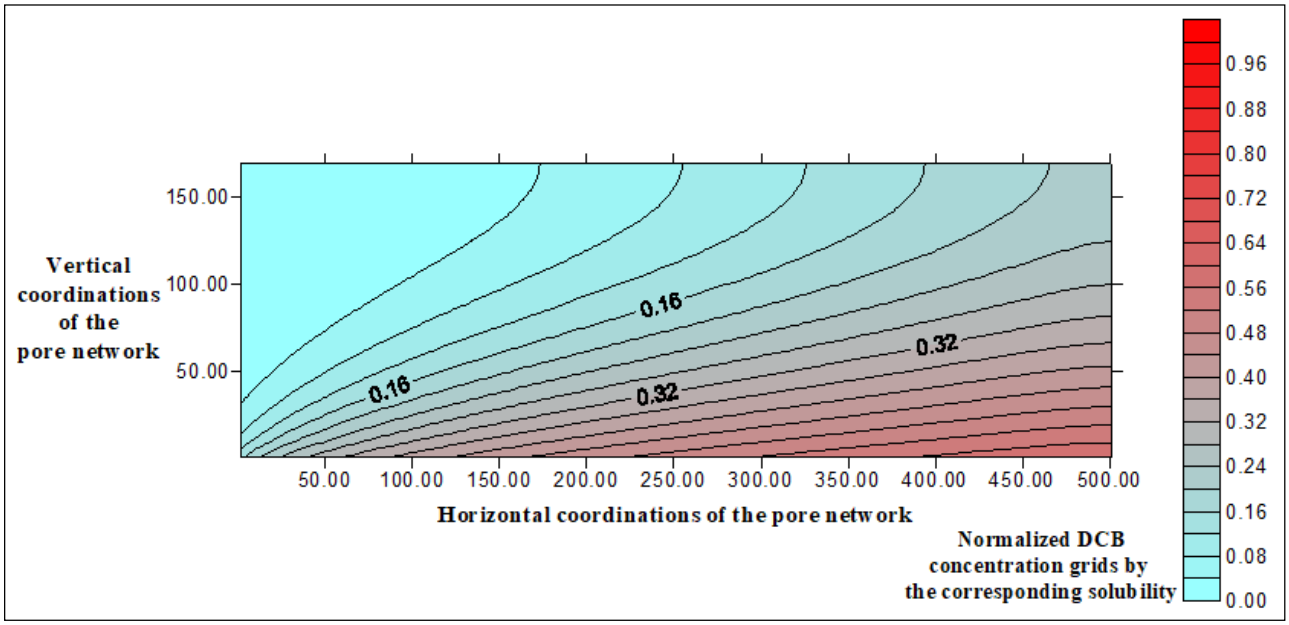

Figure 5.44. Contour plot of the normalized DCB distribution computed with the pore network model for Q = 1 mL/min, EtOH = 20 % (sand).

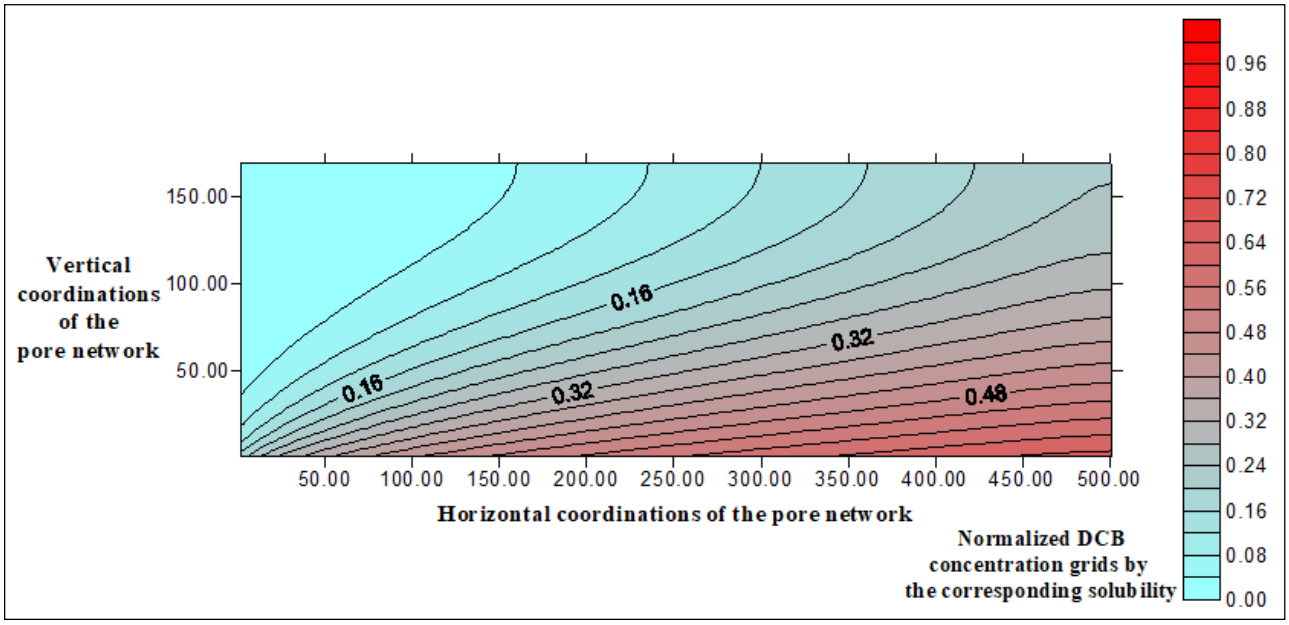

Figure 5.45. Contour plot of the normalized DCB distribution computed with the pore network model for Q = 1 mL/min, EtOH = 30 % (sand).

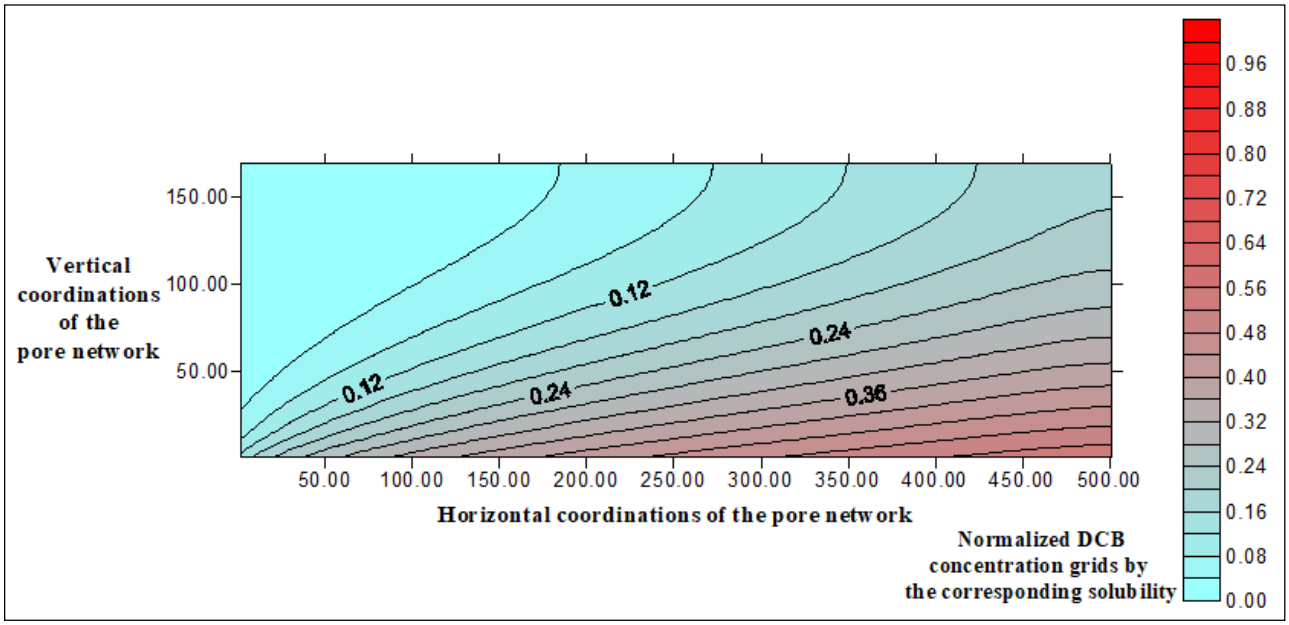

Figure 5.46. Contour plot of the normalized DCB distribution computed with the pore network model for Q = 1 mL/min, EtOH = 40 % (sand).

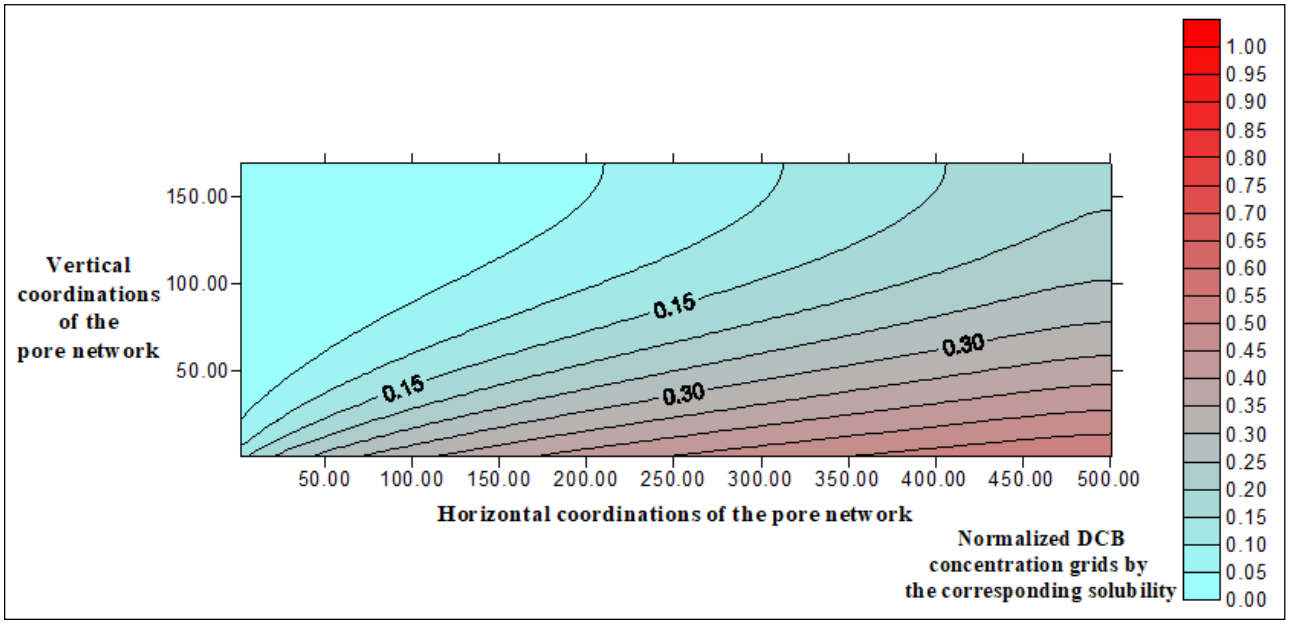

Figure 5.47. Contour plot of the normalized DCB distribution computed with the pore network model for Q = 2 mL/min, EtOH = 0 % (sand).

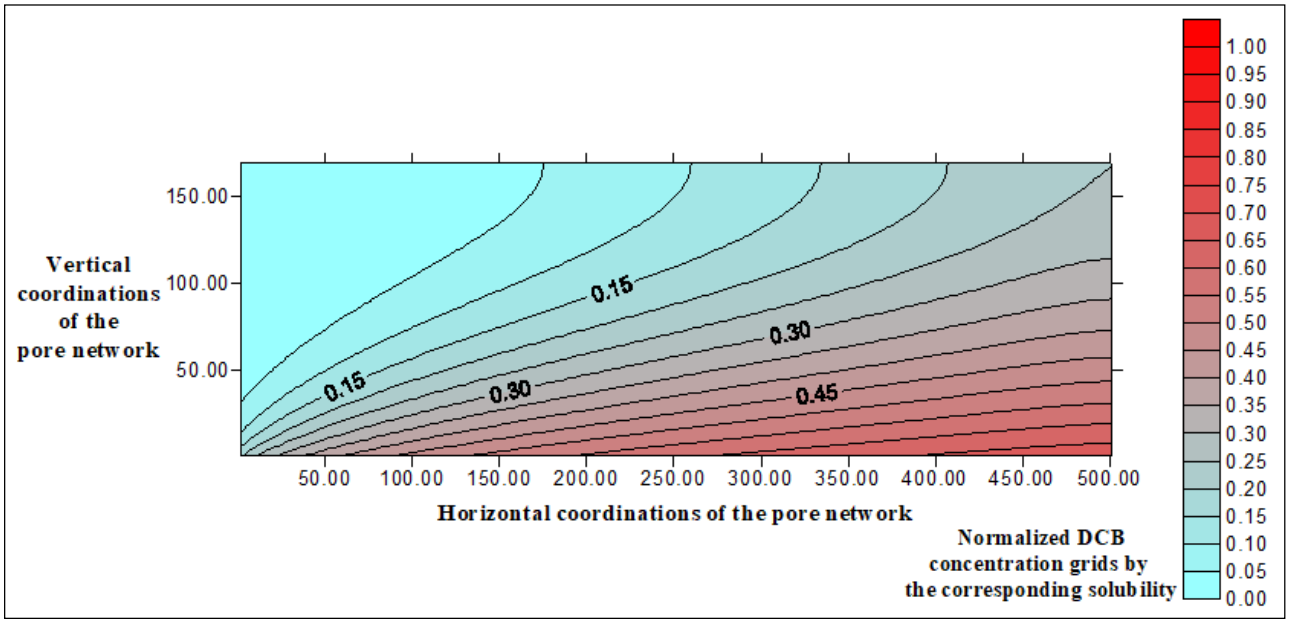

Figure 5.48. Contour plot of the normalized DCB distribution computed with the pore network model for Q = 2 mL/min, EtOH = 10 % (sand).

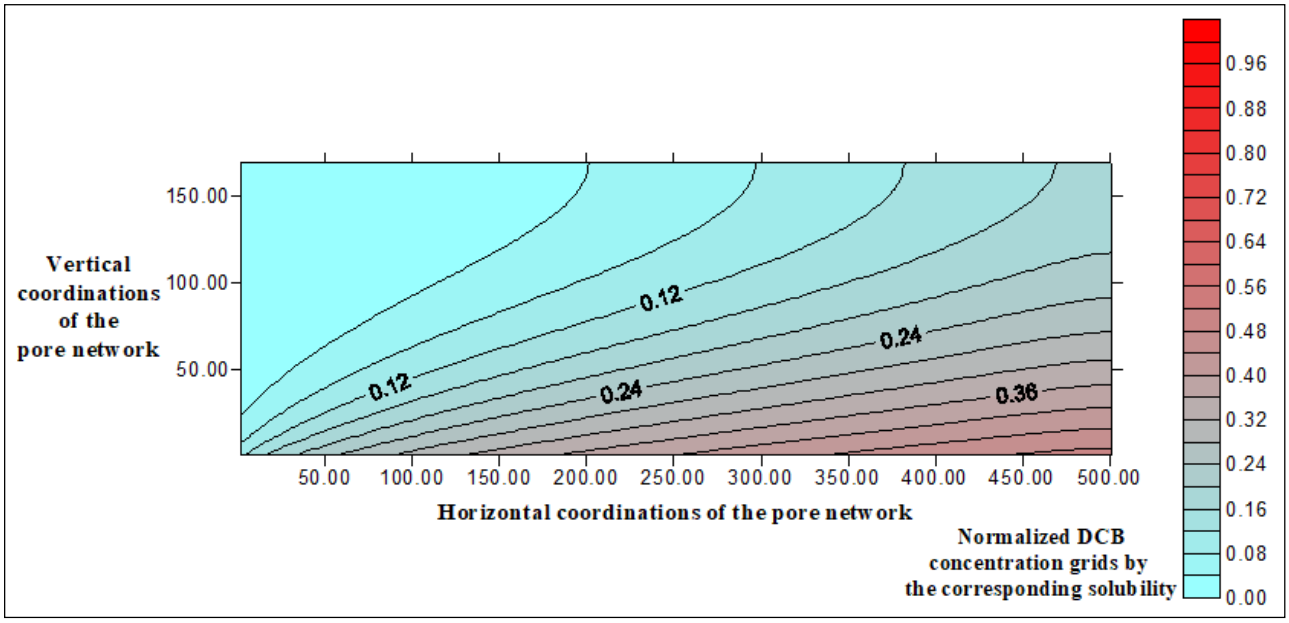

Figure 5.49. Contour plot of the normalized DCB distribution computed with the pore network model for Q = 2 mL/min, EtOH = 20 % (sand).

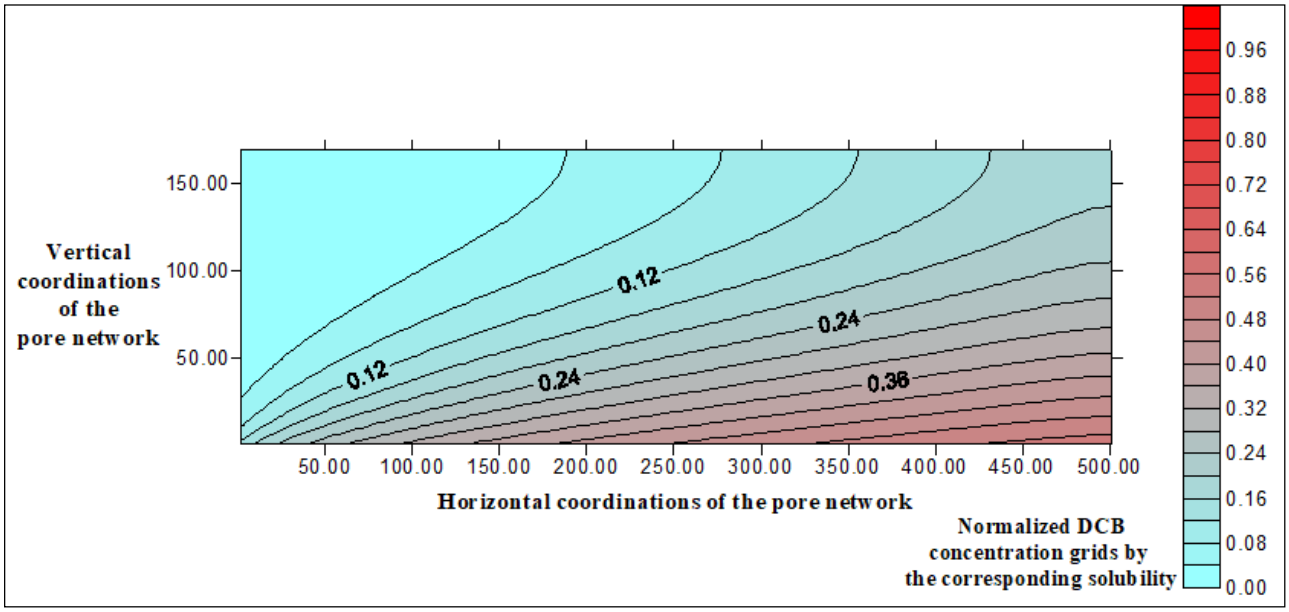

Figure 5.50. Contour plot of the normalized DCB distribution computed with the pore network model for Q = 2 mL/min, EtOH = 30 % (sand).

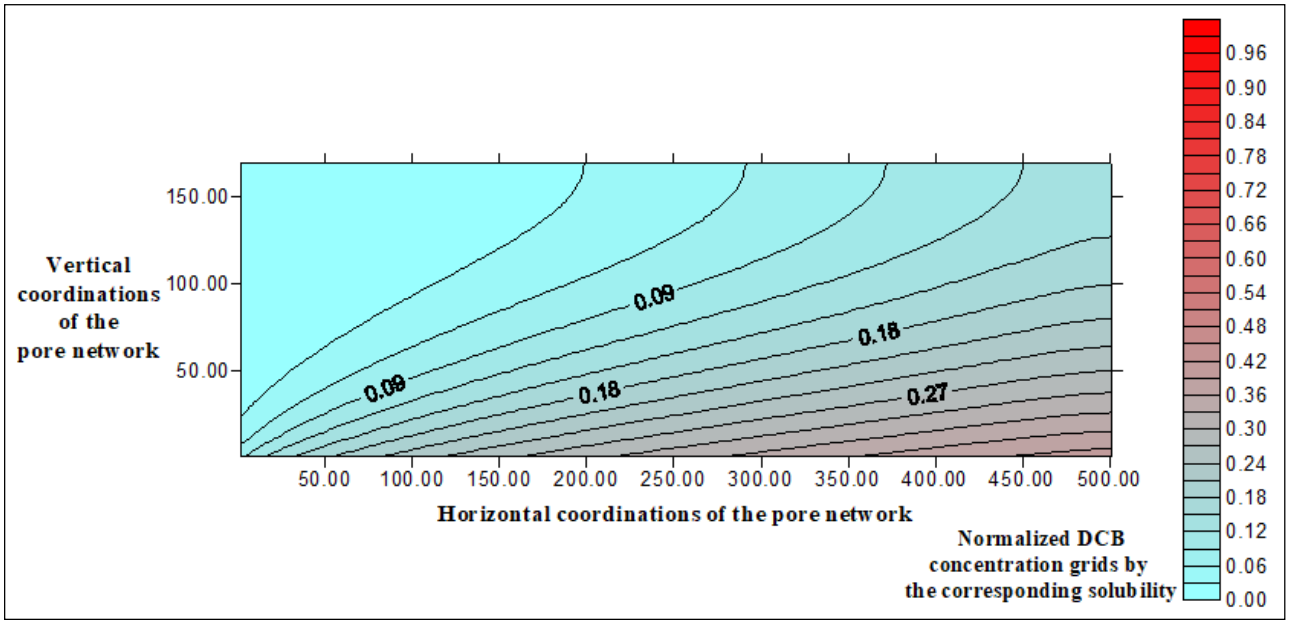

Figure 5.51. Contour plot of the normalized DCB distribution computed with the pore network model for Q = 2 mL/min, EtOH = 40 % (sand).

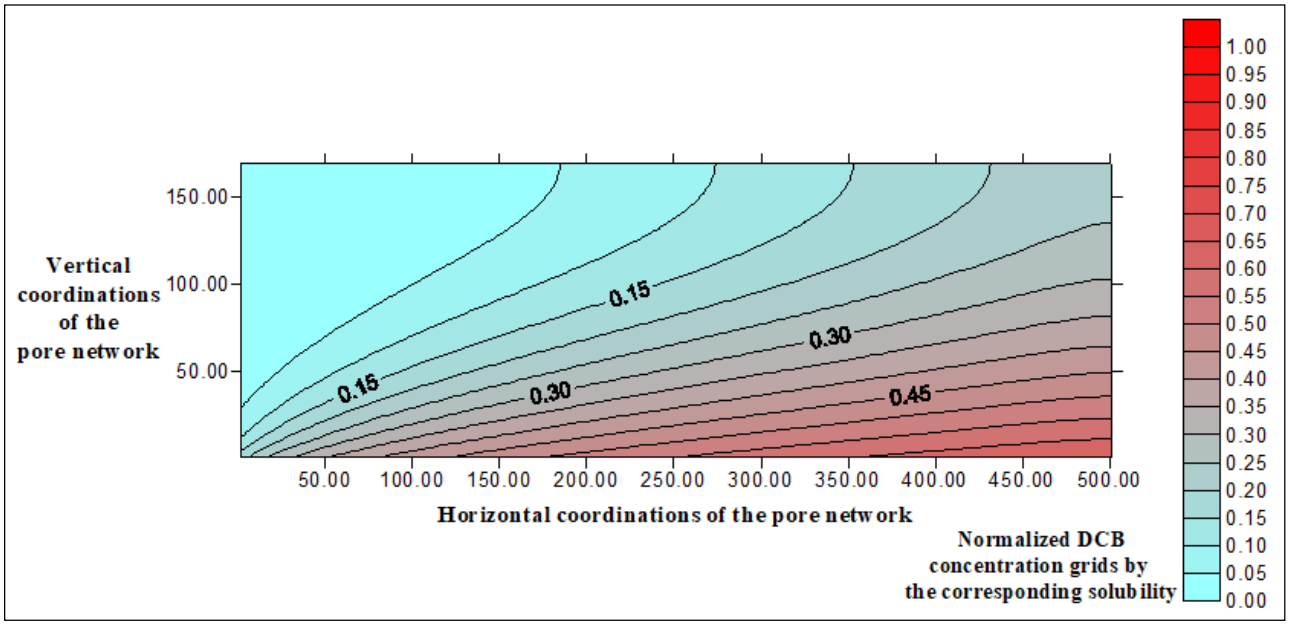

Figure 5.52. Contour plot of the normalized DCB distribution computed with the pore network model for Q = 5 mL/min, EtOH = 0 % (sand).

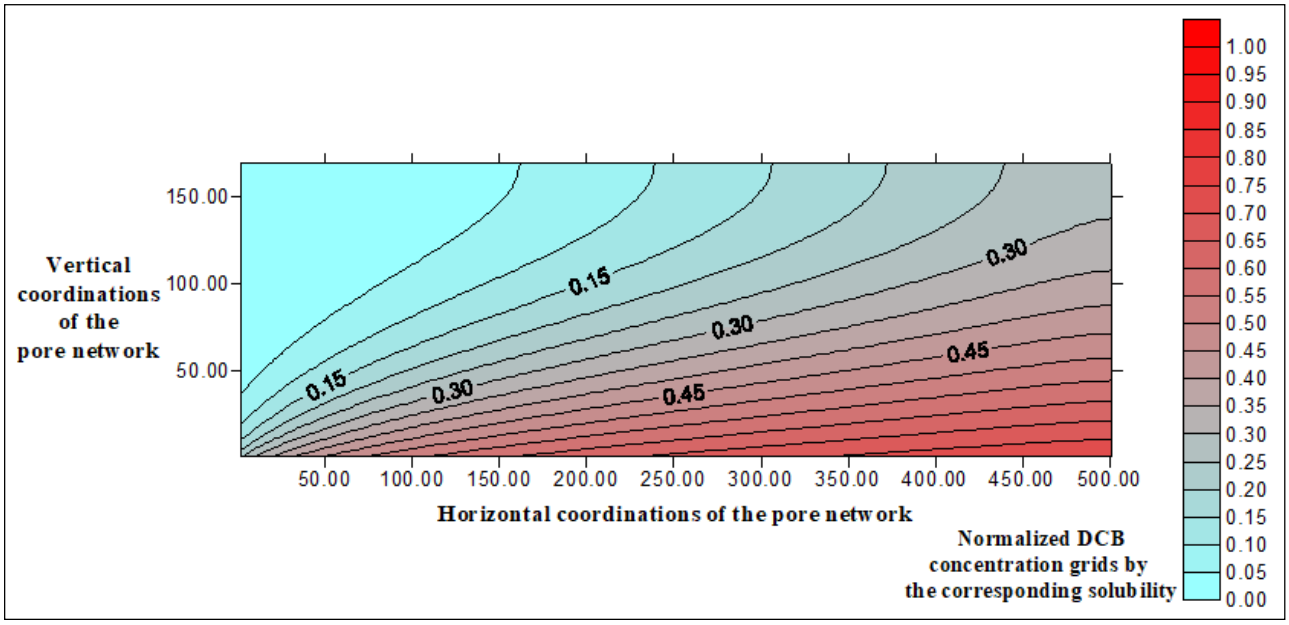

Figure 5.53. Contour plot of the normalized DCB distribution computed with the pore network model for Q = 5 mL/min, EtOH = 10 % (sand).

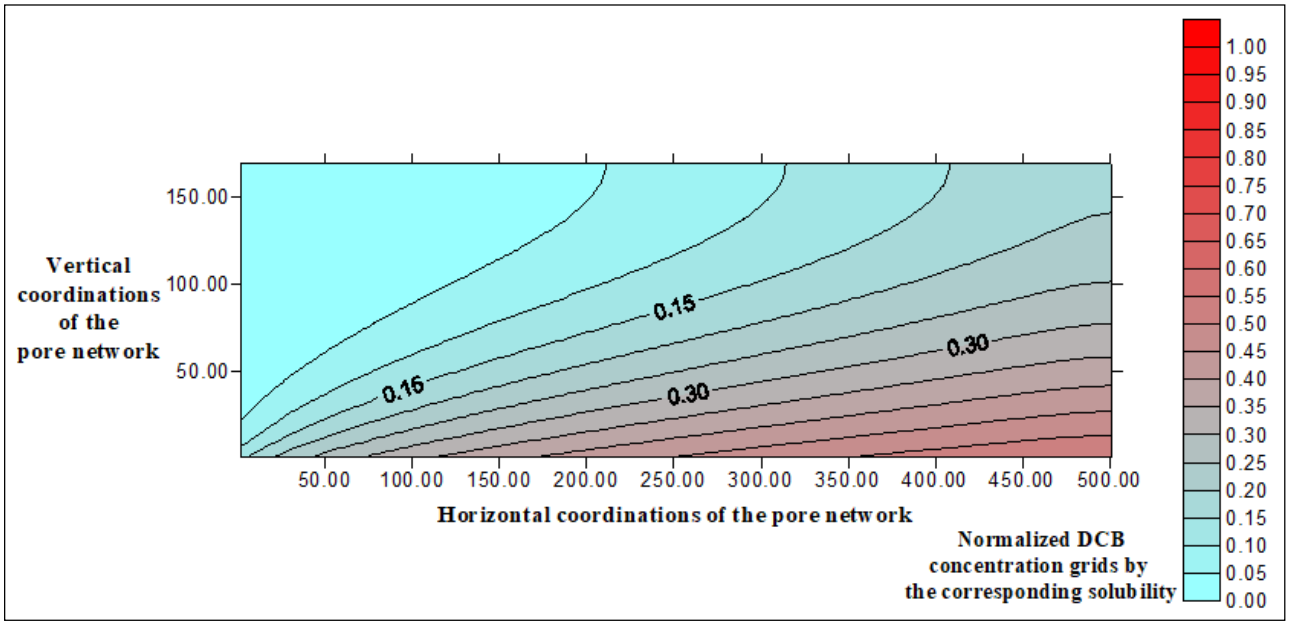

Figure 5.54. Contour plot of the normalized DCB distribution computed with the pore network model for Q = 5 mL/min, EtOH = 20 % (sand).

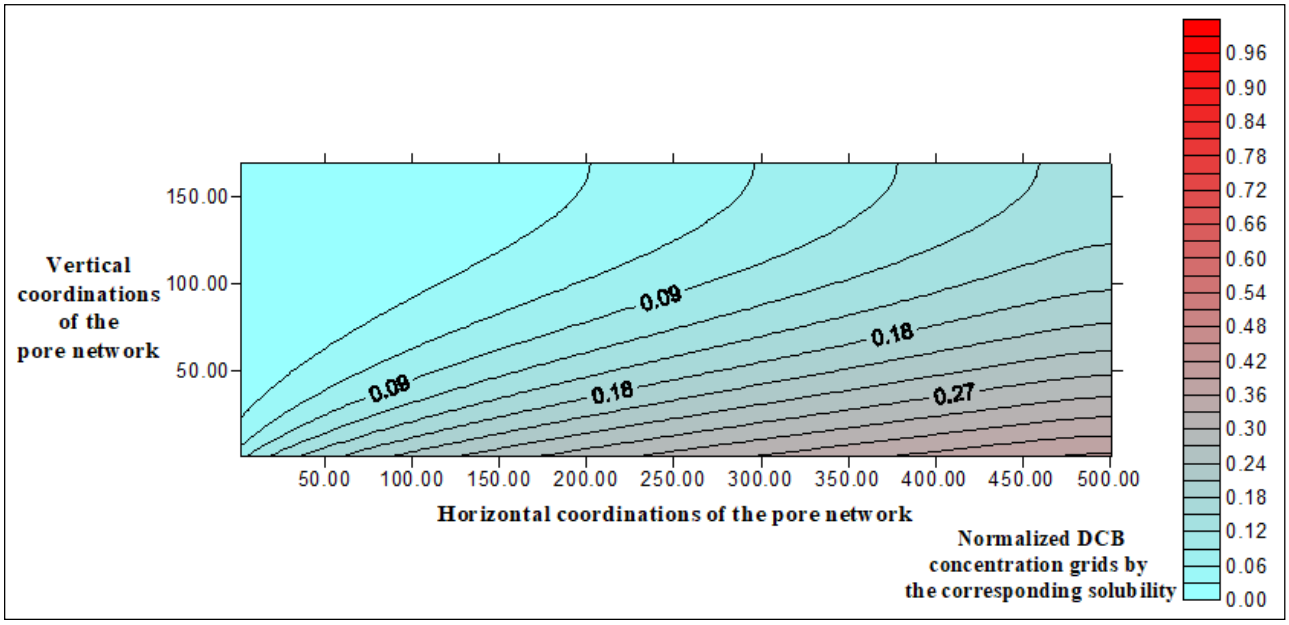

Figure 5.55. Contour plot of the normalized DCB distribution computed with the pore network model for Q = 5 mL/min, EtOH = 30 % (sand).

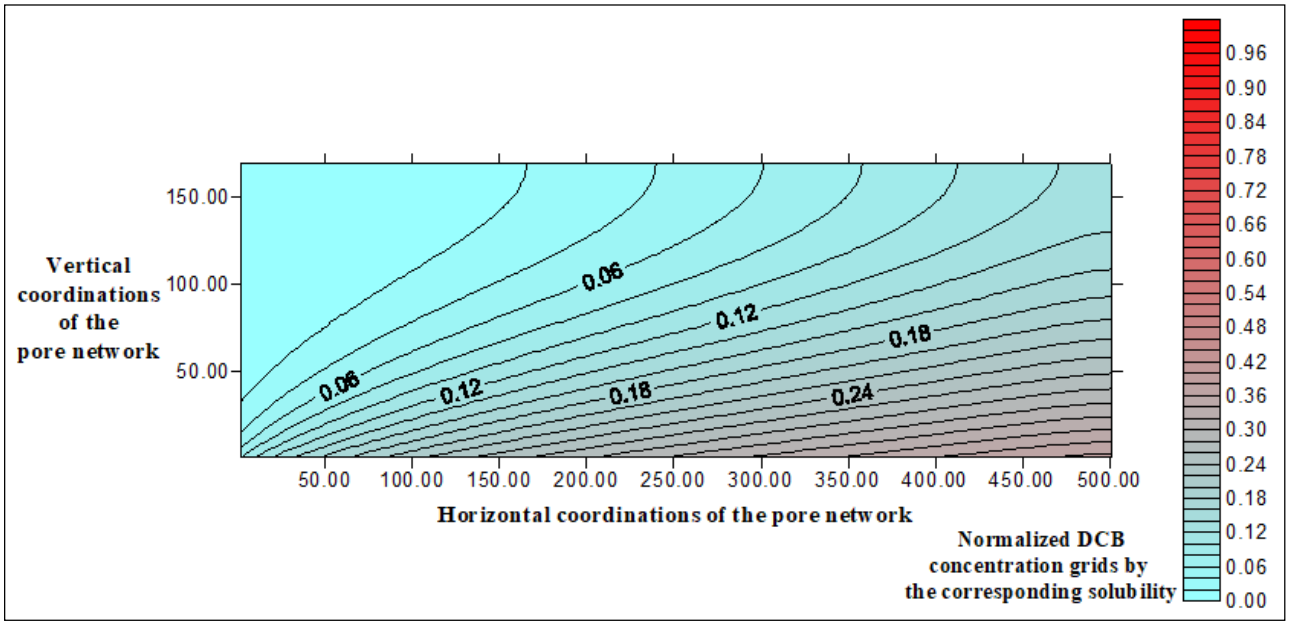

Figure 5.56. Contour plot of the normalized DCB distribution computed with the pore network model for Q = 5 mL/min, EtOH = 40 % (sand).

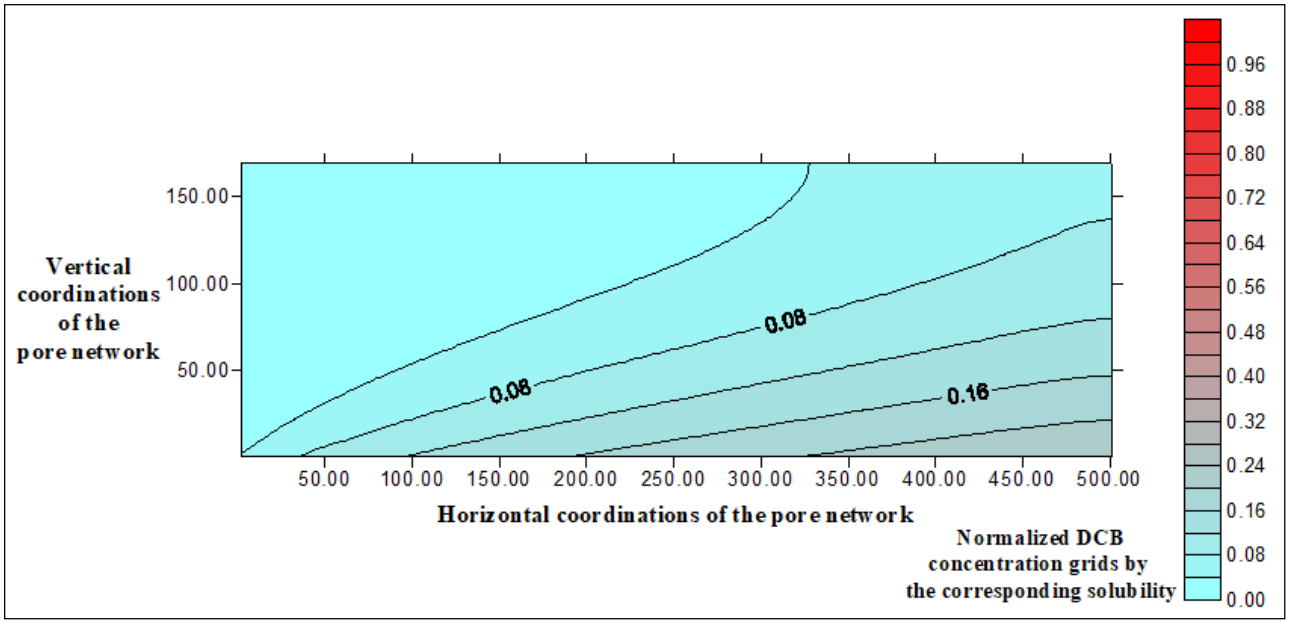

Figure 5.57. Contour plot of the normalized DCB distribution computed with the pore network model for Q = 11 mL/min, EtOH = 0 % (sand).

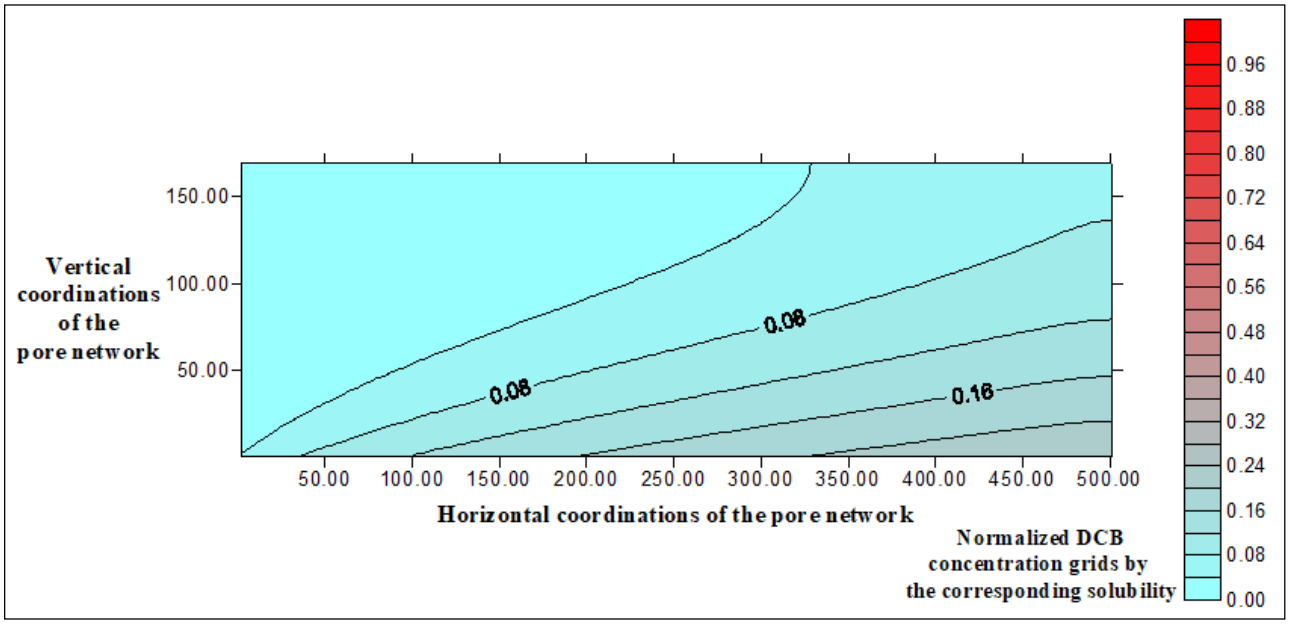

Figure 5.58. Contour plot of the normalized DCB distribution computed with the pore network model for Q = 11 mL/min, EtOH = 0 % (sand).

5.4. Development of Sherwood Correlations

The data presented in Section 5.3 are further used to develop Sherwood correlations. For generating the correlations, the data are expressed in terms of the non-dimensional parameters: Péclet number, Schmidt number and Sherwood number for corresponding computation methods (1D

analytical or 2D pore network), which are shown in Table 5.10 for the glass beads medium and Table 5.11 for the sand medium.

Table 5.10. Péclet, Schmidt and Sherwood number calculations for glass beads experiment sets.

Péclet number	**Schmidt number**	**Sherwood number**	
		1D Analytical equation	**2D Pore network model**
9.49	1004	0.95	1.54
9.49	1310	0.90	1.43
9.49	1860	0.51	0.75
9.49	2402	0.25	0.35
40.85	1004	2.41	3.56
40.85	1310	2.06	3.00
40.85	1860	1.10	1.53
40.85	2402	1.00	1.40
81.70	1004	4.12	6.00
81.70	1310	6.48	10.05
81.70	1860	2.82	4.00
81.70	2402	2.17	3.02
204.25	1004	11.00	16.20
204.25	1310	10.34	15.10
204.25	1860	8.20	11.75
204.25	2402	4.39	6.05
1021.24	1004	38.00	54.50
1021.24	1310	38.43	54.80
1021.24	1860	27.34	38.00
1021.24	2402	20.59	28.35

The Péclet number, Schmidt number and Sherwood number are calculated using Equation 4.6, Equation 4.7 and Equation 4.5 respectively. Mass transfer coefficients presented in Table 5.8 and Table 5.9 are incorporated in the calculations of Sherwood numbers. Previously specified mean grain diameter values (in meter) are used in the calculation of Péclet and Sherwood numbers. Velocities calculated from the flow rates via Equation 4.4 are used in the calculation of Péclet numbers. The molecular diffusion coefficient, D_m, is assumed to be 1×10^{-9} m^2/s for all the both sets of experiments (Gabler et al., 1996). The flushing solution viscosity and density appearing in the Schmidt number were from the work of Khattab and colleagues (Khattab et al., 2012).

Table 5.11. Péclet, Schmidt and Sherwood number calculations for sand experiment sets.

Péclet number	Schmidt number	Sherwood number	
		1D Analytical equation	2D Pore network model
1.06	1004	0.18	0.48
1.06	2762	0.07	0.13
1.27	1004	0.14	0.31
1.27	1310	0.12	0.24
1.27	1860	0.07	0.13
1.27	2402	0.09	0.17
6.81	1004	1.75	8.40
6.81	1310	1.58	6.30
6.81	1860	0.97	2.41
6.81	2402	1.11	3.02
6.81	2762	0.86	2.03
13.62	1004	1.74	4.10
13.62	1310	2.34	6.73
13.62	1860	1.50	3.35
13.62	2402	1.69	3.95
13.62	2762	1.17	2.39
34.04	1004	5.42	14.60
34.04	1310	6.77	22.20
34.04	1860	4.32	10.20
34.04	2402	2.86	5.82
34.04	2762	2.76	5.59

The values corresponding to the sand experiments of flow rates at 11 mL/min are excluded from the calculation of Sherwood numbers. It can be noticed clearly from Figure 5.12 that the results from this experiment reveal a significant degree of error relative to the rest of the results. This was confirmed at the regression analysis stage while crosschecking the predicted Sherwood number values with the calculated ones yielded more than 450 % deviation. It is likely that the referred values are outliers in the data sets and excluding them from the calculations of Sherwood correlations result help developing consistent and harmonious Sherwood expressions. The most notable cause for the inconsistency of the results for flow rates 11 mL/min is the potential exhaustion of NAPL mass at the interfacial area of the aqueous phase as that particular experimental set was performed after liters of flushing, including 30 % and 40 % ethanol contents. Also, such higher flow rate possibly caused

mobilization of the NAPL, which was already observed at the case of 20 % ethanol flushing experiment.

Sherwood correlations developed from multivariate regression are presented below. The obtained correlations are presented in Table 5.12: Equation 5.1 for glass beads, Equation 5.2 for sand and Equation 5.3 for both data sets together using the mass transfer coefficient calculated with the 1D analytical solution; the accuracy of these results is considered lower because the 1D solution does not account for dispersion in the flow cell (Equation 4.1).

Table 5.12. Sherwood correlations from 1D analytical solution.

Sherwood correlation	Condition	R^2	Correlation number
$Sh = 197.08\frac{(Pe)^{0.87}}{(Sc)^{1.07}}$	For glass beads (d_m = 0.001 m)	0.9773	(5.1)
$Sh = 12.58\frac{(Pe)^{1.12}}{(Sc)^{0,66}}$	For sand (d_m = 0.0002 m)	0.9590	(5.2)
$Sh = 0.163\frac{(Pe)^{0.97}}{(Sc)^{0.80}(d_m)^{0.67}}$	For 0.0002 m < d_m < 0.001 m	0.9595	(5.3)

The corresponding Sh correlations generated with the mass transfer coefficients determined from the 2D pore network model are presented in Table 5.13: Equation 5.4 for glass beads, Equation 5.5 for sand and Equation 5.6 for both data sets. The aforementioned correlations are considered to be more reliable than the ones developed from 1D solution, as explained further in this section.

Table 5.13. Sherwood correlations from 2D pore network model.

Sherwood correlation	Condition	R^2	Correlation number
$Sh = 590.99\frac{(Pe)^{0.85}}{(Sc)^{1.16}}$	For glass beads (d_m = 0.001 m)	0.9719	(5.4)
$Sh = 391.96\frac{(Pe)^{1.18}}{(Sc)^{1.01}}$	For sand (d_m = 0.0002 m)	0.9118	(5.5)
$Sh = 0.105\frac{(Pe)^{0.98}}{(Sc)^{1.04}(d_m)^{1.03}}$	For 0.0002 m < d_m < 0.001 m	0.9220	(5.6)

The corresponding EXCEL regression outputs for the 6 regression correlations are given in Table 5.14 to Table 5.19. The R^2 values of all the regressions equations are consistently greater than 0.9, indicating good agreement between the experimental data and developed correlations. While correlations for particular porous media (Equation 5.4 and 5.5) are valid for the specific porous media (Figure 5.59 – Figure 5.61), the one incorporating mean grain diameter term (Equation 5.6) can be used for porous media with mean grain diameters in the range $0.0002\ m < d_m < 0.001\ m$. Yet, because only two porous media were used in the development of this correlation, further experimental and modeling work is recommended to extend its validity to other soil types.

The correlations are developed within the range of 1 – 1021 for Péclet numbers, and 1004 – 2762 for Schmidt numbers. The corresponding range in the Sherwood numbers is 0.07 – 54.80. While glass beads correlations are generated within a relatively narrower range of ethanol content but broader velocity range, sand correlations are for narrower range of velocities and broader range of ethanol contents. It is important to note that flushing NAPLs (especially DNAPLs) should be done with extreme caution for ethanol contents above 50% by volume (Schmidt numbers above 3300 for the case of this study). At this high cosolvent content, the NAPL and flushing solutions become miscible or near-miscible which may lead to undesired NAPL mobility.

The reliability of the Sherwood correlations developed in this study are next compared to available data from the literature. The only published Sherwood correlations that included the Schmidt number are in the study of Miller and colleagues (Miller et al., 1990) and the book of Wakao and colleagues (Wakao and Kaguei, 1982). Miller and colleagues conducted experiments with a one-dimensional experimental apparatus to measure mass transfer between toluene and water. Using glass beads as porous media (nominal particle diameters in a range of 0.2 – 0.65 mm), the rate of interphase mass transfer was investigated as a function of flushing velocity, fluid saturations and porous media characteristics. The results were reported to be computed with a 1D analytical solution in a similar manner as Equation 2.2, 2.3, 2.8, 2.9. The Sherwood correlation they developed was $\boldsymbol{Sh = \beta \times \theta_n^x \times Re^{0.75} Sc^{0.5}}$ where the term β is an independent coefficient and equals 12 ± 2 and θ stands for the volume fraction of the NAPL mass. In addition to this, the correlations provided in the book (Wakao and Kaguei, 1982) were proposed for the dissolution of solid spheres in fluidized beds. The Sh correlation presented in this publication is $\boldsymbol{Sh = 2 + 1.1 Re^{0.6} Sc^{0.33}}$. Experimental data for different fluid systems were used to support the validity of this expression, and it was stated to be reliable for a wide range of Reynolds number from 3 to 3000.

The two correlations found in the literature are not directly comparable to the results produced in this study as the NAPL distribution porous media properties are not similar. However, it should be noted that Reynolds number appearing in the above correlations can be expressed in terms of Péclet and Schmidt numbers ($Re = Pe/Sc$). Applying the relationship to the correlations presented in the aforementioned works yield a positive exponent for the Peclet number and a negative exponents for the Schmidt number parameters, which are parallel to the findings of this study.

Incorporating the Schmidt numbers in Sherwood correlations enables their applicability to a variety of cosolvent agents, unrestricted to ethanol. The Schmidt number is a unitless generic expression, which is not solvent specific. Besides, the use of Schmidt numbers instead of ethanol contents is also desirable as it allows for the incorporation of the results of the experiment with 0% ethanol content.

For the determination of coefficients to form Sherwood correlations, the data in Table 5.10 and Table 5.11 are processed with Ordinary Least Squares (OLS) regression tool in Microsoft Excel software. The values are first written in the form of their natural logarithms to transform the values in order that the variables in the expressions would have a linear relationship. The outputs generated by the regression analyses are presented in the following tables (Table 5.14 - Table 5.19). The R square values are distinctly higher for the sets where only values from the glass beads experiments are correlated, than values from the sand experiments, for both the 1D and 2D mass transfer calculations. As mentioned previously, the NAPL entrapment method in the sand experiments have a potential impact on the results. Having two distinct porous media to help place the DNAPL pool, possible "air bubbles" or uneven formation of DCB surface were more likely to happen leading to a less even interface between the two phases. This issue highlights the challenge for remediating NAPLs in field scale which would be under immensely more complex conditions, foremost due to the heterogeneity of natural soils and its impact on the distribution of the NAPL and flushing solutions.

Sherwood numbers estimated by the correlations of Equation 5.4, Equation 5.5 and Equation 5.6 are compared with the values computed via 2D pore network model in Table 5.10 and Table 5.11. The relationship between the Sherwood values are visualized in Figure 5.59, Figure 5.60 and Figure 5.61 and the comparisons between the calculated and estimated Sherwood numbers are presented in bar charts in Figure 5.62 for Equation 5.4, Figure 5.63 for Equation 5.5 and Figure 5.64 for Equation 5.6. Since the Sherwood values range in 0.07 to 54.80, logarithmic scale (to the base of e) is facilitated for the comparison. It can be noticed that for the case of estimations where the grain size parameter

is incorporated into the correlation (Figure 5.64), the deviation from the computed values are slightly higher than the former two, specifically for the lower flow rate values (indicated with *Pé* – Péclet numbers) of sand experiments and the higher flow rates of glass beads experiments. Overall, the correlations developed in this study are a useful tool for the estimation of the mass transfer coefficient in porous media for different flushing solutions and for a wide range of Peclet numbers.

Table 5.14. Regression output for the 1D analytical calculation, glass beads (Equation 5.1).

SUMMARY OUTPUT

Regression Statistics	
Multiple R	0.9886
R Square	0.9773
Adjusted R Square	0.9747
Standard Error	0.2314
Observations	20

ANOVA

	df	*SS*	*MS*	*F*	*Significance F*
Regression	2	39.247	19.623	366.522	1.049E-14
Residual	17	0.910	0.054		
Total	19	40.157			

	Coefficients	*Standard Error*	*t Stat*	*P-value*	*Lower 95%*	*Upper %95*
Intercept	5.284	1.155	4.573	2.700E-04	2.846	7.721
ln(Pe)	0.865	0.033	26.187	3.516E-15	0.795	0.935
ln(Sc)	-1.071	0.156	-6.877	2.684E-06	-1.399	-0.742

Table 5.15. Regression output for the 1D analytical calculation, sand (Equation 5.2).

SUMMARY OUTPUT

Regression Statistics	
Multiple R	0.9793
R Square	0.9590
Adjusted R Square	0.9544
Standard Error	0.3163
Observations	21

ANOVA

	df	*SS*	*MS*	*F*	*Significance F*
Regression	2	42.114	21.057	210.475	3.279E-13
Residual	18	1.801	0.100		
Total	20	43.914			

	Coefficients	*Standard Error*	*t Stat*	*P-value*	*Lower 95%*	*Upper %95*
Intercept	2.532	1.336	1.895	7.430E-02	-0.275	5.339
ln(Pe)	1.124	0.055	20.446	6.579E-14	1.008	1.239
ln(Sc)	-0.657	0.180	-3.648	1.838E-03	-1.036	-0.279

Table 5.16. Regression output for the 1D analytical calculation, glass beads and sand combined (Equation 5.3).

SUMMARY OUTPUT

Regression Statistics	
Multiple R	0.9795
R Square	0.9594
Adjusted R Square	0.9562
Standard Error	0.3412
Observations	41

ANOVA

	df	*SS*	*MS*	*F*	*Significance F*
Regression	3	101.911	33.970	291.777	8.612E-26
Residual	37	4.308	0.116		
Total	40	106.219			

	Coefficients	*Standard Error*	*t Stat*	*P-value*	*Lower 95%*	*Upper %95*
Intercept	-1.814	1.271	-1.427	1.619E-01	-4.388	0.761
ln(Pe)	0.972	0.038	25.833	2.842E-25	0.895	1.048
ln(Sc)	-0.801	0.148	-5.409	3.962E-06	-1.101	-0.501
$\ln(d_m)$	-0.671	0.090	-7.476	6.644E-09	-0.853	-0.489

Table 5.17. Regression output for the 2D model, glass beads (Equation 5.4).

SUMMARY OUTPUT

Regression Statistics	
Multiple R	0.9858
R Square	0.9719
Adjusted R Square	0.9685
Standard Error	0.2564
Observations	20

ANOVA

	df	*SS*	*MS*	*F*	*Significance F*
Regression	2	38.588	19.294	293.500	6.607E-14
Residual	17	1.118	6.57E-02		
Total	19	39.706			

	Coefficients	*Standard Error*	*t Stat*	*P-value*	*Lower 95%*	*Upper %95*
Intercept	6.382	1.280	4.985	1.130E-04	3.681	9.083
ln(Pe)	0.852	0.037	23.273	2.480E-14	0.775	0.929
ln(Sc)	-1.162	0.173	-6.734	3.500E-06	-1.526	-0.798

Table 5.18. Regression output for the 2D model, sand (Equation 5.5).

SUMMARY OUTPUT

Regression Statistics	
Multiple R	0.9549
R Square	0.9118
Adjusted R Square	0.9020
Standard Error	0.5037
Observations	21

ANOVA

	df	*SS*	*MS*	*F*	*Significance F*
Regression	2	47.236	23.618	93.077	3.2199E-10
Residual	18	4.567	0.254		
Total	20	51.803			

	Coefficients	*Standard Error*	*t Stat*	*P-value*	*Lower 95%*	*Upper %95*
Intercept	5.971	2.128	2.806	1.169E-02	1.500	10.442
ln(Pe)	1.178	0.088	13.456	7.822E-11	0.994	1.362
ln(Sc)	-1.013	0.287	-3.531	2.388E-03	-1.616	-0.410

Table 5.19. Regression output for the 2D model, glass beads and sand combined (Equation 5.6).

SUMMARY OUTPUT

Regression Statistics	
Multiple R	0.9602
R Square	0.9220
Adjusted R Square	0.9157
Standard Error	0.4603
Observations	41

ANOVA

	df	*SS*	*MS*	*F*	*Significance F*
Regression	3	92.726	30.909	145.865	1.506E-20
Residual	37	7.840	0.212		
Total	40	100.566			

	Coefficients	*Standard Error*	*t Stat*	*P-value*	*Lower 95%*	*Upper %95*
Intercept	-2.255	1.714	-1.316	0.196	-5.728	1.218
ln(Pe)	0.984	0.051	19.399	5.555E-21	0.882	1.087
ln(Sc)	-1.040	0.200	-5.202	7.540E-06	-1.444	-0.635
$\ln(d_m)$	-1.034	0.121	-8.536	2.848E-10	-1.279	-0.788

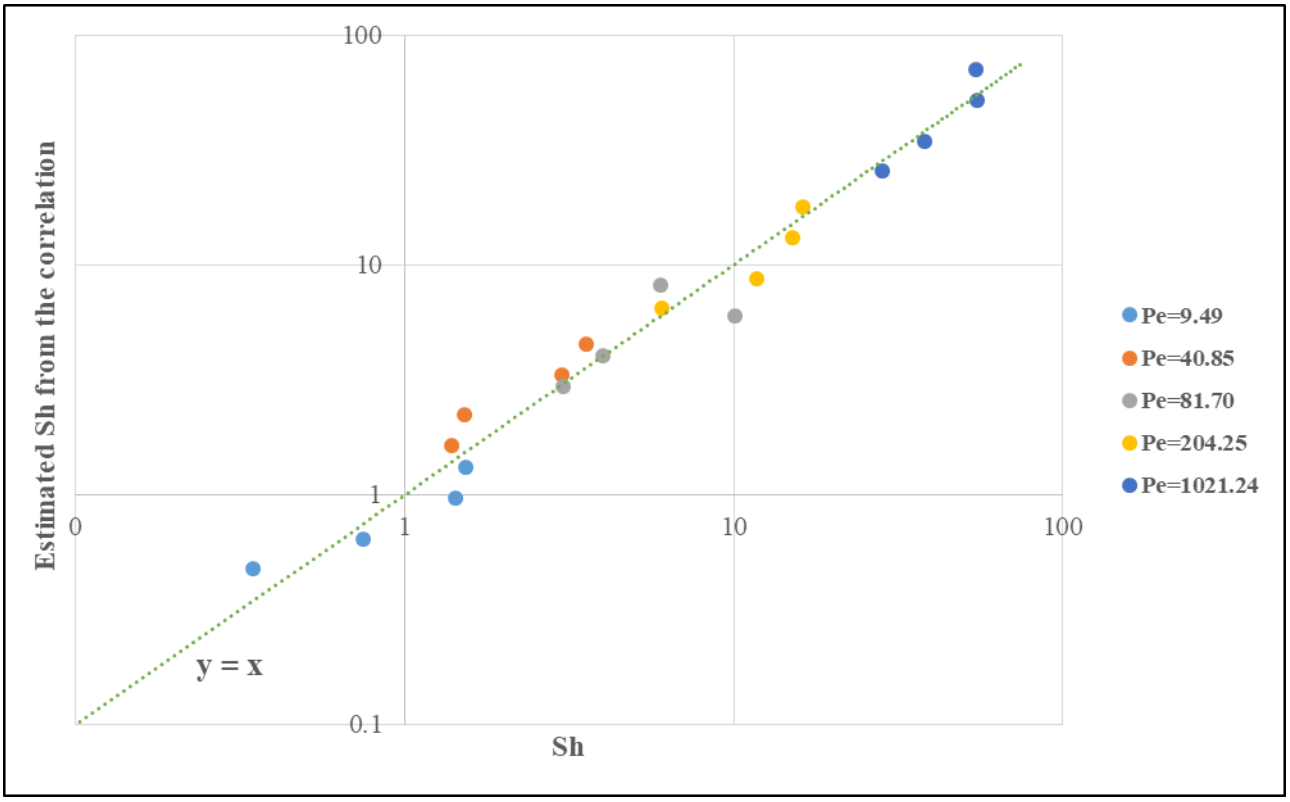

Figure 5.59. Comparison of Sherwood numbers, calculated via 2D model and Equation 5.4 (Glass beads).

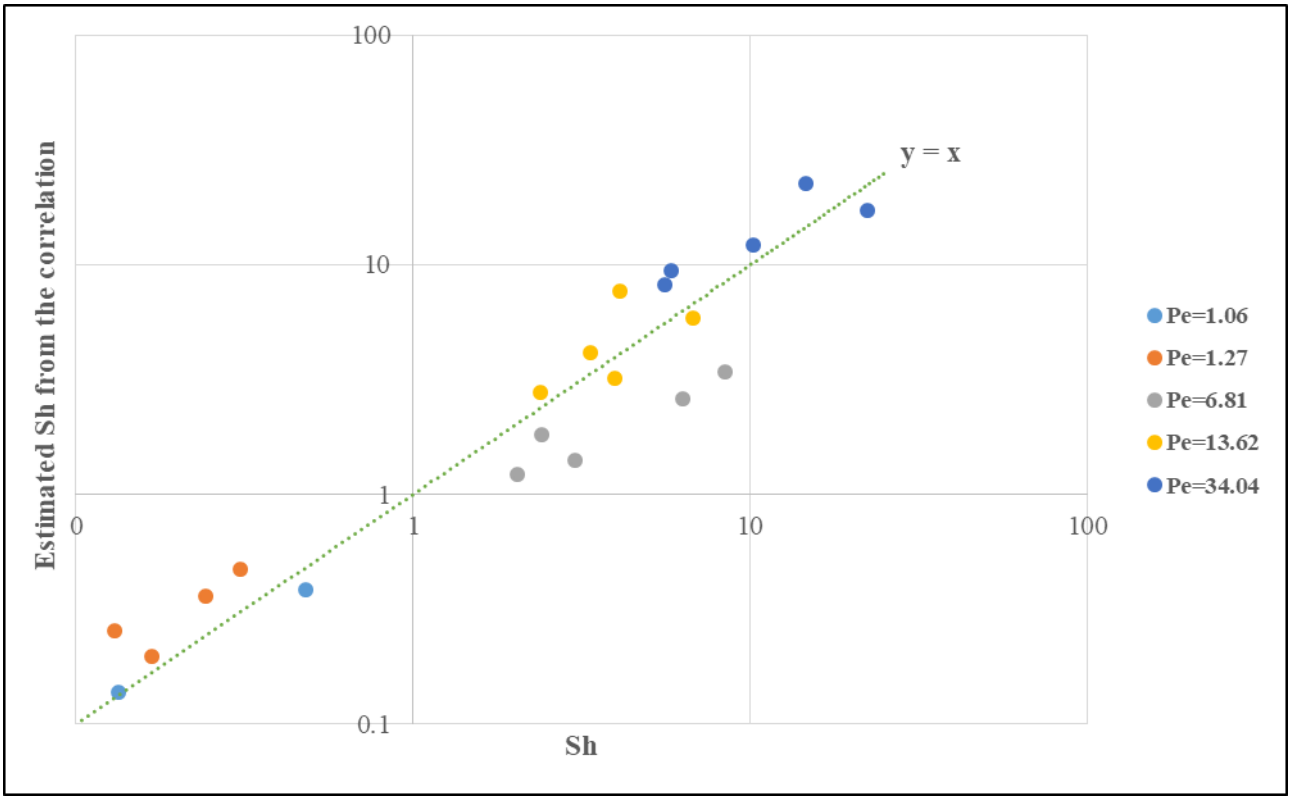

Figure 5.60. Comparison of Sherwood numbers, calculated via 2D model and Equation 5.5 (Sand).

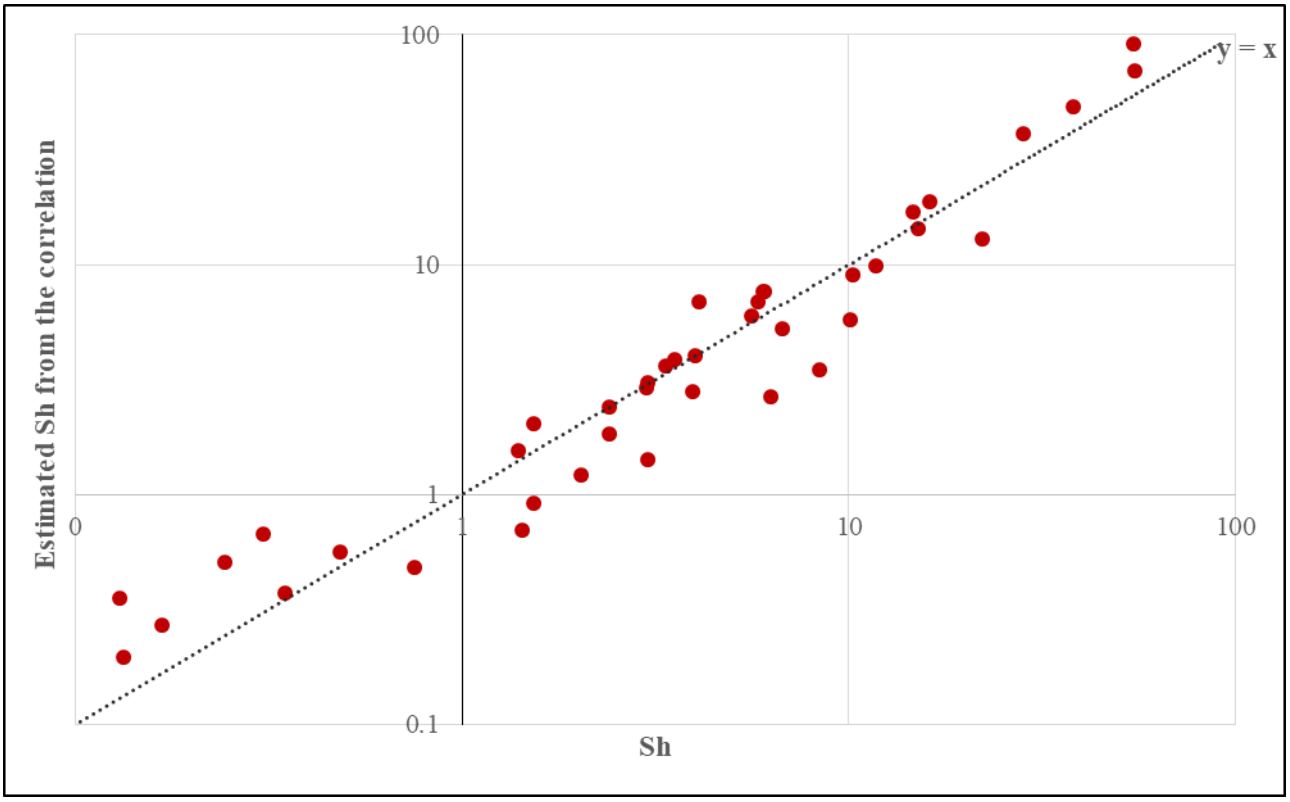

Figure 5.61. Comparison of Sherwood numbers, calculated via 2D model and Equation 5.6 (Glass beads and sand).

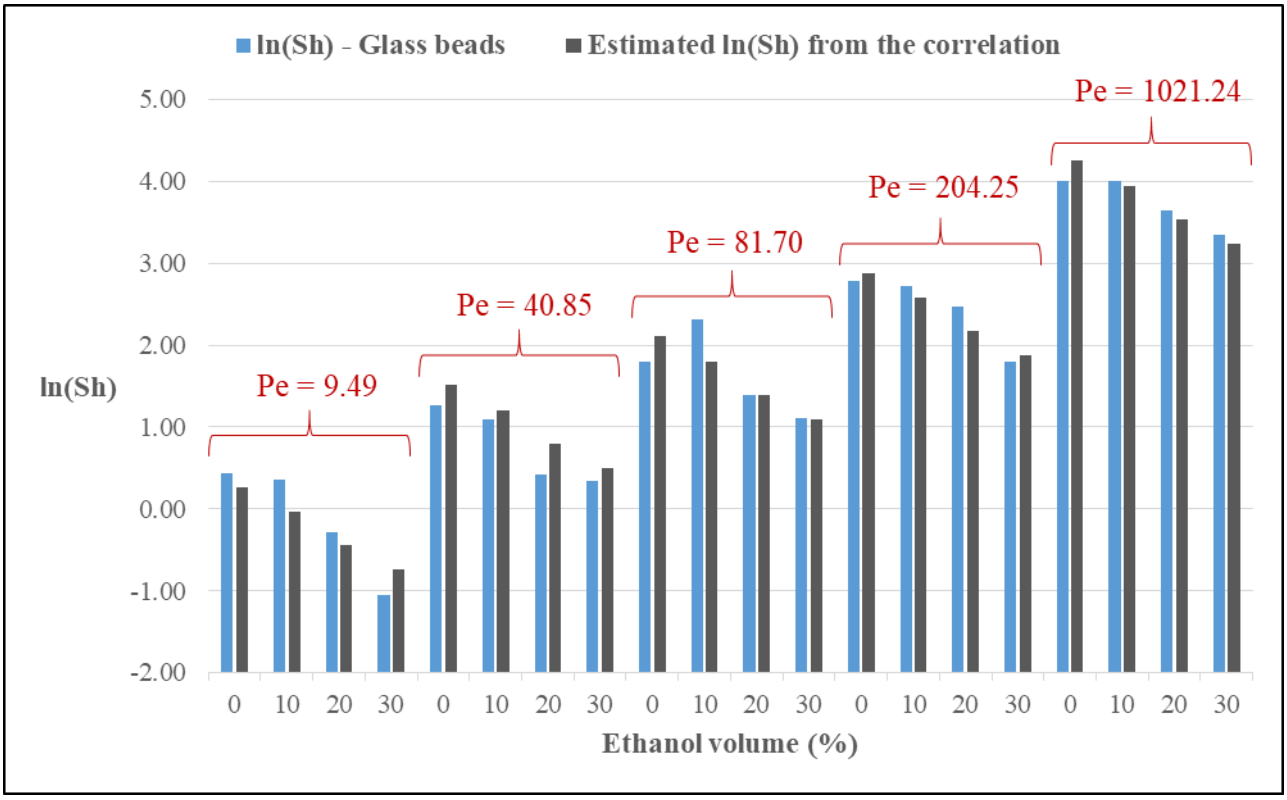

Figure 5.62. Comparison of Sherwood numbers, calculated via 2D model and Equation 5.4 (Glass beads).

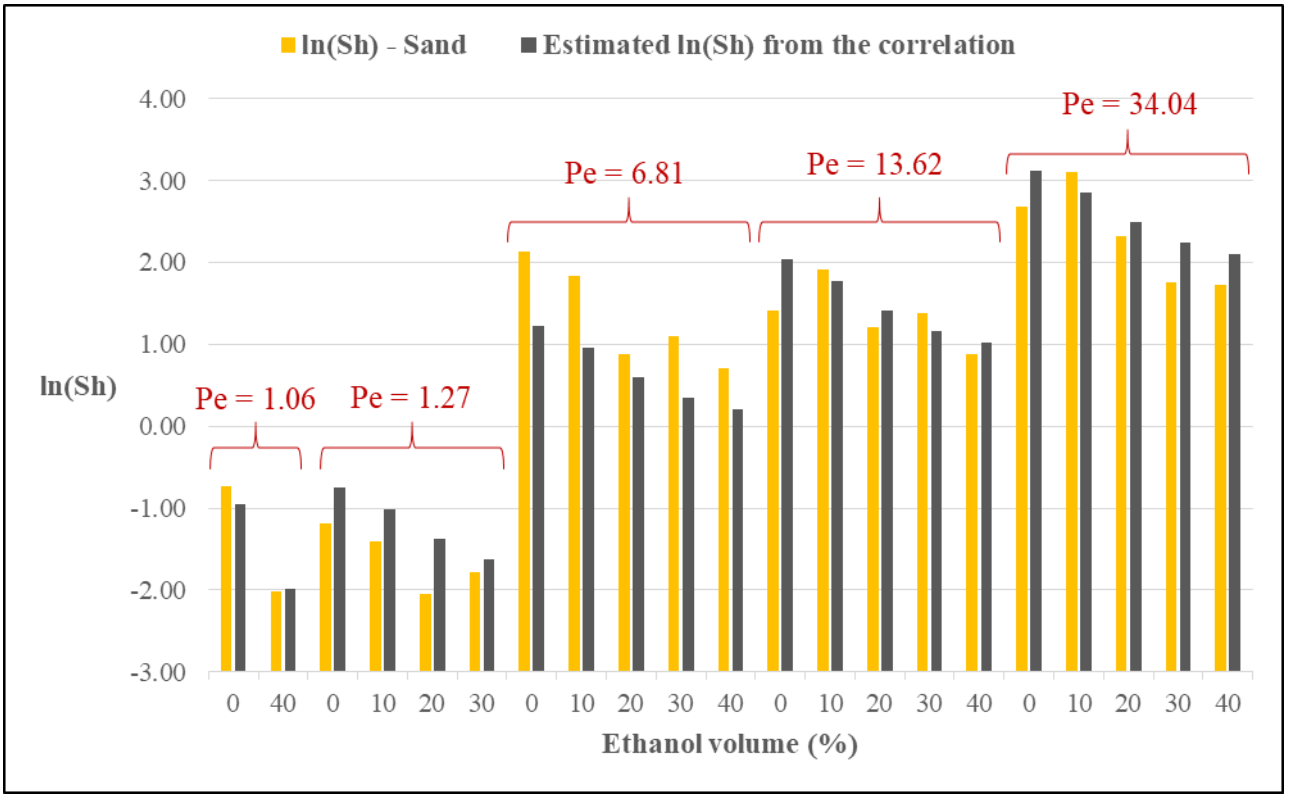

Figure 5.63. Comparison of Sherwood numbers, calculated via 2D model and Equation 5.5 (Sand).

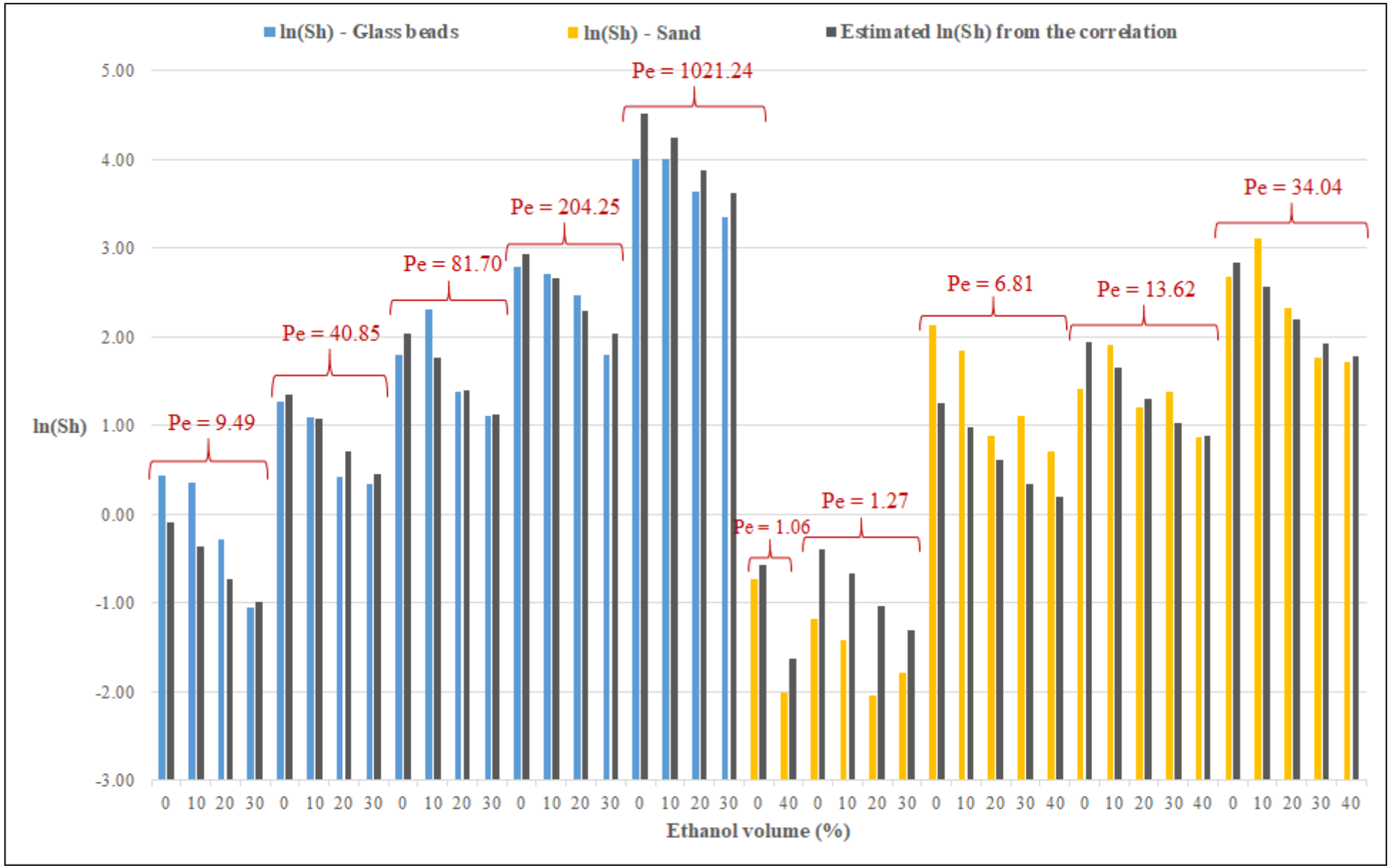

Figure 5.64. Comparison of Sherwood numbers, calculated via 2D model and Equation 5.6 (Glass beads and sand).

6. CONCLUSIONS

Contamination of groundwater with non-aqueous phase liquids (NAPLs) is a significant threat to both public health and the environment. Cosolvent flushing has been proposed as a promising technology for successful remediation of groundwater resources contaminated with such organic compounds. This thesis investigated the effect of cosolvents on the interphase mass transfer phenomena, a key factor that controls this remediation technology. To achieve this goal, a series of flow cell experiments were performed to calculate mass transfer coefficients of a chlorinated organic compound (1,2-dichlorobenzene – DCB) for various experimental conditions. The DNAPL was assumed to be in pooled form. The cosolvent used throughout the experiments is ethanol.

The parameters tested with the flow cell experiments are cosolvent content in the flushing solutions, velocity of the flushing solutions and mean grain diameters of the porous media. The experimental results were used to estimate the interphase mass transfer coefficients using two approaches; a simplified 1D analytical method and a 2D pore network model written in Fortran programming language. The results of the two sets varied due to the fact that the simplified 1D analytical expression excludes dispersion. In particular, the lateral dispersivity is an important parameter in mass transfer processes as it is the primary mechanism responsible for the spread of the dissolved contaminant away from the interface which in turn leads to further dissolution. As such, the 2D model results are more reliable to those predicted with the simplified 1D solution. As expected, the mass transfer coefficient values are proportional with velocity of the aqueous phases and inversely proportional with the ethanol content of the flushing solutions.

The outcomes of the work is next evaluated to develop non-lumped Sherwood expressions. Although lumped Sherwood correlations are frequent in the literature, only a few such correlations have been developed for the non-lumped Sherwood expression due to the difficulty of defining the interfacial area between the NAPL and aqueous phases, a required parameter for the definition of the non-lumped Sherwood correlation. Moreover, very few studies have considered the effect of fluid composition on interface mass transfer and the ensuing Sherwood number correlation. In this study, the Sherwood correlations were expressed in terms of Péclet and Schmidt numbers, representing the system properties. The Schmidt number in the correlations stand for the effect of cosolvent content on the Sherwood number. Coefficients of the Schmidt number parameters highlighted the importance of cosolvent content on the interphase mass transfer. These Sherwood correlations are expected to help fill the gap in the existing literature.

The experimental work and evaluation of the results supported the fact that mass transfer in porous media is a complex process, influenced by numerous factors. Improving the precision of modeling and application of this technology requires extensive efforts, primarily experimental work and detailed interpretation of these results. Future research can address the following issues:

- The experiments conducted in this study are limited to two porous media. Future studies can consider porous media with a wider range of mean grain diameters. Both uniform as well as non-uniform grain size distributions can be considered.
- Mass transfer calculations with varieties of cosolvents as well as NAPLs are also suggested to extend the applicability of the correlations to various flushing reagents and enhance the reliability of the Schmidt number factors in Sherwood correlations.
- Heterogeneity of the porous media, namely the spatial variability of the porous media and flow properties, is a salient property of practically all natural soils. Future studies can consider this phenomenon in conjunction with other parameters such as cosolvent content and velocity. Comprehensive experimental data would be needed to broadly evaluate and quantify the factors that influence interphase mass transfer rates.
- The spatial distribution of the NAPL remains the most limiting factor in many instances for the effective remediation of subsurface systems. Because of irregular non-uniform soil properties, NAPL distributions exhibit complex spatial distributions. In the present study, an attempt was made to emplace the NAPL in pool form with an even interface with the flushing solution. Future studies can consider other spatial distributions of the NAPL. Because the analysis of the mass transfer needs detailed knowledge of the interfacial area, recent developments in imaging techniques such as x-ray micro-tomography may be required to better define the NAPL distribution.

Overall, this study provides some useful interphase mass transfer data, analyses and correlations that can be used in future modeling works and field investigations involving cosolvent flushing of NAPLs in porous media.

REFERENCES

Adams, G. O., Fufeyin, P. T., Okoro, S. E., Ehinomen, I., 2015. Bioremediation, Biostimulation and Bioaugmention: A Review. International Journal of Environmental Bioremediation & Biodegradation, 3, 28-39.

Agaoglu, B., Copty, N., Scheytt, T., 2012. Laboratory-Scale Experiments and Numerical Modeling of Cosolvent Flushing of Multi-Component NAPLs in Saturated Porous Media. Journal of Contaminant Hydrology, 140-141, 80-94.

Agaoglu, B., Copty, N., Scheytt, T., Hinkelmann, R., 2015. Interphase mass transfer between fluids in subsurface formations; A review. Advances in Water Resources, 79, 162-194.

Agaoglu, B., Scheytt, T., Copty, N. K., 2016. Impact of NAPL architecture on interphase mass transfer: A pore network study. Advances in Water Resources, 95, 138-151.

Akyol, N. H., Yolcubal, I., 2013. Oxidation of nonaqueous phase trichloroethylene with permanganate in epikarst. Water, Air, and Soil Pollution, 224, 1573.

Akyol, N. H., 2018. Surfactant-enhanced permanganate oxidation on mass-flux reduction and mass removal relationship for pool-dominated TCE source zones in heterogeneous porous media. Water, Air, and Soil Pollution, 229: 285.

Akyol, N. H., Turkkan, S., 2018. Effect of Cyclodextrin-enhanced dissolution on Mass Removal and Mass Discharge Reduction for TCE Source Zones in Heterogeneous Porous Media. Water, Air, and Soil Pollution, 229: 30.

Anwar, A. F., Tien, T. H., Inoue, Y., Takagi, F., 2003. Mass transfer correlation for nonaqueous phase liquid volatilization in porous media. Environmental Science and Technology, 37, 1277-1283.

Arpe, H.-J., 2010. Industrial Organic Chemistry, Wiley-VCH, Weinheim, Germany.

Atlas, R. M., Philp, J., 2005. Bioremediation: Applied Microbial Solutions for Real-world Environmental Cleanup. ASM Press.

Aydin, G. A., Agaoglu, B., Kocasoy, G., Copty, N. K., 2011. Effect of temperature on cosolvent flooding for the enhanced solubilization and mobilization of NAPLs in porous media. Journal of Hazardous Materials, 186, 636–644.

Aydin-Sarikurt, D., 2018. Remediation of DNAPLs in Saturated Porous Media: Cosolvent Flushing and Sherwood Correlation, Ph.D. Thesis, Bogazici University, Turkey.

Aydin-Sarikurt, D., Dokou, Z., Copty, N. K., Karatzas, G. P., 2016. Experimental Investigation and Numerical Modeling of Enhanced DNAPL Solubilization in Saturated Porous Media. Water, Air, & Soil Pollution, 227, 441.

Aydin-Sarikurt, D., Gokdemir, C., Copty, N. K., 2017. Sherwood correlation for dissolution of pooled NAPL in porous media. Journal of Contaminant Hydrology, 206, 67-74.

Balseiro-Romero, M., Monterroso, C., Casares, J. J., 2018. Environmental Fate of Petroleum Hydrocarbons in Soil: Review of Multiphase Transport, Mass Transfer, and Natural Attenuation Processes. Pedosphere, 28, 833-847.

Banerjee, S., Yalkowsky, S. H., Valvani, S. C., 1980. Water Solubility and Octanol/Water Partition Coefficients of Organics. Limitations of the Solubility-Partition Coefficient Correlation. Environmental Science & Technology, 14, 1227-1229.

Berg, M. V., Birnbaum, L., Bosveld, A. T., Brunström, B., Cook, P., Feeley, M., Giesy, J. P., Hanberg, A., Hasegawa, R., Kennedy, S. W., Larsen, J. C., Leeuwen, F. X. R. V., Liem, A. K. D., Nolt, C., Younes, M., Wærn, F., Zacharewski, T., 1998. Toxic Equivalency Factors (TEFs) for PCBs, PCDDs, PCDFs for Humans and Wildlife. Environmental Health Perspectives, 106, 775-792.

Besha, A. T., Bekele, D. N., Naidu, R., Chadalavada, S., 2018. Recent advances in surfactant-enhanced In-Situ Chemical Oxidation for the remediation of non-aqueous phase liquid contaminated soils and aquifers. Environmental Technology & Innovation, 9, 303-322.

Birak, P. S., Miller, C. T., 2008. Dense Nonaqueous Phase Liquids at Former Manufactured Gas Plants: Challenges to Modeling and Remediation. Journal of Contaminant Hydrology, 105, 81-98.

Boshoff, G. A., Bone, B. D., 2005. Permeable Reactive Barriers. International Association of Hydrological Sciences (IAHS) Publication.

Bradley, P., 2003. History and ecology of chloroethene biodegradation: a review. Bioremediation Journal, 7, 81-109.

Brooks, M. C., Annable, M. D., Rao, P. S., Hatfield, K., Jawitz, J. W., Wise, W. R., Wood, A. L., Enfield, C. G., 2004. Controlled release, blind test of DNAPL remediation by ethanol flushing. Journal of Contaminant Hydrology, 69, 281-297.

Brooks, R. H., Corey, A. T., 1966. Properties of porous media affecting fluid flow. Journal of the Irrigation and Drainage Division, 92, 61-90.

Brusseau, M. L., Wood, A. L., Rao, P. S., 1991. Influence of organic cosolvents on the sorption kinetics of hydrophobic organic chemicals. Environ. Sci. Technol., 25, 903–910.

Brusseau, M., Carroll, K., Allen, T., Baker, J., DiGuiseppi, W., Hatton, J., Morrison, C., Russo, A., Berkompas, J., 2011. Impact of in situ chemical oxidation on contaminant mass discharge: linking source-zone and plume-scale characterizations of remediation performance. Environmental Science and Technology, 45, 5352-5358.

Carter, R. E., 2011. Organic Solvents: Properties, Toxicity, and Industrial Effects. Nova Science Publisher's.

Chao, H., Hsieh, L. C., Tran, H. N., 2018. Increase in volatilization of organic compounds using air sparging through addition in alcohol in a soil-water system. Journal of Hazardous Materials, 344, 942-949.

Chaudhry, G. R., Chapalamadugu, S., 1991. Biodegradation of halogenated organic compounds. Microbiol Reviews, 55, 59-79.

Childs, J., Acosta, E., Annable, M. D., Brooks, M. C., Enfield, C. G., Harwell, J. H., Shiau, B., 2006. Field demonstration of surfactant-enhanced solubilization of DNAPL at Dover Air Force Base, Delaware. Journal of Contaminant Hydrology, 82, 1-22.

Cho, J., Annable, M. D., Rao, P. S., 2005. Measured Mass Transfer Coefficients in Porous Media Using Specific Interfacial Area. Environmental Science & Technology, 39, 7883-7888.

Christ, J. A., Lemke, L. D., Abriola, L. M., 2005. Comparison of two-dimensional and three-dimensional simulations of dense nonaqueous phase liquids (DNAPLs): Migration and entrapment in a nonuniform permeability field. Water Resources Research, 41, 1-12.

Chu, M., Kitanidis, P. K., McCarty, P. L., 2007. Dependence of lumped mass transfer coefficient on scale and reactions kinetics for biologically enhanced NAPL dissolution. Advances in Water Resources, 30, 1618-1629.

Cohen, R. M., Mercer, J. W., 1993. DNAPL Site Evaluation - EPA/600/R-93/022. Oklahoma, USA: U.S. Environmental Protection Agency.

Davis, E. L., 1997. Ground Water Issue: How Heat Can Enhance In-Situ Soil and Aquifer Remediation: Important Chemical Properties and Guidance on Choosing the Appropriate Technique - EPA/540/S-97/502. US Environmental Protection Agency.

Dillard, N., Leslie, A., Blunt, M. J., 2000. Development of a pore network simulation model to study nonaqueous phase liquid dissolution. Water Resources Research, 36, 439-454.

Eberhardt, C., Grathwohl, P., 2002. Time scales of organic contaminant dissolution from complex source zones: Coal tar pools vs. blobs. Journal of Contaminant Hydrology, 59, 45-66.

European Environment Agency., 2015. Remediated sites and brownfields, Success stories in Europe, A report of the European Information and Observation Network's National Reference Centres for Soil (Eionet NRC Soil). European Information and Observation Network.

European Environment Agency., 2018. Water quality and pollution by hazardous substances. Copenhagen, Denmark.

Faisal, A. A. H., Sulaymon, A. H., Khaliefa, Q. M., 2018. A review of permeable reactive barrier as passive sustainable technology for groundwater remediation. International Journal of Environmental Science and Technology, 15, 1123–1138.

Falta, R. W., Kueper, B. H., 2014. Modeling Plume Responses to Source Treatment. In: B. H. Kueper, H. F. Stroo, C. M. Vogel, C. H. Ward, Chlorinated Solvent Source Zone Remediation, 145-186, New York, U.S.A.: Springer Science and Business Media.

Fu, F., Dionysiou, D. D., Liu, H., 2014. The use of zero-valent iron for groundwater remediation and wastewater treatment: A review. Journal of Hazardous Materials, 267, 194-205.

Gabler, T., Paschke, A., Schüürmann, G., 1996. Diffusion coefficients of substituted benzenes at high dilution in water. Journal of Chemical and Engineering Data, 41, 33-36.

Gauthier, M., Kueper, B. H., 2006. Removal of PCB-DNAPL from a rough-walled fracture using alcohol/polymer flooding. Journal of Contaminant Hydrology, 84, 1-20.

Geller, J. T., Hunt, J. R., 1993. Mass Transfer From Nonaqueous Phase Organic Liquids in Water-Saturated Porous Media. Water Resour Res., 29, 833–845.

Gerhard, J. I., Kueper, B. H., Sleep, B. E., 2014. Modeling Source Zone Remediation. In: B. H. Kueper, H. F. Stroo, C. M. Vogel, C. H. Ward, Chlorinated Solvent Source Zone Remediation, 113-144, New York, U.S.A.: Springer Science and Business Media.

Gerstl, Z., Chen, Y., Mingelgrin, U., Yaron, B., 1989. Toxic Organic Chemicals in Porous Media. Springer-Verlag Berlin Heidelberg.

Goldstein, R. J., Cho, H. H., 1995. A review of mass transfer measurements using naphthalene sublimation. Experimental Thermal and Fluid Science, 10, 416-434.

González, B., Calvar, N., Gómez, E., Domínguez, Á., 2007. Density, dynamic viscosity, and derived properties of binary mixtures of methanol or ethanol with water, ethyl acetate, and methyl acetate at T = (293.15, 298.15, and 303.15) K. Journal of Chemical Thermodynamics, 39, 1578-1588.

Grodowska, K., Parczewski, A., 2010. Organic solvents in the pharmaceutical industry. Acta Poloniae Pharmaceutica, 67, 3-12.

Grubb, D. G., Sitar, N., 1994. Evaluation Of Technologies For Cleanup Of DNAPL Contaminated Sites. US Environmental Protection Agency.

Guerrero-Barajas, C., Ordaz, A., Garibay-Orijel, C., García-Solares, S. M., Bastida-González, F., Zárate-Segur, P. B., 2014. Enhanced Sulfate Reduction and Trichloroethylene (TCE) Biodegradation in a UASB Reactor Operated with a Sludge Developed from Hydrothermal Vents Sediments: Process and Microbial Ecology. International Biodeterioration & Biodegradation, 94, 182-191.

Hoffmann, B., 1969. Über die Ausbreitung gelöster Kohlenwasserstoffe im Grundwasserleiter. Technische Universität Hannover.

Hu, L. M., Meegoda, J. N., Lo, I. M., Liu, Y., Gao, S. Y., Wu, Z. Q., 2009. Gasoline Contaminated Sites: Pollutant Transport and Remediation. Advances in Environmental Geotechnics, 221-235.

Huling, S. G., Weaver, J. W., 1991. Ground Water Issue - Dense Nonaqueous Phase Liquids. U.S. Environmental Protection Agency (EPA).

Illangasekare, T. H., Armbruster III, E. J., Yates, D. N., 1995. Non-aqueous-phase fluids in heterogeneous aquifers - Experimental study. Journal of Environmental Engineering, 121, 571-579.

Imhoff, P. T., Gleyzer, S. N., McBride, J. F., Vancho, L. A., Okuda, I., Miller, C. T., 1995. Cosolvent-Enhanced Remediation of Residual Dense Nonaqueous Phase Liquids: Experimental Investigation. Environmental Science and Technology, 29, 1966–1976.

Imhoff, P. T., Jaffé, P. R., Pinder, G. F., 1994. An experimental study of complete dissolution of a nonaqueous phase liquid in saturated porous media. Water Resources Research, 30, 307-320.

Jawitz, J. W., Sillan, R. K., Annable, M. D., Rao, P. S., Warner, K., 2000. In-situ alcohol flushing of a DNAPL source zone at a dry cleaner site. Environmental Science and Technology, 34, 3722-3729.

Jia, C., Shing, K., Yortsos, Y. C., 1999. Visualization and simulation of non-aqueous phase liquids solubilization in pore networks. Journal of Contaminant Hydrology, 35, 363-387.

Jin, M., Hirasaki, G. J., Jackson, R. E., Kostarelos, K., Pope, G. A., 2007. Control of downward migration of dense nonaqueous phase liquid during surfactant flooding by design simulations. Water Resources Research, 43, 1-14.

Joekar-Niasar, V., Hassanizadeh, S. M., 2012. Analysis of fundamentals of two-phase flow in porous media using dynamic pore-network models: a review. Critical reviews in environmental science and technology, 42, 1895-1976.

Johnson, R. L., Pankow, J. F., 1992. Dissolution of dense chlorinated solvents into groundwater. 2. Source functions for pools of solvent. Environmental Science and Technology, 26, 901-908.

Johnson, R., Johnson, P., McWhorter, D., Hinchee, R., Goodman, I., 1993. An Overview of In Situ Air Sparging. Groundwater Monitoring & Remediation, 13, 127-135.

Kavanaugh, M. C., Rao, P. S., 2003. The DNAPL remediation challenge: Is there a case for source depletion? Washington DC: U.S. Environmental Protection Agency.

Khattab, I. S., Bandarkar, F., Fakhree, M. A., Jouyban, A., 2012. Density, viscosity, and surface tension of water+ethanol mixtures from 293 to 323K. Korean Journal of Chemical Engineering, 29, 812-817.

Ko, S., Crimi, M., Marvin, B. K., Holmes, V., Huling, S. G., 2012. Comparative study on oxidative treatments of NAPL containing chlorinated ethanes and ethenes using hydrogen peroxide and persulfate in soils. Journal of Environmental Management, 108, 42-48.

Kokkinaki, A., O'Carroll, D. M., Werth, C. J., Sleep, B. E., 2013. An evaluation of Sherwood-Gilland models for NAPL dissolution and their relationship to soil properties. Journal of Contaminant Hydrology, 155, 87-98.

Kueper, B. H., Davies, K. L., 2014a. DNAPL Source Zone Characterization and Delineation. In: B. H. Kueper, H. F. Stroo, C. M. Vogel, C. H. Ward, Chlorinated Solvent Source Zone Remediation, 63-82, New York, USA: Springer Science and Business Media.

Kueper, B. H., Stroo, H. F., Vogel, C. M., Ward, C. H., 2014b. Source Zone Remediation: The State of the Practice. In: B. H. Kueper, H. F. Stroo, C. M. Vogel, C. H. Ward, Chlorinated Solvent Zone Remediation, 1-28, New York, U.S.A: Springer Science and Business Media.

Kueper, B. H., Wealthall, G. P., Smith, J. W., Leharne, S. A., Lerner, D. N., 2003. An Illustrated Handbook of DNAPL Transport and Fate in the Subsurface. Bristol, U.K.: Environment Agency.

Lee, J., Woo, H. J., Jeong, K., 2019. Removal of non-aqueous phase liquids (NAPLs) from TPH-saturated sandy aquifer sediments using in situ air sparging combined with soil vapor extraction. Journal of Environmental Science and Health, Part A, 53, 1253-1266.

Lenormand, R., Touboul, E., Zarcone, C., 1988. Numerical models and experiments on immiscible displacements in porous media. Journal of Fluid Mechanics, 189, 165-187.

Lewis, J., Sjöstrom, J., 2010. Optimizing the experimental design of soil columns in saturated and unsaturated transport experiments. Journal of Contaminant Hydrology, 115, 1-13.

Liu, Y., Illangasekare, T. H., Kitanidis, P. K., 2014. Long-term mass transfer and mixing-controlled reactions of a DNAPL plume from persistent residuals. Journal of Contaminant Hydrology, 157, 11-24.

Llamas, M. R., Custodio, E., 2002. Intensive Use of Groundwater: Challenges and Opportunities. The Netherlands: CRC Press.

Loop, C. M., 2012. Contamination of Cave Waters by Nonaqueous Phase Liquids. In: W. B. White, D. C. Culver, Encyclopedia of Caves, 166-172, Academic Press.

Lowe, D. F., Oubre, C. L., Ward, C. H., Simpkin, T. J., 1999. Surfactants and cosolvents for NAPL remediation: A technology practices manual. U.S.A.: CRC Press.

Luciano, A., Viotti, P., Papini, M. P., 2010. Laboratory investigation of DNAPL migration in porous media. Journal of Hazardous Materials, 176, 1006-1017.

Lunn, S. R., Kueper, B. H., 1997. Removal of pooled dense, nonaqueous phase liquid from saturated porous media using upward gradient alcohol floods. Water Resources Research, 33, 2207-2219.

Lunn, S. R., Kueper, B. H., 1999a. Manipulation of density and viscosity for the optimization of DNAPL recovery by alcohol flooding. Journal of Contaminant Hydrology, 38, 427-445.

Lunn, S. R., Kueper, B. H., 1999b. Risk reduction during chemical flooding: Preconditioning DNAPL density in situ prior to recovery by miscible displacement. Environmental Science Technology, 33, 1703–1708.

Mahmoodlu, M. G., Hassanizadeh, S., Hartog, N., Raoof, A., van Genuchten, M. T., 2015. Evaluation of a horizontal permeable reactive barrier for preventing upward diffusion of volatile organic compounds through the unsaturated zone. Journal of Environmental Management, 163, 204-213.

Maji, R., Sudicky, E. A., 2008. Influence of mass transfer characteristics for DNAPL source depletion and contaminant flux in a highly characterized glaciofluvial aquifer. Journal of Contaminant Hydrology, 102, 105–119.

Mateas, D. J., Tick, R., Carroll, K. C., 2017. In situ stabilization of NAPL contaminant source-zones as a remediation technique to reduce mass discharge and flux to groundwater. Journal of Contaminant Hydrology, 204, 40-56.

McCarty, P. L., 2010. Groundwater Contamination by Chlorinated Solvents: History, Remediation Technologies and Strategies. In: H. F. Stroo, C. H. Ward, In Situ Remediation of Chlorinated Solvent Plumes, 1-28, New York: Springer Science+Business Media.

McCarty, P. L., Semprini, L., 1994. Ground-Water Treatment for Chlorinated Solvents. In: R. D. Norris, Handbook of Bioremediation, 87-116, Michigan: CRC Press.

McDade, J. M., McGuire, T. M., Newell, C. J., 2005. Analysis of DNAPL source-depletion costs at 36 field sites. Remediation, 15, 9-18.

McGuire, T. M., McDade, J. M., Newell, C. J., 2006. Performance of DNAPL Source Depletion Technologies at 59 Chlorinated Solvent-Impacted Sites. Ground Water Monitoring & Remediation, 26, 73-84.

Mercer, J. W., Cohen, R. M., 1990. A review of immiscible fluids in the subsurface: Properties, models, characterization and remediation. Journal of Contaminant Hydrology, 6, 107-163.

Miller, C. T., Christakos, G., Imhoff, P. T., McBride, J. F., Pedit, J. A., 1998. Multiphase flow and transport modeling in heterogeneous porous media: challenges and approaches. Advances in Water Resources, 21, 77-120.

Miller, C. T., Poirier-McNeil, M. M., Mayer, A. S., 1990. Dissolution of Trapped Nonaqueous Phase Liquids: Mass Transfer Characteristics. Water Resources Research, 26, 2783–2796.

Molins, S., Mayer, K. U., Amos, R. T., Bekins, B. A., 2010. Vadose zone attenuation of organic compounds at a crude oil spill site - Interactions between biogeochemical reactions and multicomponent gas transport. Journal of Contaminant Hydrology, 112, 15-29.

Morris, K. R., Abramowitz, R., Pinal, R., Davis, P., Yalkowsky, S. H., 1988. Solubility of aromatic pollutants in mixed solvents. Chemosphere, 17, 285-298.

Mulligan, C. N., Yong, R. N., Gibbs, B. F., 2001. Surfactant-Enhanced Remediation of Contaminated Soil: a Review. Engineering Geology, 60, 371-380.

Nagasawa, Y., Samoto, H., Ukai, H., Okamoto, S., Itoh, K., Hanada, T., Kanemaru, A., Fukui, Y., Kojima, S., Moriguchi, J., Sakuragi, S., Ohashi, F., Takada, S., Kawakami, T., Ikeda, M., 2013. Use of organic solvents in large research institutions in Japan. Environ Health Prev Med., 18, 341–348.

Nambi, I. M., Powers, S. E., 2000. NAPL dissolution in heterogeneous systems: an experimental investigation in a simple heterogeneous system. Journal of Contaminants Hydrology, 44, 161-184.

Nambi, I. M., Powers, S. E., 2003. Mass transfer correlations for nonaqueous phase liquid dissolution from regions with high initial saturations. Water Resources Research, 39.

Newell, C. J., Acree, S. D., Ross, R. R., Huling, S. G., 1995. Ground Water Issue - Light Nonaqueous Phase Liquids. Washington: U.S. Environmental Protection Agency.

Nkedi-Kizza, P., Rao, P. S., Hornsby, A. G., 1985. Influence of organic cosolvents on sorption of hydrophobic organic chemicals by soils. Environ. Sci. Technol., 19, 975–979.

Obiri-Nyarko, F., Grajales-Mesa, S. J., Malina, G., 2014. An overview of permeable reactive barriers for in situ sustainable groundwater remediation. Chemosphere, 111, 243-259.

O'Hannesin, S. F., Gillham, R. W., 1998. Long-Term Performance of an In Situ “Iron Wall” for Remediation of VOCs. Groundwater, 36, 164-170.

Pankow, J. F., Feenstra, S., Cherry, J. A., 1996. Dense Chlorinated Solvents in Groundwater: Background and History of the Problem. In: J. F. Pankow, J. A. Cherry, Dense Chlorinated Solvents and other DNAPLs in Groundwater: History, Behavior, and Remediation, 1-52, Ontario, Canada: Waterloo Press.

Paria, S., 2008. Surfactant-enhanced remediation of organic contaminated soil and water. Advances in Colloid and Interface Science, 131, 24-58.

Park, E., Parker, J. C., 2005. Evaluation of an upscaled model for DNAPL dissolution kinetics in heterogeneous aquifers. Advances in Water Resources, 28, 1280-1291.

Pennell, K. D., Abrlola, L. M., Jr., W., J., W., 1993. Surfactant-enhanced solubilization of residual dodecane in soil columns. 1. Experimental investigation. Environmental science & technology, 27, 2332-2340.

Pennell, K. D., Ca´piro, N. L., Walker, D. I., 2014. Surfactant and Cosolvent Flushing. In: B. H. Kueper, H. F. Stroo, C. M. Vogel, C. H. Ward, Chlorinated Solvent Source Zone Remediation, 353-394, New York: Springer Science+Business Media.

Pennell, K. D., Pope, G. A., Abriola, L. M., 1996. Influence of viscous and buoyancy forces on the mobilization of residual tetrachloroethylene during surfactant flushing. Environmental Science & Technology, 30, 1328-1335.

Pennell, K., Jin, M., Abriola, L., Pope, G. A., 1994. Surfactant Enhanced Remediation of Soil Columns Contaminated by Residual Tetrachloroethylene. Journal of Contaminant Hydrology, 16, 35-53.

Perry, A. S., Muszkat, L., Perry, R. Y., 1989. Pollution Hazards from Toxic Organic Chemicals. In: Z. Gerstl, Y. Chen, U. Mingelgrin, B. Yaron, Toxic Organic Chemicals in Porous Media, 16-36, Springer-Verlag Berlin Heidelberg.

Pfannkuch, H. O., 1984. Determination of the contaminant source strength from mass exchange processes at the petroleum groundwater interface in shallow aquifer systems, Proceedings of the NWWA/API conference on petroleum hydrocarbons and organic chemicals in ground water: Prevention, detection, and restoration, 5-7, National Water Well Association, Houston, Texas.

Phenrat, T., Fagerlund, F., Illangasekare, T., Lowry, G. V., Tilton, R. D., 2011. Polymer-Modified Fe^0 Nanoparticles Target Entrapped NAPL in Two Dimensional Porous Media: Effect of Particle Concentration, NAPL Saturation, and Injection Strategy. Environmental Science and Technology, 45, 6102–6109.

Powers, S. E., Abriola, L. M., Weber Jr., W. J., 1992. An experimental investigation of nonaqueous phase liquid dissolution in saturated subsurface systems: Steady state mass transfer rates. Water Resources Research, 16, 2691–2705.

Powers, S. E., Abriola, L. M., Weber, W. J., 1994b. An experimental investigation of nonaqueous phase liquid dissolution in saturated subsurface systems: Transient mass transfer rates. Water Resources Research, 30, 321–332.

Powers, S. E., Abriola, L. M., Dunkin, J. S., Weber, W. J., 1994a. Phenomenological models for transient NAPL- water mass-transfer processes. Journal of Contaminant Hydrology, 16, 1–33.

Rao, P. S., Annable, M. D., Sillan, R. K., Dai, D. P., Hatfield, K., Graham, W. D., Wood, A. L., Enfield, C. G., 1997. Field-scale evaluation of in situ cosolvent flushing for enhanced aquifer remediation. Water Resources Research, 33, 2673–2686.

Rathfelder, K. M., Abriola, L. M., Singletary, M. A., Pennell, K. D., 2003. Influence of surfactant-facilitated interfacial tension reduction on chlorinated solvent migration in porous media: observations and numerical simulation. Journal of Contaminant Hydrology, 64, 227-252.

Rivett, M. O., 2006. Organic Contaminant Remediation in Urban Groundwater. In: J. H. Tellam, M. O. Rivett, R. G. Israfilov, Urban Groundwater Management and Sustainability, 347-357, Springer Science+Business Media B.V.

Roudet, M., Billet, A.-M., Cazin, S., Risso, F., Roig, V., 2017. Experimental investigation of interfacial mass transfer mechanisms for a confined high-reynolds-number bubble rising in a thin gap. AIChE Journal, 63, 2394-2408.

Rubin, H., Narkis, N., Carberry, J. B., 2013. Overview of NAPL Contamination and Reclamation. In: H. Rubin, N. Narkis, J. Carberry, Soil and Aquifer Pollution: Non-Aqueous Phase Liquids - Contamination and Reclamation, 1-18, New York: Springer-Verlag Berlin Heidelberg.

Russell, H. H., Matthews, J. E., Sewell, G. W., 1992. TCE Removal from Contaminated Soil and Ground Water - EPA Ground Water Issue. Washington DC: US EPA.

Saba, T., Illangasekare, T. H., 2000. Effect of groundwater flow dimensionality on mass transfer from entrapped nonaqueous phase liquid contaminants. Water Ressources Research, 36, 971-979.

Schaefer, C. E., Lavorgna, G. M., White, E. B., Annable, M. D., 2017. Bioaugmentation in a Well-Characterized Fractured Rock DNAPL Source Area. Groundwater Monitoring & Remediation, 37, 35-42.

Shafieiyoun, S., Thomson, N. R., 2018. The role of intra-NAPL diffusion on mass transfer from MGP residuals. Journal of Contaminant Hydrology, 213, 49-61.

Sheu, Y., Tsang, D. C. W., Dong, C.,Chen, C., Luo, S., Kao, C., 2018. Enhanced bioremediation of TCE-contaminated groundwater using gamma poly-glutamic acid as the primary substrate. Journal of Cleaner Production, 178, 108-118.

Shevah, Y., Waldman, M., 1995. In-Situ and On-Site Treatment of Groundwater. Pure and Applied Chemistry, 67, 1549-1561.

Shukla, A. K., Upadhyay, S. N., Dubey, S. K., 2014. Current Trends in Trichloroethylene Biodegradation: a Review. Critical Reviews in Biotechnology, 34, 101-114.

Siegrist, R. L., Crimi, M., Simpkin, T. J., 2011. In Situ Chemical Oxidation for Groundwater Remediation. New York: Springer Science+Business Media.

Song, D., Seibert, A. F., Rochelle, G. T., 2014. Effect of liquid viscosity on the liquid phase mass transfer coefficient of packing. Energy Procedia, 63, 1268-1286.

Stroo, H. F., Ward, C. H., 2010. In Situ Remediation of Chlorinated Solvent Plumes. New York, USA: Springer Science & Business Media.

Stroo, H. F., West, M. R., Kueper, B. H., Borden, R. C., Major, D. W., Ward, C. H., 2014. In Situ Bioremediation of Chlorinated Ethene Source Zones. In: B. Kueper, H. F. Stroo, C. Vogel, C. H. Ward, Chlorinated Solvent Source Zone Remediation, 395-457, New York: Springer Science+Business Media.

Suthersan, S., Horst, J., Schnobrich, M., Welty, N., McDonough, J., 2017. Remediation Engineering - Design Concepts. Boca Raton, Florida USA: CRC Press.

Testa, S. M., Winegardner, D. L., 2000. Restoration of Contaminated Aquifers: Petroleum Hydrocarbons and Organic Compounds, Second Edition. U.S.A.: CRC Press.

The Interstate Technology and Regulatory Council (ITRC)., 2005. Technical and Regulatory Guidance for In Situ Chemical Oxidation of Contaminated Soil and Groundwater. Environmental Research Institute of the States (ERIS).

Tomlinson, D. W., Thornton, S. F., Thomas, A. O., Leharne, S. A., Wealthall, G. P., 2014. Illustrated Handbook of LNAPL Transport and Fate in the Subsurface. London, U.K.: CL:AIRE.

Tratnyek, P. G., Johnson, R. L., Lowry, G. V., Brown, R. A., 2014. In Situ Chemical Reduction for Source Remediation. In: B. Kueper, H. Stroo, C. Vogel, C. Ward, Chlorinated Solvent Source Zone Remediation, 307-351, New York: Springer Science+Business Media.

U.S. Environmental Protection Agency., 1991. Engineering Bulletin In Situ Soil Flushing - EPA/540/2-91/021. U.S. EPA.

U.S. Environmental Protection Agency., 1995a. In Situ Remediation Technology Status Report: Surfactant Enhancements - EPA 542-K-94-003. U.S. EPA.

U.S. Environmental Protection Agency., 1995b. Subsurface Volatilization and Ventilation System (SVVS) Innovative Technology Evaluation Report - EPA/540/R-94/529.

U.S. Environmental Protection Agency., 1996. Pump-and-Treat Ground-Water Remediation: A Guide for Decision Makers and Practitioners - EPA/625/R-95/005.

U.S. Environmental Protection Agency., 2004. Site Characterization Technologies for DNAPL Investigations - EPA 542-R-04-017. U.S. EPA/National Service Center for Environmental Publications.

U.S. Environmental Protection Agency., 2009. Underground Storage Tank Program: 25 Years of Protecting Our Land and Water - EPA-510-B-09-001. U.S. EPA/Office of Solid Waste and Emergency Response.

U.S. Environmental Protection Agency. (2018, November 24). Learn about Polychlorinated Biphenyls (PCBs). Retrieved from https://www.epa.gov/pcbs/learn-about-polychlorinated-biphenyls-pcbs

USGS., 1998. Ground Water Contamination by Crude Oil near Bemidji, Minnesota. U.S. Geological Survey.

Van Valkenburg, M. E., Annable, M. D., 2002. Mobilization and entry of DNAPL pools into finer sand media by cosolvents: two-dimensional chamber studies. Journal of Contaminant Hydrology, 59, 211–230.

Verginelli, I., Capobianco, O., Hartog, N., Baciocchi, R., 2017. Analytical model for the design of in situ horizontal permeable reactive barriers (HPRBs) for the mitigation of chlorinated solvent vapors in the unsaturated zone. Journal of Contaminant Hydrology, 197, 50-61.

Wakao, N., Kaguei, S., 1982. Heat and Mass Transfer in Packed Beds. New York: Gordon and Breach Science.

Wang, W., Schnoor, J. L., Doi, J., 1996. Volatile Organic Compounds in the Environment (Astm Special Technical Publication). Astm Intl.

Wei, J., Dahmani, A., Ahlfeld, D. P., Lin, J. D., Hill III, E., 1993. Laboratory Study of Air Sparging: Air Flow Visualization. Groundwater Monitoring & Remediation, 13, 115-126.

West, C. C., Harwell, J. H., 1992. Surfactants and subsurface remediation. Environmental Science and Technology, 26, 2324-2330.

Wilkin, R. T., Acree, S. D., Ross, R. R., Puls, R. W., Lee, T. R., Woods, L. L., 2014. Fifteen-year Assessment of a Permeable Reactive Barrier for Treatment of Chromate and Trichloroethylene in Groundwater. Science of The Total Environment, 468-469, 186-194.

Willingham, T., Zhang, C., Werth, C. J., Valocchi, A. J., Oostrom, M., Wietsma, T. W., 2010. Using dispersivity values to quantify the effects of pore-scale flow focusing on enhanced reaction along a transverse mixing zone. Advances in Water Resources, 33, 525-535.

Wypych, G., 2014. Handbook of Solvents (Second Edition). Toronto, CA: ChemTec Publishing.

Yalkowsky, S. H., He, Y., Jain, P., 2010. Handbook of Aqueous Solubility Data, Second Edition. Boca Raton, FL: CRC Press LLC.

Yang, J.-S., Yanga, J.-W., 2018. Partitioning effects of nonionic surfactants on the solubilization of single or binary chlorinated solvents: Batch and column experiments. Journal of Industrial and Engineering Chemistry, 58, 140-147.

Yang, L., Wang, X., Mendoza-Sanchez, I., Abriola, L. M., 2018. Modeling the influence of coupled mass transfer processes on mass flux downgradient of heterogeneous DNAPL source zones. Journal of Contaminant Hydrology, 211, 1-14.

Yoon, H., Kim, J. H., Liljestrand, H. M., Khim, J., 2002. Effect of water content on transient nonequilibrium NAPL–gas mass transfer during soil vapor extraction. Journal of Contaminant Hydrology, 54, 1-18.

Zhong, L., Mayer, A. S., Pope, G. A., 2003. The Effects of Surfactant Formulation on Nonequilibrium NAPL Solubilization. Journal of Contaminant Hydrology, 60, 55-75.